Modeling Human Control Behavior in Command-following Tasks

Sajad Koushkbaghi

University of Kentucky, koushkbaghi@gmail.com

Author ORCID Identifier:

iD https://orcid.org/0000-0001-9655-5809

Digital Object Identifier: https://doi.org/10.13023/etd.2022.052

Right click to open a feedback form in a new tab to let us know how this document benefits you.

MODELING HUMAN CONTROL BEHAVIOR IN
COMMAND-FOLLOWING TASKS

—————————————————

DISSERTATION

—————————————————

A dissertation submitted in partial fulfillment of the
requirements for the degree of Doctor of Philosophy in the
College of Engineering
at the University of Kentucky

By

Sajad Koushkbaghi

Lexington, Kentucky

Director: Dr. T. Michael Seigler, Professor of Mechanical Engineering

Lexington, Kentucky

ABSTRACT OF DISSERTATION

MODELING HUMAN CONTROL BEHAVIOR IN COMMAND-FOLLOWING TASKS

Humans interact with a variety of complex dynamic systems on a daily basis. However, they are often the lesser understood component of human-in-the-loop (HITL) systems. In this dissertation, we present the results of two HITL experiments to investigate the control strategies that humans use when performing command-following tasks. The first experiment is designed to investigate the control strategies that humans use to interact with nonlinear dynamic systems. Two groups of human subjects interact with a dynamic system and perform a command-following task. One group interacts with a linear time-invariant (LTI) dynamic system and the other group interacts with a Wiener system, which consists of the same LTI dynamics cascaded with a static output nonlinearity. In the second experiment, we examine the impacts of a relaxed command-following control objective on the control strategies used by humans. Two groups of human subjects interact with the same dynamic system and perform a command-following task; however, the groups have different control objectives. One group's control objective is to follow the reference command as closely as possible at all times, while the other group's control objective is to follow the reference command with some allowable error.

We develop and utilize a new subsystem identification (SSID) algorithm to model control behavior of the human subjects participating in these HITL experiments. This SSID algorithm can identify the feedback and feedforward controllers used by human subjects, and is applicable to both linear and nonlinear dynamic systems. The SSID results of the first experiment indicate that adaptive feedforward inversion is the main control strategy used by human subjects for both linear and nonlinear plants. The results of the second experiment suggest that not all the human subjects who are instructed to perform a relaxed command-following task adopt adaptive feedforward inversion as their primary control strategy. The control behavior of those human subjects contains significant nonlinearities, which cannot be captured by a LTI control model. We present a nonlinear feedforward control architecture that can model several aspects of their control behavior.

KEYWORDS: Subsystem Identification, Human Control Behavior, Feedforward Inversion, Human-in-the-Loop Systems, Command-following Task

Sajad Koushkbaghi
April 24, 2022

MODELING HUMAN CONTROL BEHAVIOR IN COMMAND-FOLLOWING TASKS

By

Sajad Koushkbaghi

Dr. T. Michael Seigler

Director of Dissertation

Dr. Jesse B. Hoagg

Director of Graduate Studies

April 24, 2022

To my parents

Table of Contents

List of Tables

List of Figures

Chapter 1   Introduction

1.1   Motivation

Humans learn to control a variety of complex dynamic systems, such as aircraft, bicycles, and automobiles. Humans often act as an operator for these systems to accomplish the required task. They also have the ability to adapt to changes in those dynamics systems as well as external disturbances.

Understanding the learning process and mathematically modeling the control strategies used by humans can potentially lead to methods that speed up the learning process. For example, a lot of training is required for humans to learn how to control complex dynamic systems such as cranes, aircraft, and automobiles. By studying the human learning process we may better understand which characteristics of those systems make learning more difficult. Using this knowledge, it may be possible to develop equipment and training methods to make the learning process faster and easier. Another example is patients with amputated limbs who use prosthetic limbs. Their brain must learn how to use this new "actuator". A better understanding of how the brain treats and controls other natural actuators could lead to improved prosthetic devices and training.

Modeling the control strategies used by humans can also make it easier to mimic human behavior which is of interest in a wide range of applications. Humans possess multiple advantages over current robotic systems. For example, humans are capable of adapting their control strategies based on characteristics of the dynamic system they are trying to control. Moreover, the human brain can form control structures
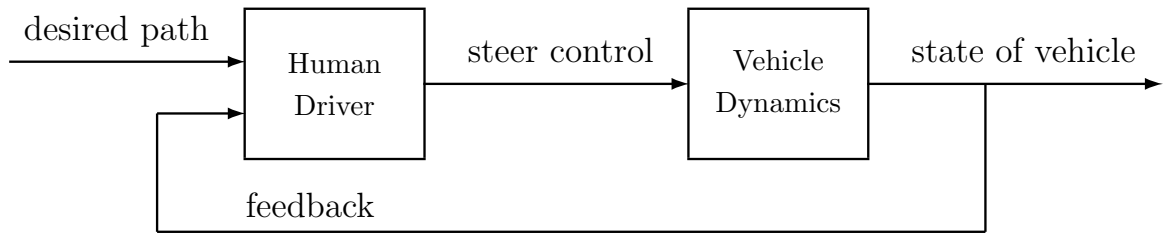
Figure 1.1: An HITL system where a human driver interacts with vehicle dynamics and manipulates the state of the vehicle on the road.

that are adaptive to uncertainties of the system without any prior knowledge of those uncertainties. The human brain is also able to learn from previous experiences and improve its performance. Since nowadays supercomputers that possess high computational power are more accessible, if we successfully mimic the functions used by the human brain then with the help of these supercomputers, we would be able to solve problems that seem to be unsolvable today.

1.2 Human-in-the-Loop Systems

Human-in-the-loop (HITL) systems are defined as systems where human interactions affect the output of the system. For example, an automobile driven by a human driver is a HITL system. As shown by the block diagram of the system in Fig. 1.1, the steer command implemented by the human driver passes through the dynamics of the vehicle and affects the state of the vehicle on the road. This steer command depends on many factors such as the general human driver skills and characteristics, the vehicle dynamics, the desired path, the current state of the vehicle, etc. Other examples of HITL systems include a human pilot flying an airplane, a human operator controlling a crane, or a gamer playing videos games.

Humans are often the least-understood component of a HITL system. There are many engineering principles and analysis techniques that can be used to predict and design the behavior of dynamic systems, such as aircraft, construction machinery, haptic devices, and telerobotic systems. Predicting how humans will interact with

those systems is more challenging. An improved understanding of human control strategies is likely to yield significant advancements in HITL technologies.

It has been suggested that when interacting with dynamic systems, the central nervous system constructs adaptive internal models of the system that it is trying to control [1–6]. This hypothesis, which is usually referred to as the Internal Model Hypothesis (IMH), has been extensively investigated using reaching experiments [7–11] and grip-force experiments [12,13]. For example, subjects in [8] are asked to grasp and move a robotic manipulator between 2 points in a horizontal plane; however, the robotic manipulator is actuated by velocity-dependent forces. These forces initially cause subjects' hand motions to deviate from a straight line. After practice, subjects adjust to the forces and are able to move the manipulator in a straight line. However, when the force is subsequently removed, the subjects deviate from the straight line in a manner that mirrors the initial deviations. These experiments are often interpreted with internal models; however, these results do not confirm the IMH [14].

The IMH has also been explored by comparing the results of human-in-the-loop experiments with mathematical models built on the IMH [15–26]. The internal models used by humans can be employed as part of the feedback or feedforward control [8, 22, 27–30]. Early work on modeling human control behavior was directed at modeling human pilot behaviour and designing aircraft control systems. [31] proposed the earliest model of human pilot behaviour, which was called the *tustin model*. This model, which was established using the servomechanism theory, was later shown to lack accuracy.

In [32–39], system identification methods and experimental data were used to obtain models of human control behavior. For example, [33] proposed the *cross-over model*, which was used to describe the open-loop behavior of a human pilot in compensatory tracking tasks. A series of experiments were conducted to validate the model under different flight conditions. This model demonstrated that humans adapt their control

strategy based on the dynamics of the controlled system. Using the cross-over model, [40] proposed the *precision model* which is the most-used describing function for human control dynamics in compensatory tasks. An extension of [33] is given in [38], which uses a model of human pilot control behavior that consists of feedback and feedforward controllers. Although [32–40] provide approximations of feedback and feedforward controllers, they are not capable of identifying the best-fit feedback and feedforward controllers. These models reproduce certain qualitative features observed in the experiments. However, different control strategies can yield similar dynamic behavior.

Command-following tasks are the focus of more recent studies [41–46]. The experimental results showed that human's control strategy considerably changes in a command-following task compared to the compensatory experiments. It has been proposed that in command-following tasks humans apply a feedforward control on the target signal and a feedback control on the error. In [47–50], frequency-domain Subsystem Identification (SSID) techniques are used in order to model the feedback and feedforward controllers humans use when interacting with linear dynamic systems. The identified controllers support the idea that the central nervous system constructs an approximate inverse model of the dynamic system in feedforward for many linear systems.

Multiple studies have investigated whether or not the central nervous system is able to form internal models of nonlinear systems. In [51–56], human subjects are asked to perform a tracking task where the joystick they control and the output they see on the screen have a static nonlinear relationship. In these experiments eliminating the visual feedback is used as a tool to find the relative extent of contribution for feedback and feedforward control. Based on the measured control signals applied by the subjects, it has been concluded that similar to the linear systems, humans are capable of constructing internal models of the systems with static nonlinearities. [57] provides

the results of an experiment in which participants control the position of a cursor on a computer display screen using a joystick and are instructed to follow target signals with Gaussian probability density functions. The participants perform linear and nonlinear tasks. For the linear task there is a proportional and one-to-one relationship between the position of the joystick and the position of the response cursor. For the nonlinear task this relationship follows a static nonlinear or non-proportional pattern. The results imply that participants form an internal representation of the static nonlinearity. These studies, however, do not explicitly identify the controllers used by the human subjects. Moreover, the nonlinear systems used in [51–57] are only static, and thus human control strategies for nonlinear systems having dynamics remains unclear. In this dissertation, we are interested to have an improved understanding of the command-following control strategies that humans use to interact with nonlinear systems. More specifically, we want to be able to explicitly identify the controllers humans learn to use when interacting with nonlinear systems that have dynamics.

Moreover, some studies have investigated the impact of changes in the reference command on the control strategies adopted by humans in a command-following task. The results in [58, 59] suggest that certain reference commands are more difficult for humans to follow than others. Moreover, these results suggest that as long as the reference command is predictable, adaptive feedforward inversion remains as their primary control strategy, even after the reference command has changed. However, to the best of our knowledge, so far no study has been conducted to investigate the possible impacts of relaxing the command-following control objectives on human control behavior in a pursuit tracking task. Many real-world human-machine interactions do not require a human operator to strictly follow a reference command, but rather a relaxed command-following is required. For example, the control objective of a human driver usually is not to keep the vehicle on an exact path trajectory along the road at all time, but rather to maintain the vehicle within the boundaries of a certain lane

on the road. Therefore, achieving a better understanding of human control behavior when performing a relaxed command-following task could have application to many real-world HITL technologies. In this dissertation, we want to know whether relaxing the control task objectives changes the control strategies utilized by humans.

1.3 Experimental Approach to Studying Human Learning

Multiple HITL experiments were conducted during this study to investigate impacts of output nonlinearities and relaxed control objectives on strategies used by humans in command-following tasks. Subjects use a rotational joystick to control the motion of an object that is displayed on a computer screen. The experimental setup is shown in Fig. 1.2. The computer monitor displays two rectangular markers, one above the other. The top rectangular marker is called the *reference object* and its horizontal position is denoted r. The bottom rectangular marker is called the *control object* and its horizontal position is denoted y. The reference object follows a predetermined path, which is the same for all subjects and all trials. Alternatively, the control object's position is dependent on the joystick's angular position, which is denoted by u. The control object's position y is related to the joystick input by a time-invariant differential equation, which is being numerically simulated by the computer shown in Fig. 1.2(a). The subjects are provided no information about how the joystick affects the motion of the control object. Subjects are instructed to use the joystick to make the control object mimic the motion of the reference object. The time signals r, y, and u are recorded for all subjects and all trials.

Figure 1.3 shows the closed-loop HITL system which consists of the human subject and the computer-simulated dynamic system. During the experiments the time signals r, y, and u are recorded. These signals provide an insight into the control behavior of human subjects. We model the feedback and feedforward control strategies
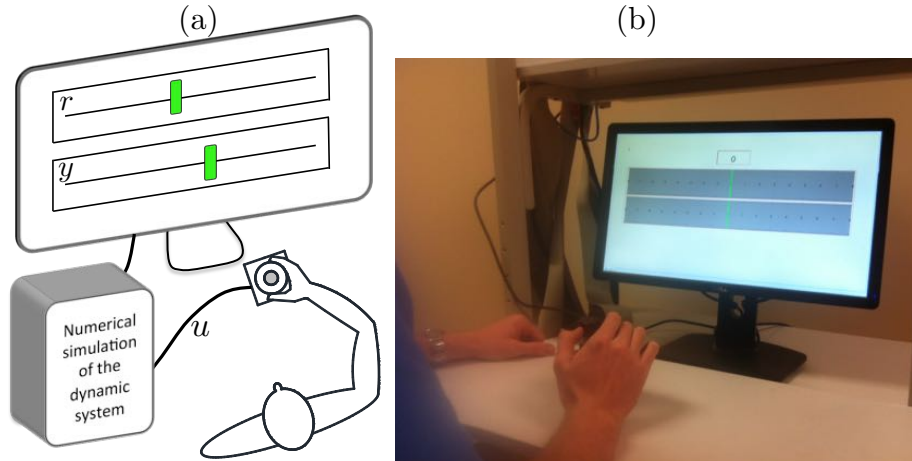
Figure 1.2: Subjects use a joystick to affect the motion of an object on a computer screen. The object's position y represents output of a dynamic system, which is simulated by a computer as shown in (a), and the joystick position u represents the input to the dynamic system. Figure (b) shows a subject performing the experiment.
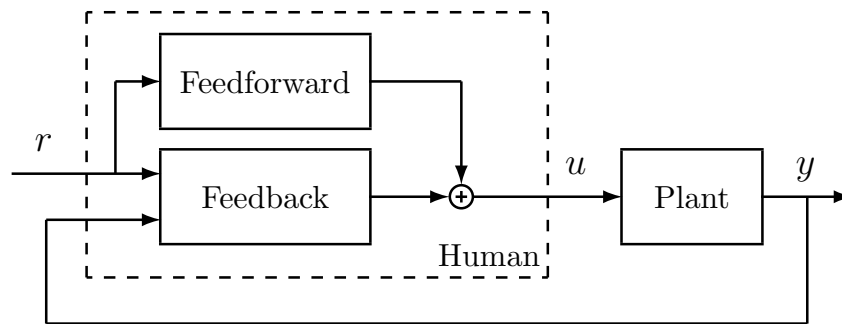
Figure 1.3: Human interacts with a dynamic system, receives external information r and feedback y from the dynamic system, and generates control u.

human subjects learn to use during the experiments using subsystem identification techniques. These subsystem identification techniques determine models that are best-fit to the experimental data.

1.4 Modeling Human Control Strategies Using Subsystem Identification

Subsystem identification (SSID) is a methodology that builds mathematical models of unknown subsystems from measured data. The closed-loop HITL system demonstrated in Fig. 1.3 depicts a scenario in which a human interacts with a dynamic

system by using feedback y and a command r to generate a control u that achieves a desired behavior. In this case, the human is the unknown subsystem. The human's control strategy can be modeled by a combination of feedback and feedforward controllers. Modeling the human's control strategy can be viewed as a SSID problem, where the signals r, u, and y are measured, the plant is known, and the feedback and feedforward controllers are the subsystems to be identified.

Methods for SSID are given in [60–70]. Specifically, [60–62] focus on open-loop SSID, while [63–65] present methods for closed-loop static SSID. Techniques for closed-loop dynamic SSID are given in [66–70]. In [50, 71], a SSID technique is presented that identifies the best-fit feedback and feedforward controller of each subject. This technique, however, model both the plant and the controller as linear systems.

This dissertation presents a new nonlinear time-domain and a linear frequency-domain SSID technique. These new nonlinear time-domain identification technique uses concepts from [71] and [72] and can accommodate nonlinearities in the plant and controller. Both identification techniques use a convexification approach that involves using a candidate pool to find the best-fit subsystem models. It can be shown that if the data noise is sufficiently small and the feedback candidate pool is sufficiently dense, then the identified control parameters are arbitrarily close to the true parameters.

1.5 Overview of Dissertation

Chapter 2. This chapter presents a frequency-domain and a new time-domain SSID algorithm to identify best-fit feedback and feedforward controllers of a closed-loop system where these controllers are connected to a known plant. These SSID algorithms use a candidate pool to search among all the candidate feedback controllers. Then, a convex optimization problem is solved to determine the best-fit feedforward controller. The frequency-domain algorithm is applicable to a closed-loop

8

system where the plant is linear while the time-domain algorithm is also applicable to a closed-loop system where the plant and/or the feedforward controller contain nonlinear components.

Chapter 3. This chapter presents results of an experiment where 22 human subjects each interact with a dynamic system 40 times over a one-week period. The subjects are divided into 2 groups of 11 subjects. The first group interacts with a LTI system, and the second group interacts with a Wiener system, which consists of the same LTI dynamics cascaded with a static output nonlinearity. Each subject's command-following behavior is modeled by a discrete-time control architecture consisting of a feedback time delay, a linear feedback controller, and a nonlinear feedforward controller. We compare the time-domain performance and control behavior of these two groups. By comparing the time-domain performance and control behavior of these two groups, we investigate the effects of output nonlinearity on control strategies used by human subjects. We also use a time-domain subsystem identification algorithm to model the control strategies (feedforward, feedback, and feedback time delay) that each subject uses on each trial. We use the identification results of this chapter's experiment to improve our understanding of the effects that system nonlinearities have on control strategies used by humans.

Chapter 4. This chapter presents results of an experiment where 22 human subjects each interact with a dynamic system 40 times over a one-week period. The subjects are divided into 2 groups of 11 subjects. Each group interacts with the same dynamic system and performs a command-following task; however, the groups have different control objectives. One group's control objective is to follow the reference command as closely as possible at all time. In contrast, the other group's control objective is to follow the reference command with some allowable error. We use the experimental results to examine the effects of a relaxed command-following control objective. We also use a frequency-domain subsystem identification algorithm to model

the control strategies (feedforward, feedback, and feedback time delay) that each subject uses on each trial. We use the identification results of this chapter's experiment to improve our understanding of the effects that changes in control objectives has on control strategies used by humans.

Chapter 2   Subsystem Identification Techniques

In this chapter, we present subsystem identification algorithms used for identifying each human subject's control strategy. These subsystem identification algorithms, performed in time domain and frequency domain, identify estimates of the feedback and feedforward controllers using the knowledge of dynamic system and recorded input and output data. They do not require knowledge of any internal signals and are applicable to a wide range of systems including LTI systems, LTI systems with static nonlinearities in the plant and controller, and systems with pre-filter in controller.

2.1   Introduction

Subsystem identification (SSID) refers to a process where the observed input and output data of a system are used to find best-fit models of unknown subsystems assuming they are interconnected with some known subsystems. As an example, consider the HITL system shown in Fig. 2.1, where a human interacts with a dynamic system and uses the input signal r (e.g., the reference command), and the feedback from the output signal y to manipulate the control signal u in a manner that the output signal y mimics the input signal r. In this example, the SSID process involves utilizing the measured input signal r and the measured output signal y to identify the unknown subsystems in the human control structure (e.g., feedback and feedforward controllers) assuming the dynamic system the human is interacting with is known but all the internal signals (e.g., the internal signals that construct the control signal u) are inaccessible.
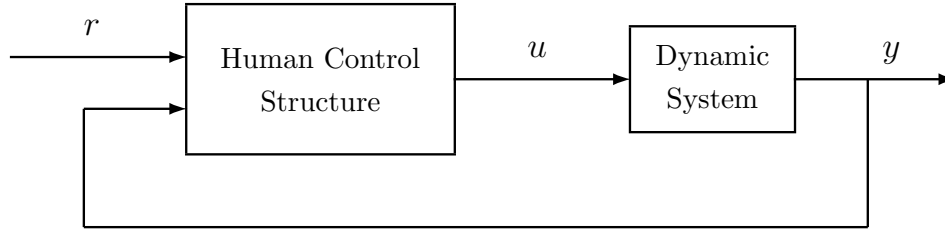
Figure 2.1: A HITL system where a human interacts with a dynamic system and uses the input signal r (e.g., the reference command) and the feedback from the output signal y to manipulate the control signal u in a manner that the output signal y mimics the input signal r.

Methods for SSID are given in [60–70]. Specifically, [60–62] focus on open-loop SSID, while [63–65] present methods for closed-loop static SSID. Techniques for closed-loop dynamic SSID are given in [66–70]. In [47–50, 71], a SSID technique is presented that identifies the best-fit feedback and feedforward controller of each subject. This technique, however, model both the plant and the controller as linear systems.

This chapter first presents a review of the frequency-domain SSID technique developed in [71]. Then, a new time-domain SSID technique is developed that uses concepts from [71] and [72] and can accommodate nonlinearities in the plant and controller. This SSID technique uses a convexification approach that involves using a candidate-pool to find the best-fit subsystem models. It can be shown that if the data noise is sufficiently small and the feedback candidate pool is sufficiently dense, then the identified control parameters are arbitrarily close to the true parameters.

2.2 Problem Statement

Consider the time-invariant system shown in Fig. 2.2, where $G : \mathbb{C} \to \mathbb{C}$ is a real rational transfer function, $h : \mathbb{R} \to \mathbb{R}$ is a continuous and one-to-one function, $r_k \in \mathbb{R}$ is the input, $u_k \in \mathbb{R}$ is the control, $v_k \in \mathbb{R}$ is the output of the linear dynamics, and $y_k \in \mathbb{R}$ is the output. Note that $k \in \{1, 2, \cdots, N_\mathrm{s}\}$ where N_s is the number of time response data. The controller consists of a feedback transfer function
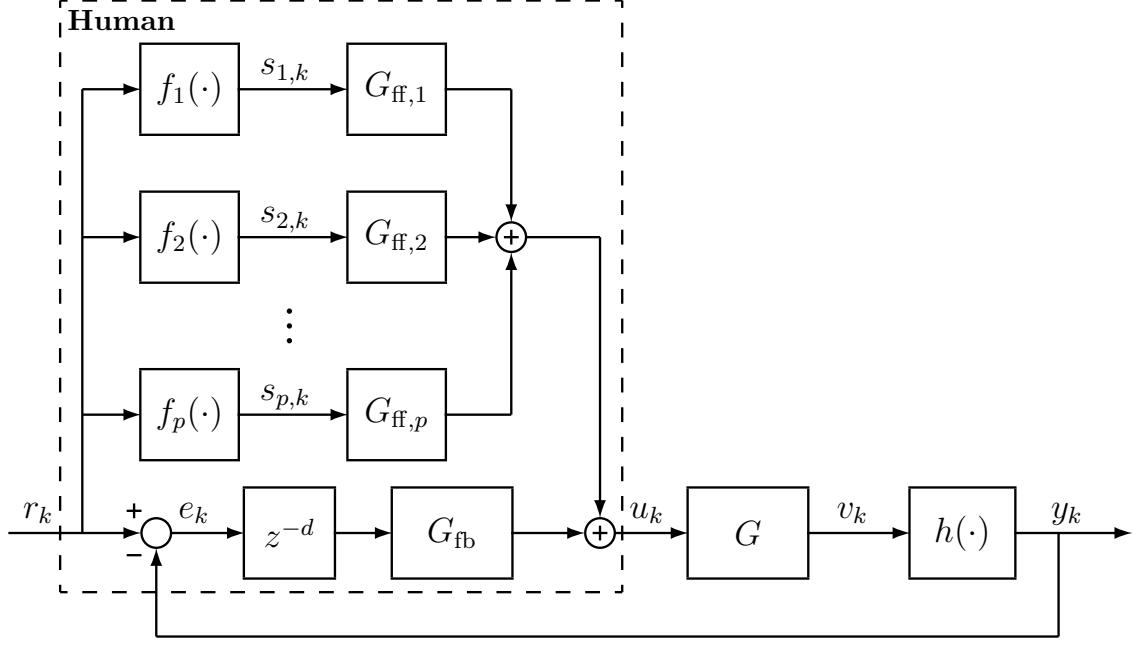
Figure 2.2: A time-invariant system, where the input r_k, the output y_k, and the signals v_k and u_k are accessible, but all internal signals are inaccessible.

$G_{\mathrm{fb}} : \mathbb{C} \to \mathbb{C}$; a feedback delay d, which is a nonnegative integer (the feedback time delay in seconds is dT_{s}, where T_{s} is the sampling time); feedforward transfer functions $G_{\mathrm{ff},1}, ..., G_{\mathrm{ff},p} : \mathbb{C} \to \mathbb{C}$; and basis functions $f_1, ..., f_p : \mathbb{R} \to \mathbb{R}$. The basis functions $f_1, ..., f_p$ allow for static-input nonlinearities in the feedforward controller.

The SSID problem is to estimate the feedback pair (d, G_{fb}) and feedforward transfer functions $(G_{\mathrm{ff},1}, ..., G_{\mathrm{ff},p})$ from knowledge of G and h, basis functions $f_1, ..., f_p$, and discrete-time signals r_k and v_k.

2.3 Notation

The following assumptions and notation are used for the rest of this section. Unless otherwise specified, all references to the subscript j are for all $j \in \{1, 2, ..., p\}$. Let $\mathbb{Z}^+$ denote the set of positive integers. Let $\| \cdot \|_2$ denote the two-norm on $\mathbb{F}^n$ and A^* denote the complex conjugate transpose of $A \in \mathbb{F}^{n \times m}$, where $\mathbb{F}$ is either $\mathbb{R}$ or $\mathbb{C}$. Let N and D be the coprime polynomials of degree n_y and d_y satisfying $G = ND^{-1}$. The

feedback transfer function G_{fb} has the factorization $G_{\mathrm{fb}} = N_{\mathrm{fb}} D_{\mathrm{fb}}^{-1}$, where N_{fb} and D_{fb} are polynomials of degree n_{fb} and d_{fb}, where $d_{\mathrm{fb}} \geq n_{\mathrm{fb}}$. The feedforward transfer function $G_{\mathrm{ff},j}$ is order n_{ff} finite impulse response (FIR), which implies that it can be expressed as $G_{\mathrm{ff},j} = N_{\mathrm{ff},j} z^{-n_{\mathrm{ff}}}$, where $N_{\mathrm{ff},j}$ is a polynomial of degree n_{ff}. The FIR assumption does not significantly restrict the range of feedforward behavior relative to an infinite impulse response (IIR) transfer function, since a sufficiently large order FIR transfer function can be used to approximate an IIR transfer function to arbitrary accuracy. Next, the discrete signals r_k, u_k, v_k, and y_k have N_{s} samples and sampling time T_{s}. Finally, the operator q denotes the forward shift operator (i.e., if x_k is a sequence, then $\mathrm{q} x_k = x_{k+1}$).

2.4 Frequency-domain Subsystem Identification

In this section, we present a SSID algorithm which is performed in the frequency domain and is applicable to linear time-invariant systems. The time-invariant system shown in Fig. 2.2 is linear if we assume h and f_1 are identity functions and $f_j = 0$ for $j = 2, 3, \cdots, p$. This implies that $y_k = v_k$, $s_{1,k} = r_k$, and for all $j \in \{2, 3, \ldots, p\}$, $s_{j,k} = 0$ for all $k \in \{1, 2, \cdots, N_{\mathrm{s}}\}$.

Let $\hat{y}(z)$ and $\hat{u}(z)$ denote the z-transforms of output y_k and control u_k, and it follows that

$$\hat{y}(z) = G(z)\hat{u}(z). \tag{2.1}$$

The control based on the architecture of Fig. 2.2 is

$$\hat{u}(z) = G_{\mathrm{fb}}(z) z^{-d} \hat{e}(z) + G_{\mathrm{ff},1}(z) \hat{r}(z), \tag{2.2}$$

where $\hat{e}(z)$ is the z-transform of $e_k = r_k - y_k$, and $\hat{r}(z)$ is the z-transforms of r_k.

Combining (2.1) and (2.2) yields

$$\hat{y}(z) = G(z)G_{\text{fb}}(z)z^{-d}\hat{e}(z) + G(z)G_{\text{ff},1}(z)\hat{r}(z). \tag{2.3}$$

Thus, the closed-loop transfer function from r_k to y_k can be defined as

$$\begin{aligned}
\tilde{G}_{yr}(z) &\triangleq \frac{G(z)[G_{\text{ff},1}(z) + G_{\text{fb}}(z)z^{-d}]}{1 + G(z)G_{\text{fb}}(z)z^{-d}} \\
&= \frac{N(z)D_{\text{fb}}(z)N_{\text{ff},1}(z)z^{-n_{\text{ff}}} + N(z)N_{\text{fb}}(z)z^{-d}}{D(z)D_{\text{fb}}(z) + N(z)N_{\text{fb}}(z)z^{-d}}.
\end{aligned} \tag{2.4}$$

Let $r_{\text{dft}}(\omega_k)$ and $y_{\text{dft}}(\omega_k)$ denote the discrete Fourier transforms of the sequences $\{r_k\}_{k=1}^{N_{\text{s}}}$ and $\{y_k\}_{k=1}^{N_{\text{s}}}$ at frequencies $\omega_k \in (0, \infty)$, where $k \in \{1, 2 \dots, N_{\text{f}}\}$ and $\omega_1 < \omega_2 < \cdots < \omega_{N_{\text{f}}}$. Let $\sigma_k \triangleq e^{j\omega_k T_{\text{s}}}$ and define the closed-loop frequency response data $H(\omega_k) \triangleq y_{\text{dft}}(\omega_k)/r_{\text{dft}}(\omega_k)$. We seek to find $G_{\text{ff},1}$, G_{fb}, and d such that $\{\tilde{G}_{yr}(\sigma_k)\}_{k=1}^{N_{\text{f}}}$, which is the closed-loop frequency response of the modeled control structure shown in Fig. 2.2, approximates $\{H(\omega_k)\}_{k=1}^{N_{\text{f}}}$, which is the closed-loop frequency response obtained from the input and output data. In other words, the SSID algorithm determines $G_{\text{ff},1}$, G_{fb}, and d that minimize the cost function

$$\begin{aligned}
J(d, G_{\text{fb}}, G_{\text{ff},1}) &\triangleq \frac{1}{2}\sum_{k=1}^{N_{\text{f}}}\left|\tilde{G}_{yr}(\sigma_k) - H(\omega_k)\right|^2 \\
&= \frac{1}{2}\sum_{k=1}^{N_{\text{f}}}\left|\frac{G(\sigma_k)\left[G_{\text{ff},1}(\sigma_k) + G_{\text{fb}}(\sigma_k)\sigma_k^{-d}\right]}{1 + G(\sigma_k)G_{\text{fb}}(\sigma_k)\sigma_k^{-d}} - H(\omega_k)\right|^2,
\end{aligned}$$

given the constraint that $\tilde{G}_{yr}$ is asymptotically stable. To identify $G_{\text{ff},1}$, G_{fb}, and d, we first generate a *candidate pool* that contains N_{c} possible models of the feedback pair (d, G_{fb}). The cost J is convex in the numerator coefficients of $G_{\text{ff},1}$. For each feedback pair (d, G_{fb}) in the candidate pool, a convex optimization is solved to determine the best-fit $G_{\text{ff},1}$ that minimizes $J(G_{\text{ff},1})$. This computation generates N_{c} models of $(d, G_{\text{fb}}, G_{\text{ff},1})$, from which we select the element that minimizes $J(d, G_{\text{fb}}, G_{\text{ff},1})$.

Subsection 2.4.1 provides a more detailed description of this SSID algorithm. Properties of this SSID algorithm are given in [71], which shows that if the data noise is sufficiently small and the feedback candidate pool is sufficiently dense, then the identified control parameters are arbitrarily close to the true parameters. Some numerical examples that demonstrate the application and effectiveness of this SSID method are given in Subsection 2.4.2.

2.4.1 SSID Algorithm

To formulate the SSID algorithm in terms of coefficients of the feedback and feedforward controllers, define the candidate polynomials

$$\mathcal{N}_{\text{fb}}(z, \theta) \triangleq [z^{n_{\text{fb}}} \quad z^{n_{\text{fb}}-1} \quad \cdots \quad 1 \quad 0_{1 \times d_{\text{fb}}}] \theta,$$

$$\mathcal{D}_{\text{fb}}(z, \theta) \triangleq z^{d_{\text{fb}}} + [0_{1 \times (n_{\text{fb}}+1)} \quad z^{d_{\text{fb}}-1} \quad \cdots \quad 1] \theta,$$

$$\mathcal{N}_{\text{ff},1}(z, \phi_1) \triangleq [z^{n_{\text{ff}}} \quad z^{n_{\text{ff}}-1} \quad \cdots \quad 1] \phi_1,$$

where $\theta \in \mathbb{R}^{n_{\text{fb}}+d_{\text{fb}}+1}$ contains the numerator and denominator coefficients of the candidate feedback transfer function $\mathcal{G}_{\text{fb}}(z, \theta)$, and $\phi_1 \in \mathbb{R}^{n_{\text{ff}}+1}$ contains the numerator coefficients of the candidate feedforward transfer function $\mathcal{G}_{\text{ff},1}(z, \phi_1)$. Hence, $\mathcal{G}_{\text{fb}}(z, \theta) \triangleq \mathcal{N}_{\text{fb}}(z, \theta) \mathcal{D}_{\text{fb}}^{-1}(z, \theta)$ and $\mathcal{G}_{\text{ff},1}(z, \phi_1) \triangleq \mathcal{N}_{\text{ff},1}(z, \phi_1) z^{-n_{\text{ff}}}$. Also, let the positive integer δ denote the candidate feedback delay.

Let $\theta_* \in \mathbb{R}^{n_{\text{fb}}+d_{\text{fb}}+1}$, $\phi_{1,*} \in \mathbb{R}^{n_{\text{ff}}+1}$, and $\delta_* \in \mathbb{Z}^+$ be such that, $N_{\text{fb}}(z) \equiv \mathcal{N}_{\text{fb}}(z, \theta_*)$, $D_{\text{fb}}(z) \equiv \mathcal{D}_{\text{fb}}(z, \theta_*)$, $N_{\text{ff},1}(z) \equiv \mathcal{N}_{\text{ff},1}(z, \phi_{1,*})$, and $d \equiv \delta_*$. Thus, $G_{\text{fb}}(z) \equiv \mathcal{G}_{\text{fb}}(z, \theta_*)$ and $G_{\text{ff},1}(z) \equiv \mathcal{G}_{\text{ff},1}(z, \phi_{1,*})$.

Next, let $\tilde{\mathcal{G}}_{yr}(z, \delta, \theta, \phi_1)$ be the closed-loop transfer function obtained using δ, θ, and ϕ_1. It follows from (2.4) that

$$\tilde{\mathcal{G}}_{yr}(z, \delta, \theta, \phi_1) = \frac{G(z) \left[\mathcal{G}_{\text{ff},1}(z, \phi_1) + \mathcal{G}_{\text{fb}}(z, \theta) z^{-\delta} \right]}{1 + G(z) \mathcal{G}_{\text{fb}}(z, \theta) z^{-\delta}}$$

$$= \frac{N(z)\mathcal{D}_{\text{fb}}(z,\theta)\mathcal{N}_{\text{ff},1}(z,\phi_1)z^{-n_{\text{ff}}} + N(z)\mathcal{N}_{\text{fb}}(z,\theta)z^{-\delta}}{D(z)\mathcal{D}_{\text{fb}}(z,\theta) + N(z)\mathcal{N}_{\text{fb}}(z,\theta)z^{-\delta}}.$$

Note that $\tilde{G}_{yr}(z) \equiv \tilde{\mathcal{G}}_{yr}(z,\delta_*,\theta_*,\phi_{1,*})$. Our objective is to determine δ, θ, and ϕ_1 such that δ approximates d, and $\mathcal{G}_{\text{fb}}$ and $\mathcal{G}_{\text{ff},1}$ approximate G_{fb} and $G_{\text{ff},1}$, respectively. In order to achieve this, consider the cost function

$$\mathcal{J}(\delta,\theta,\phi_1) \triangleq J(\delta,\mathcal{G}_{\text{fb}}(\sigma_k,\theta),\mathcal{G}_{\text{ff},1}(\sigma_k,\phi_1))$$
$$= \frac{1}{2}\sum_{k=1}^{N_{\text{f}}} \left|\tilde{\mathcal{G}}_{yr}(\sigma_k,\delta,\theta,\phi_1) - H(\omega_k)\right|^2, \tag{2.5}$$

and define

$$\tilde{\mathcal{N}}_1(z,\theta) \triangleq N(z)\mathcal{D}_{\text{fb}}(z,\theta)[1 \quad z^{-1} \quad \cdots \quad z^{-n_{\text{ff}}}], \tag{2.6}$$

$$\tilde{\mathcal{N}}_2(z,\delta,\theta) \triangleq N(z)\mathcal{N}_{\text{fb}}(z,\theta)z^{-\delta}, \tag{2.7}$$

$$\tilde{\mathcal{D}}(z,\delta,\theta) \triangleq D(z)\mathcal{D}_{\text{fb}}(z,\theta) + N(z)\mathcal{N}_{\text{fb}}(z,\theta)z^{-\delta}, \tag{2.8}$$

$$a_k(\delta,\theta) \triangleq \frac{\tilde{\mathcal{N}}_1(\sigma_k,\theta)}{\tilde{\mathcal{D}}(\sigma_k,\delta,\theta)}, \tag{2.9}$$

$$b_k(\delta,\theta) \triangleq H(\omega_k) - \frac{\tilde{\mathcal{N}}_2(\sigma_k,\delta,\theta)}{\tilde{\mathcal{D}}(\sigma_k,\delta,\theta)}. \tag{2.10}$$

It follows from (2.5)-(2.10) that

$$\mathcal{J}(\delta,\theta,\phi_1) = \frac{1}{2}\sum_{k=1}^{N_{\text{f}}} \left|a_k(\delta,\theta)\phi_1 - b_k(\delta,\theta)\right|^2.$$

Next, let $\mathcal{I}_{\text{c}} \triangleq \{1,...,N_{\text{c}}\}$, where N_{c} is a positive integer. For all $i \in \mathcal{I}_{\text{c}}$, define distinct candidate feedback pairs (δ_i,θ_i). Let $\Gamma \subset \mathcal{S}$ be a set with N_{c} elements where $\gamma_i \triangleq [\delta_i \quad \theta_i^{\text{T}}]^{\text{T}} \in \mathbb{R}^{n_{\text{fb}}+d_{\text{fb}}+2}$ are its elements and $\mathcal{S} \triangleq \{[\delta \quad \theta^{\text{T}}]^{\text{T}} \in \mathbb{Z}^+ \times \mathbb{R}^{n_{\text{fb}}+d_{\text{fb}}+1} \mid$ if $\lambda \in \mathbb{C}$ and $\tilde{\mathcal{D}}(z,\delta,\theta) = 0$, then $|\lambda| < 1\}$ which is the set of (δ,θ) such that $\tilde{\mathcal{D}}(z,\delta,\theta)$ is asymptotically stable. We call Γ the *candidate pool*. For each $\gamma_i \in \Gamma$, define the

quadratic cost function

$$\mathcal{J}_i(\phi_1) \triangleq \frac{1}{2} \|A_i \phi_1 - b_i\|_2^2, \tag{2.11}$$

where

$$A_i \triangleq [a_1^{\mathrm{T}}(\delta_i, \theta_i) \;\; a_2^{\mathrm{T}}(\delta_i, \theta_i) \;\; \cdots \;\; a_{N_{\mathrm{f}}}^{\mathrm{T}}(\delta_i, \theta_i)]^{\mathrm{T}},$$

$$b_i \triangleq [b_1(\delta_i, \theta_i) \;\; b_2(\delta_i, \theta_i) \;\; \cdots \;\; b_{N_{\mathrm{f}}}(\delta_i, \theta_i)]^{\mathrm{T}}.$$

For all $i \in \mathcal{I}_{\mathrm{c}}$, $\mathcal{J}_i$ is quadratic with respect to the unknown feedforward parameters ϕ_1. If N_{f} is sufficiently large, then it can be shown that $A_i^* A_i$ is positive definite. For each $i \in \mathcal{I}_{\mathrm{c}}$, define

$$\phi_{1,i} \triangleq \left(\Re\left(A_i^* A_i\right)\right)^{-1} \Re\left(A_i^* b_i\right),$$

which is the unique global minimizer of $\mathcal{J}_i$.

Let $\kappa \in \mathcal{I}_{\mathrm{c}}$ be the smallest integer such that $\mathcal{J}_\kappa = \min_{i \in \mathcal{I}_{\mathrm{c}}} \mathcal{J}_i$. The identified feedback time delay is $d^+ \triangleq \delta_\kappa$; the numerator and denominator polynomials of the identified feedback transfer function are $N_{\mathrm{fb}}^+(z) \triangleq \mathcal{N}_{\mathrm{fb}}(z, \theta_\kappa)$ and $D_{\mathrm{fb}}^+(z) \triangleq \mathcal{D}_{\mathrm{fb}}(z, \theta_\kappa)$; the numerator polynomial of the identified feedforward transfer function is $N_{\mathrm{ff},1}^+(z) \triangleq \mathcal{N}_{\mathrm{ff},1}(z, \phi_{1,\kappa})$; and the identified feedback and feedforward transfer functions are $G_{\mathrm{fb}}^+(z) \triangleq \mathcal{G}_{\mathrm{fb}}(z, \theta_\kappa)$ and $G_{\mathrm{ff},1}^+(z) \triangleq \mathcal{G}_{\mathrm{ff},1}(z, \phi_{1,\kappa})$.

This SSID algorithm is summarized by the following steps:

Step 1) Generate the candidate pool $\Gamma \subset \mathcal{S}$ and the sequence $\{\gamma_i\}_{i=1}^{N_{\mathrm{c}}}$.

Step 2) For each $i \in \mathcal{I}_{\mathrm{c}}$, calculate $\phi_{1,i} \triangleq \left(\Re\left(A_i^* A_i\right)\right)^{-1} \Re\left(A_i^* b_i\right)$ which is the unique global minimizer of $\mathcal{J}_i$.

Step 3) Find the smallest integer $\kappa \in \mathcal{I}_{\mathrm{c}}$ such that $\mathcal{J}_\kappa = \min_{i \in \mathcal{I}_{\mathrm{c}}} \mathcal{J}_i$.

Step 4) The identification results are $d^+ \triangleq \delta_\kappa$, $G_{\text{fb}}^+(z) \triangleq \mathcal{G}_{\text{fb}}(z, \theta_\kappa)$, and $G_{\text{ff},1}^+(z) \triangleq \mathcal{G}_{\text{ff},1}(z, \phi_{1,\kappa})$.

2.4.2 Numerical Examples

We present two numerical examples using the SSID technique described in this chapter. For both examples, the plant components are $G(z) = 1/(z + 0.2)$ and h and f_1 are identity functions and $f_j = 0$ for $j = 2, 3, \cdots, p$. We numerically simulate the closed-loop system shown in Fig. 2.2 for a given feedback system (d, G_{fb}) and feedforward transfer function G_{ff} where all initial conditions are zero. The numerical simulations yield data signals r_k and y_k, which are used to compute best-fit models (d^+, G_{fb}^+) and G_{ff}^+.

Example 1. Consider $d = 8$, $G_{\text{fb}}(z) = 0.43/(z - 0.31)$, and $G_{\text{ff}}(z) = (3z - 6)/z$. Let $n_{\text{ff}} = 1$ and define the candidate pools

$$
\begin{aligned}
\Gamma_1 &\triangleq \{\gamma \in \mathbb{R}^3 : e_1\gamma, e_2\gamma \in \{-1 + 0.25\tau\}_{\tau=0}^8, \\
&\qquad e_3\gamma \in \{4 + \tau\}_{\tau=0}^{21}\}, \\
\Gamma_2 &\triangleq \{\gamma \in \mathbb{R}^3 : e_1\gamma, e_2\gamma \in \{-1 + 0.125\tau\}_{\tau=0}^{16}, \\
&\qquad e_3\gamma \in \{4 + \tau\}_{\tau=0}^{21}\}, \\
\Gamma_3 &\triangleq \{\gamma \in \mathbb{R}^3 : e_1\gamma, e_2\gamma \in \{-1 + 0.0625\tau\}_{\tau=0}^{32}, \\
&\qquad e_3\gamma \in \{4 + \tau\}_{\tau=0}^{21}\}.
\end{aligned}
$$

where $e_1 \triangleq [1 \ 0 \ 0]$, $e_2 \triangleq [0 \ 1 \ 0]$, and $e_3 \triangleq [0 \ 0 \ 1]$. The candidate pools define candidate pairs (d, G_{fb}). All 3 candidate pools have the same boundaries, but Γ_3 has more elements than Γ_2, and Γ_2 has more elements than Γ_1. Note that G_{fb} is not a member of the candidate pools, and thus the identification cannot yield the exact controller components. This example demonstrates how increasing the density of the candidate pool yields more accurate identifications.

For each of the 3 candidate pools, the SSID algorithm in Subsection 2.4.1 is used to obtain d^+, G_{fb}^+, and G_{ff}^+.

For Γ_1, the SSID yields $d^+ = 8$, $G_{\text{fb}}^+ = 0.5/(z - 0.25)$, and $G_{\text{ff}}^+ = (3.53z - 6.63)/z$.

For Γ_2, the SSID yields $d^+ = 8$, $G_{\text{fb}}^+ = 0.375/(z - 0.375)$, and $G_{\text{ff}}^+ = (2.82z - 5.79)/z$.

For Γ_3, the SSID yields $d^+ = 8$, $G_{\text{fb}}^+ = 0.4375/(z - 0.3125)$, and $G_{\text{ff}}^+ = (3.08z - 6.14)/z$.

Example 2. Consider the same parameters of the previous example, except $G_{\text{ff}}(z) = 2/(5z + 2)$ and $n_{\text{ff}} = 2$. Thus, G_{ff} is IIR, and we approximate it by a second-order FIR.

For Γ_1, the SSID yields $d^+ = 8$, $G_{\text{fb}}^+ = 0.5/(z - 0.25)$, and $G_{\text{ff}}^+ = (0.35z^2 - 0.11z + 0.21)/z^2$.

For Γ_2, the SSID yields $d^+ = 8$, $G_{\text{fb}}^+ = 0.375/(z - 0.375)$, and $G_{\text{ff}}^+ = (-0.21z^2 + 0.72z - 0.24)/z^2$.

For Γ_3, the SSID yields $d^+ = 8$, $G_{\text{fb}}^+ = 0.4375/(z - 0.3125)$, and $G_{\text{ff}}^+ = (0.02z^2 + 0.24z - 0.12)/z^2$.

Figure 2.3 shows the Bode plots of the identified transfer functions for each of the 3 candidate pools. The Bode plots of G_{fb}^+ and G_{ff}^+ are closest to G_{fb} and G_{ff} for the candidate pool Γ_3, which is denser than Γ_1 and Γ_2.

2.5 Time-domain Subsystem Identification

The frequency-domain SSID algorithm described in Section 2.4 is not applicable to the feedback structure of Fig. 2.2 if plant and/or controller nonlinearities are present. To address the nonlinear aspects of this SSID problem, we introduce a new approach that is performed in time domain and uses concepts from [71] and [72]. Specifically, [72] uses a feedforward architecture similar to Fig. 2.2 for Hammerstein-model identification, and [71] introduces a convexification approach that involves gridding on the parameters of the feedback pair (d, G_{fb}).
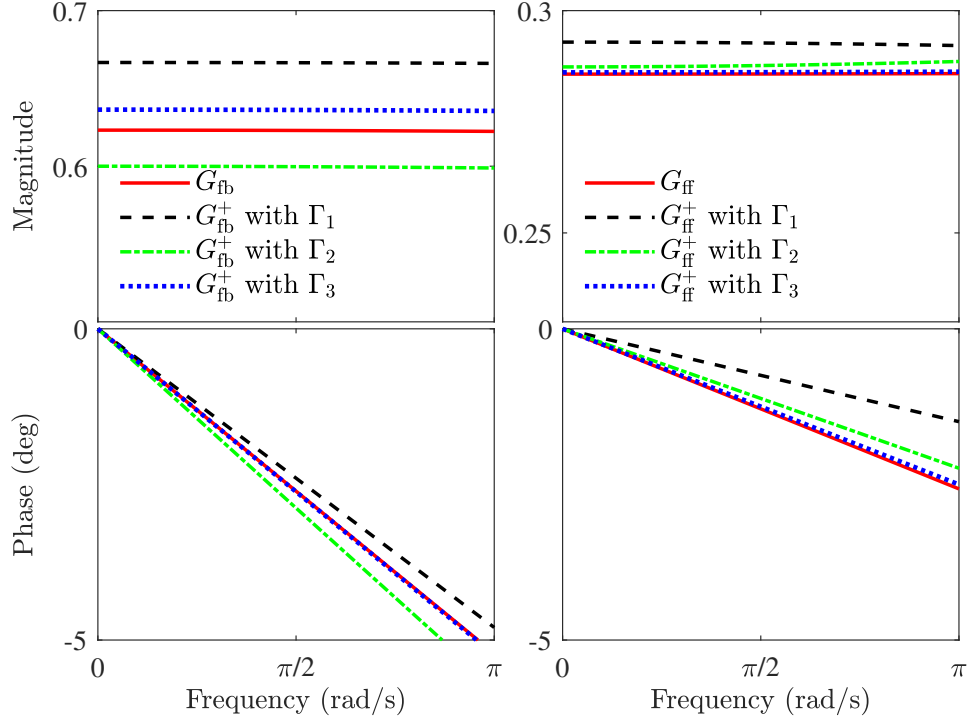
Figure 2.3: The Bode plots of the identified transfer functions G_{fb}^+ and G_{ff}^+ for the densest candidate pool Γ_3 results in the best estimates of G_{fb} and G_{ff}.

Let $\hat{v}(z)$ and $\hat{u}(z)$ denote the z-transforms of v_k and u_k, and it follows that

$$\hat{v}(z) = G(z)\hat{u}(z). \tag{2.12}$$

The control based on the architecture of Fig. 2.2 is

$$\hat{u}(z) = G_{\text{fb}}(z)z^{-d}\hat{e}(z) + \sum_{j=1}^{p} G_{\text{ff},j}(z)\hat{s}_j(z), \tag{2.13}$$

where $\hat{e}(z)$ is the z-transform of $e_k = r_k - h(v_k)$, and $\hat{s}_j(z)$ is the z-transforms of $f_j(r_k)$. Combining (2.12) and (2.13) yields

$$\hat{v}(z) = G(z)G_{\text{fb}}(z)z^{-d}\hat{e}(z) + G(z)\sum_{j=1}^{p} G_{\text{ff},j}(z)\hat{s}_j(z). \tag{2.14}$$

Substituting the polynomials N, D, N_{fb}, D_{fb}, and $N_{\text{ff},j}$ into (2.14) and multiplying

21

through by $DD_{\text{fb}}z^{d+n_{\text{ff}}}$ yields

$$D(z)D_{\text{fb}}(z)z^{d+n_{\text{ff}}}\hat{v}(z) = N(z)N_{\text{fb}}(z)z^{n_{\text{ff}}}\hat{e}(z) + N(z)D_{\text{fb}}(z)z^d \sum_{j=1}^{p} N_{\text{ff},j}(z)\hat{s}_j(z). \quad (2.15)$$

We seek feedback and feedforward parameters that make the left and right side of (2.15) approximately equal. Specifically, we seek $N_{\text{ff},1}, ..., N_{\text{ff},p}$, N_{fb}, D_{fb}, and d that minimize the cost function

$$J(d, N_{\text{fb}}, D_{\text{fb}}, N_{\text{ff},1}, ..., N_{\text{ff},p}) \triangleq \frac{1}{2} \sum_{k=1-\ell_d}^{N_{\text{s}}-\ell_d} \bigg| N(\text{q})D_{\text{fb}}(\text{q})\text{q}^d \sum_{j=1}^{p} N_{\text{ff},j}(\text{q})f_j(r_k) +$$
$$N(\text{q})N_{\text{fb}}(\text{q})\text{q}^{n_{\text{ff}}}e_k - D(\text{q})D_{\text{fb}}(\text{q})\text{q}^{d+n_{\text{ff}}}v_k \bigg|^2,$$

where $\ell_d \triangleq d + n_{\text{ff}} + d_y + d_{\text{fb}}$. To identify $N_{\text{ff},j}$, N_{fb}, D_{fb}, and d, we first generate a *candidate pool* that contains N_{c} possible models of the feedback pair (d, G_{fb}). The cost J is convex in the coefficients of $N_{\text{ff},j}$. For each feedback pair (d, G_{fb}) in the candidate pool, a convex optimization is solved to determine the best-fit $N_{\text{ff},j}$ that minimizes $J(N_{\text{ff},j})$. This computation generates N_{c} models of $(d, N_{\text{fb}}, D_{\text{fb}}, N_{\text{ff},j})$, from which we select the element that minimizes $J(d, N_{\text{fb}}, D_{\text{fb}}, N_{\text{ff},j})$. A detailed description of this SSID algorithm is given in Subsection 2.5.1. Properties of this SSID algorithm can be derived using analyses similar to those given in [71], which shows that if the data noise is sufficiently small and the feedback candidate pool is sufficiently dense, then the identified control parameters are arbitrarily close to the true parameters. Subsection 2.5.2 provides numerical examples that demonstrate the application and effectiveness of this SSID method.

2.5.1 SSID Algorithm

To formulate the SSID algorithm in terms of coefficients of the feedback and feed-forward controllers, define the candidate polynomials

$$\mathcal{N}_{\text{fb}}(\text{q}, \theta) \triangleq [\text{q}^{n_{\text{fb}}} \quad \text{q}^{n_{\text{fb}}-1} \quad \cdots \quad 1 \quad 0_{1 \times d_{\text{fb}}}]\theta,$$

$$\mathcal{D}_{\text{fb}}(\text{q}, \theta) \triangleq \text{q}^{d_{\text{fb}}} + [0_{1 \times (n_{\text{fb}}+1)} \quad \text{q}^{d_{\text{fb}}-1} \quad \cdots \quad 1]\theta,$$

$$\mathcal{N}_{\text{ff},j}(\text{q}, \phi_j) \triangleq [\text{q}^{n_{\text{ff}}} \quad \text{q}^{n_{\text{ff}}-1} \quad \cdots \quad 1]\phi_j,$$

where $\theta \in \mathbb{R}^{n_{\text{fb}}+d_{\text{fb}}+1}$ contains the numerator and denominator coefficients of feedback transfer function, and $\phi_j \in \mathbb{R}^{n_{\text{ff}}+1}$ contains the numerator coefficients of the feedforward transfer function. Next, consider the cost function

$$\mathcal{J}(\delta, \theta, \phi) \triangleq J(\delta, \mathcal{N}_{\text{fb}}(\text{q}, \theta), \mathcal{D}_{\text{fb}}(\text{q}, \theta), \mathcal{N}_{\text{ff},j}(\text{q}, \phi_j)) = \frac{1}{2} \sum_{k=1-\ell_\delta}^{N_{\text{s}}-\ell_\delta} |a_k(\delta, \theta)\phi - b_k(\delta, \theta)|^2,$$

where the positive integer δ is the feedback delay, $\ell_\delta \triangleq \delta + n_{\text{ff}} + d_y + d_{\text{fb}}$, $\phi \triangleq [\phi_1^{\text{T}} \quad \cdots \quad \phi_p^{\text{T}}]^{\text{T}} \in \mathbb{R}^{p(n_{\text{ff}}+1)}$, and for all $k \in \{1 - \ell_\delta, ..., N_{\text{s}} - \ell_\delta\}$,

$$a_k(\delta, \theta) \triangleq N(\text{q})\mathcal{D}_{\text{fb}}(\text{q}, \theta)\text{q}^\delta[\text{q}^{n_{\text{ff}}} \quad \text{q}^{n_{\text{ff}}-1} \quad \cdots \quad 1] \otimes [f_1(r_k) \quad \cdots \quad f_p(r_k)] \in \mathbb{R}^{1 \times p(n_{\text{ff}}+1)},$$

$$b_k(\delta, \theta) \triangleq D(\text{q})\mathcal{D}_{\text{fb}}(\text{q}, \theta)\text{q}^{\delta+n_{\text{ff}}}v_k - N(\text{q})\mathcal{N}_{\text{fb}}(\text{q}, \theta)\text{q}^{n_{\text{ff}}}e_k \in \mathbb{R},$$

where $\otimes$ denotes the Kronecker product.

Next, let $\mathcal{I}_{\text{c}} \triangleq \{1, ..., N_{\text{c}}\}$, where N_{c} is a positive integer. For all $i \in \mathcal{I}_{\text{c}}$, define distinct candidate feedback pairs (δ_i, θ_i). Let Γ be a set with N_{c} elements where $\gamma_i \triangleq [\delta_i \quad \theta_i^{\text{T}}]^{\text{T}} \in \mathbb{R}^{n_{\text{fb}}+d_{\text{fb}}+2}$ are its elements. We call Γ the *candidate pool*. For each $\gamma_i \in \Gamma$, define the quadratic cost function

$$\mathcal{J}_i(\phi) \triangleq \frac{1}{2} \|A_i\phi - b_i\|_2^2,$$

where

$$A_i \triangleq [a_{1-\ell_{\delta_i}}^{\mathrm{T}}(\delta_i, \theta_i) \ \ a_{2-\ell_{\delta_i}}^{\mathrm{T}}(\delta_i, \theta_i) \ \ \cdots \ \ a_{N_{\mathrm{s}}-\ell_{\delta_i}}^{\mathrm{T}}(\delta_i, \theta_i)]^{\mathrm{T}} \in \mathbb{R}^{N_{\mathrm{s}} \times p(n_{\mathrm{ff}}+1)},$$

$$b_i \triangleq [b_{1-\ell_{\delta_i}}(\delta_i, \theta_i) \ \ b_{2-\ell_{\delta_i}}(\delta_i, \theta_i) \ \ \cdots \ \ b_{N_{\mathrm{s}}-\ell_{\delta_i}}(\delta_i, \theta_i)]^{\mathrm{T}} \in \mathbb{R}^{N_{\mathrm{s}}}.$$

For all $i \in \mathcal{I}_{\mathrm{c}}$, $\mathcal{J}_i$ is quadratic with respect to the unknown feedforward parameters ϕ. If the number of samples N_{s} is sufficiently large, then it can be shown that $A_i^{\mathrm{T}} A_i$ is positive definite. For each $i \in \mathcal{I}_{\mathrm{c}}$, define

$$\phi_i \triangleq \left(A_i^{\mathrm{T}} A_i\right)^{-1} A_i^{\mathrm{T}} b_i,$$

which is the unique global minimizer of $\mathcal{J}_i$.

Let $\kappa \in \mathcal{I}_{\mathrm{c}}$ be the smallest integer such that $\mathcal{J}_\kappa = \min_{i \in \mathcal{I}_{\mathrm{c}}} \mathcal{J}_i$. The identified feedback time delay is $d^+ \triangleq \delta_\kappa$; the numerator and denominator polynomials of the identified feedback transfer function are $N_{\mathrm{fb}}^+(z) \triangleq \mathcal{N}_{\mathrm{fb}}(z, \theta_\kappa)$ and $D_{\mathrm{fb}}^+(z) \triangleq \mathcal{D}_{\mathrm{fb}}(z, \theta_\kappa)$; and the identified feedforward transfer functions are $G_{\mathrm{ff},j}^+(z) \triangleq z^{-n_{\mathrm{ff}}} \mathcal{N}_{\mathrm{ff},j}(z, \phi_{j,\kappa})$.

This SSID algorithm is summarized by the following steps:

Step 1) Generate the candidate pool $\Gamma \subset \mathcal{S}$ and the sequence $\{\gamma_i\}_{i=1}^{N_{\mathrm{c}}}$.

Step 2) For each $i \in \mathcal{I}_{\mathrm{c}}$, calculate $\phi_i \triangleq \left(A_i^{\mathrm{T}} A_i\right)^{-1} A_i^{\mathrm{T}} b_i$ which is the unique global minimizer of $\mathcal{J}_i$.

Step 3) Find the smallest integer $\kappa \in \mathcal{I}_{\mathrm{c}}$ such that $\mathcal{J}_\kappa = \min_{i \in \mathcal{I}_{\mathrm{c}}} \mathcal{J}_i$.

Step 4) The identification results are $d^+ \triangleq \delta_\kappa$, $N_{\mathrm{fb}}^+(z) \triangleq \mathcal{N}_{\mathrm{fb}}(z, \theta_\kappa)$, $D_{\mathrm{fb}}^+(z) \triangleq \mathcal{D}_{\mathrm{fb}}(z, \theta_\kappa)$, and $G_{\mathrm{ff},j}^+(z) \triangleq z^{-n_{\mathrm{ff}}} \mathcal{N}_{\mathrm{ff},j}(z, \phi_{j,\kappa})$.

2.5.2 Numerical Examples

We present two numerical examples using the SSID technique described in this chapter. For both examples, the plant components are $G(z) = 1/(z + 0.2)$ and

$h^{-1}(x) = x - 0.4x^2 + 0.2x^3$. We numerically simulate the closed-loop system shown in Fig. 2.2 for a given feedback system (d, G_{fb}) and feedforward system (f, G_{ff}) where all initial conditions are zero. The numerical simulations yield data signals r_k and v_k, which are used to compute best-fit models (d^+, G_{fb}^+) and (f^+, G_{ff}^+).

Example 3. Consider $d = 8$, $G_{\text{fb}}(z) = 0.43/(z - 0.31)$, $G_{\text{ff}}(z) = (3z - 6)/z$, and assume that $f(x) = -0.5x^3 + 0.1x^2$. Let $\alpha \in \mathbb{R}^4$ be a vector such that its elements are the coefficients of the polynomial function f. In this case, we have $\alpha = [-0.5 \ .1 \ 0 \ 0]^{\text{T}}$. Let $n_{\text{ff}} = 1$ and define the candidate pools

$$\Gamma_1 \triangleq \{\gamma \in \mathbb{R}^3 : e_1\gamma, e_2\gamma \in \{-1 + 0.25\tau\}_{\tau=0}^8,$$

$$e_3\gamma \in \{4 + \tau\}_{\tau=0}^{21}\},$$

$$\Gamma_2 \triangleq \{\gamma \in \mathbb{R}^3 : e_1\gamma, e_2\gamma \in \{-1 + 0.125\tau\}_{\tau=0}^{16},$$

$$e_3\gamma \in \{4 + \tau\}_{\tau=0}^{21}\},$$

$$\Gamma_3 \triangleq \{\gamma \in \mathbb{R}^3 : e_1\gamma, e_2\gamma \in \{-1 + 0.0625\tau\}_{\tau=0}^{32},$$

$$e_3\gamma \in \{4 + \tau\}_{\tau=0}^{21}\}.$$

where $e_1 \triangleq [1 \ 0 \ 0]$, $e_2 \triangleq [0 \ 1 \ 0]$, and $e_3 \triangleq [0 \ 0 \ 1]$. The candidate pools define candidate pairs (d, G_{fb}). All 3 candidate pools have the same boundaries, but Γ_3 has more elements than Γ_2, and Γ_2 has more elements than Γ_1. Note that G_{fb} is not a member of the candidate pools, and thus the identification cannot yield the exact controller components. This example demonstrates how increasing the density of the candidate pool yields more accurate identifications.

For each of the 3 candidate pools, the SSID algorithm in Subsection 2.5.1 is used to obtain d^+, G_{fb}^+, G_{ff}^+, and α^+.

For Γ_1, the SSID yields $d^+ = 8$, $G_{\text{fb}}^+ = 0.5/(z - 0.25)$, $G_{\text{ff}}^+ = (3.62z - 6.73)/z$, and $\alpha^+ = [-0.49527 \ 0.09407 \ 0.00195 \ 0.00016]^{\text{T}}$.

For Γ_2, the SSID yields $d^+ = 8$, $G_{\text{fb}}^+ = 0.375/(z - 0.375)$, $G_{\text{ff}}^+ = (2.78z - 5.71)/z$,

and $\alpha^+ = [-0.50342 \quad 0.10411 \quad -0.00102 \quad -0.00023]^{\mathrm{T}}$.

For Γ_3, the SSID yields $d^+ = 8$, $G_{\mathrm{fb}}^+ = 0.4375/(z - 0.3125)$, $G_{\mathrm{ff}}^+ = (3.25z - 6.28)/z$, and $\alpha^+ = [-0.49891 \quad 0.09855 \quad 0.00065 \quad -0.00002]^{\mathrm{T}}$.

Example 4. Consider the same parameters of the previous example, except $G_{\mathrm{ff}}(z) = 2/(5z + 2)$ and $n_{\mathrm{ff}} = 2$. Thus, G_{ff} is IIR, and we approximate it by a second-order FIR.

For Γ_1, the SSID yields $d^+ = 8$, $G_{\mathrm{fb}}^+ = 0.5/(z - 0.25)$, $G_{\mathrm{ff}}^+ = (0.30z^2 - 0.20z + 0.16)/z^2$, and $\alpha^+ = [-0.54127, 0.10708, -0.00066, 0.00026]^{\mathrm{T}}$.

For Γ_2, the SSID yields $d^+ = 8$, $G_{\mathrm{fb}}^+ = 0.375/(z - 0.375)$, $G_{\mathrm{ff}}^+ = (-0.26z^2 + 0.89z - 0.33)/z^2$, and $\alpha^+ = [-0.48117, 0.09672, 0.00056, -0.00016]^{\mathrm{T}}$.

For Γ_3, the SSID yields $d^+ = 8$, $G_{\mathrm{fb}}^+ = 0.4375/(z - 0.3125)$, $G_{\mathrm{ff}}^+ = (0.04z^2 + 0.31z - 0.07)/z^2$, and $\alpha^+ = [-0.51228, 0.10208, -0.00003, 0.00005]^{\mathrm{T}}$.

Figure 2.4 shows the Bode plots of the identified transfer functions for each of the 3 candidate pools. The Bode plots of G_{fb}^+ and G_{ff}^+ are closest to G_{fb} and G_{ff} for the candidate pool Γ_3, which is denser than Γ_1 and Γ_2.
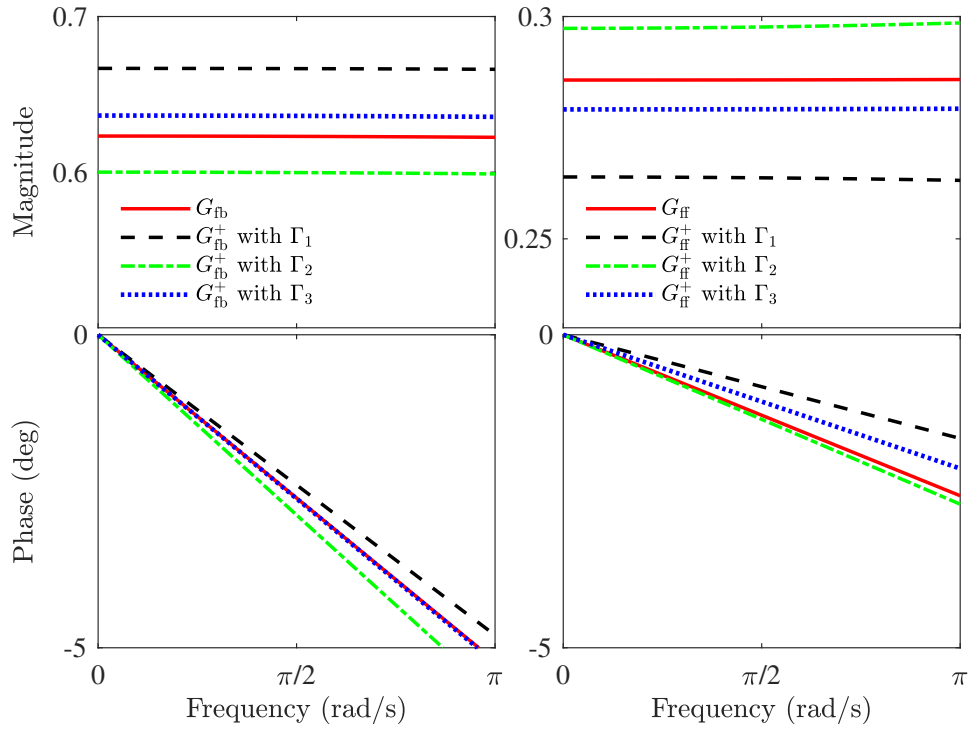
Figure 2.4: The Bode plots of the identified transfer functions G_{fb}^+ and G_{ff}^+ for the densest candidate pool Γ_3 results in the best estimates of G_{fb} and G_{ff}.

Chapter 3   The Impact of Output Nonlinearities on Human Control Strategies

In this chapter, we present the results of a human-in-the-loop experiment which is designed to investigate the control strategies that humans use to interact with nonlinear dynamic systems. Two groups of human subjects interact with a dynamic system and perform a command-following task. One group interacts with a linear time-invariant (LTI) dynamic system, while the other group interacts with a Wiener system, which consists of the same LTI dynamics cascaded with a static output nonlinearity. The time-domain subsystem identification algorithm presented in Chapter 2 is used to identify the feedback and feedforward control strategies that subjects in each group employ. Prior studies suggest that adaptive feedforward inversion is the primary control strategy used by humans for command-following tasks when interacting with linear dynamic systems. Using the identification results of this chapter's experiment, we address the open question of whether a similar control strategy is used for nonlinear systems.

3.1   Introduction

Humans are often the least-understood component of a human-in-the-loop (HITL) system. There are many engineering principles and analysis techniques that can be used to predict and design the behavior of dynamic systems, such as aircraft, construction machinery, haptic devices, and telerobotic systems. Predicting how humans will interact with those systems is more challenging. An improved understanding of
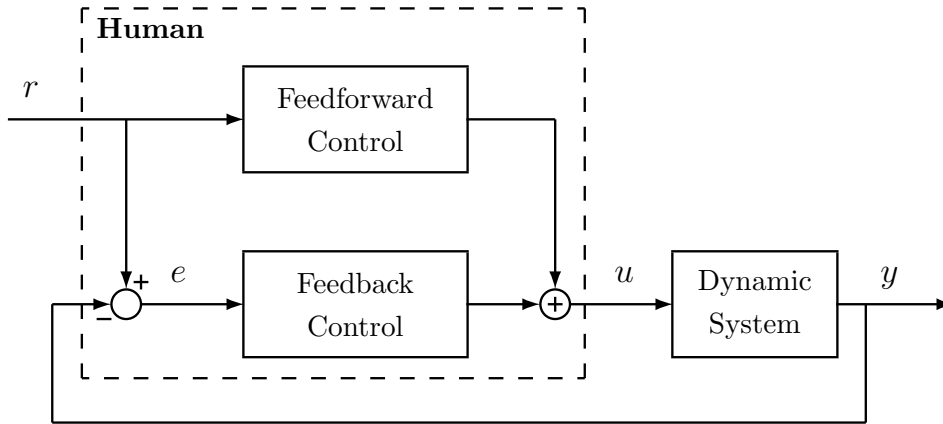
Figure 3.1: A control architecture for HITL systems.

human control strategies is likely to yield significant advancements in HITL technologies.

Many HITL systems can be modeled using the control architecture shown in Fig. 3.1. The human interacts with a dynamic system through the control input u, which is generated based on available feedback y and a command signal r. The human's goal is to interact with the dynamic system in a manner that makes the magnitude of the command-following error $e = r - y$ small.

A human's control response is complex and depends on the properties of the dynamic system and command, as well as many other factors, such as experience, effort, and ability. Although no model captures all aspects of human-control behavior, it is often possible to identify control strategies that approximate typical human behavior over a limited period of time [37, 73, 74]. Such models can be used to predict closed-loop behavior of HITL systems.

The review paper [75] provides an account of research on modeling human-control behavior. Much of the early human-control literature is based on studies of compensatory behavior, where the human only has access to the error e for feedback instead of both r and y [32, 33, 76]. The well-known *crossover model* and *precision model* provide fundamental principles that can be used to predict human compensatory behavior [40, 77, 78]. Alternatively, as discussed in [75], there is significantly less work

on HITL models for command-following.

It has long been suggested that humans may rely on models for control. The *internal model hypothesis* of neuroscience suggests that the brain constructs models (i.e., internal models) of the dynamic systems with which it interacts, and uses those models to generate control signals [2–6, 42, 79]. Forward and inverse internal models have been proposed [1, 8, 27–30, 43, 80–83]. Support for the internal model includes evidence of predictive behavior and qualitative comparisons with models [9, 12, 22, 84–92].

More direct evidence of model-based control strategies by humans is provided in [49], which analyzes command-following interactions with linear time invariant (LTI) dynamic systems. In those studies, the human control response is modeled by the feedback-feedforward control architecture shown in Fig. 3.1. The feedback control is based on e and models the human's reactive control response; the feedforward control is based only on r and models the human's anticipatory control response. Subsystem identification (SSID) techniques are used to determine best-fit linear models of the feedback and feedforward models. The results in [49] suggest that a primary command-following strategy used by humans is adaptive *feedforward inversion*. Specifically, if the LTI system is represented by the transfer function G, then over repeated interactions the human updates its feedforward controller until it approximates G^{-1}. SSID results suggest that feedforward inversion is used for many LTI systems, provided that the command is predictable or a preview of the command is available [93, 94].

The extent to which humans use adaptive feedforward inversion for control is unknown. Recent results suggest that for some nonminimum-phase LTI systems, the human's feedforward controller does not converge to an approximation of the dynamic system's inverse, but rather a different type of model-based control strategy is used [48]. Thus, it is unclear whether feedforward plant inversion is a primary

human-control strategy, even for LTI systems. Human interactions with nonlinear dynamic systems is also an open question. Some studies have investigated HITL interactions with static nonlinear systems and provide some evidence for feedforward inversion [51–57]. However, they do not explicitly identify the controllers used by the human subjects. Moreover, the nonlinear systems used in [51–57] are only static, and thus human control strategies for nonlinear systems having dynamics remains unclear. For example, [57] provides the results of an experiment in which participants control the position of a cursor on a computer display screen using a joystick and are instructed to follow target signals with Gaussian probability density functions. The participants perform linear and nonlinear tasks. For the linear task there is a proportional and one-to-one relationship between the position of the joystick and the position of the response cursor. For the nonlinear task this relationship follows a static nonlinear or non-proportional pattern. The results imply that participants form an internal representation of the static nonlinearity. This conclusion, however, is not based on identification of controllers used by the human subjects and is only based on the movements of the joystick. Furthermore, the nonlinear system used in this experiment has no dynamic component and is purely static.

The main motivation of this chapter is to investigate the command-following control strategies that humans use to interact with nonlinear systems. We present results and analysis of an experiment in which two groups of human subjects interact with two different dynamic systems to perform a command-following task. The first group interacts with a LTI system, and the second group interacts with a Wiener system, which consists of the same LTI dynamics cascaded with a static output nonlinearity. Each subject's command-following behavior is modeled by a discrete-time control architecture consisting of a feedback time delay, a linear feedback controller, and a nonlinear feedforward controller. We compare the time-domain performance, frequency-domain performance, and control behavior of these two groups. By com-

paring the time-domain performance, frequency-domain performance, and control behavior of these two groups, we investigate the effects of output nonlinearity on control strategies used by human subjects.

3.2 Experimental Methods

Twenty-two people voluntarily participated in this study, which was approved by the University of Kentucky's Institutional Review Board under IRB protocol 44649. The subjects were 18 to 35 years old and had no known neurological disorders. Subjects use a rotational joystick (Teledyne Gurley model 8225-6000-DQSD) to control the motion of an object that is displayed on a computer screen. A *trial* is a 60-s time period during which a subject operates the joystick, and a *session* consists of 10 consecutive trials completed within a period of 20 minutes. Subjects completed 4 sessions over a 7-day period, but no more than one session in a 12-hour period.

The experimental setup is shown in Fig. 3.2. The computer monitor displays two thin rectangular markers, one above the other. The top rectangular marker is called the *reference object* and its horizontal position is denoted r. The bottom rectangular marker is called the *control object* and its horizontal position is denoted y. The reference object follows a predetermined path, which is the same for all subjects and all trials. Alternatively, the control object's position is dependent on the joystick's angular position, which is denoted by u. The subjects are provided no information about how the joystick affects the motion of the control object. Subjects are instructed to use the joystick to make the control object mimic the motion of the reference object. More specifically, their objective is to generate a control u that makes the magnitude of the command-following error $e \triangleq r - y$ as small as possible.

The reference object's position for all $t \in [0, 60]$ is

$$r(t) \triangleq 2 \sin \frac{\pi t^2}{120},$$

(3.1)
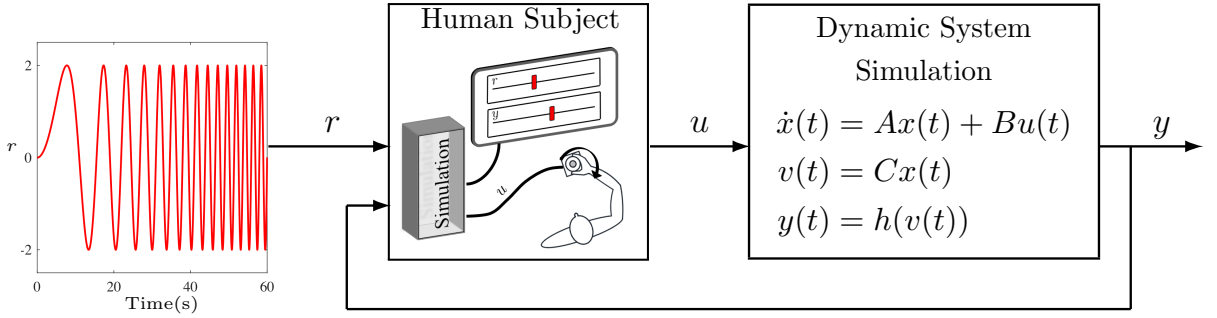
Figure 3.2: Subjects use a rotational joystick to control the position y of the bottom marker displayed on the computer screen. The subjects' objective is to make y follow the command r, whose position is displayed on the computer screen by the top marker. The joystick's angular position u is the control input of an unknown dynamic system, which is simulated by a computer, and the dynamic system's output is y.

which is a 60-second chirp signal with frequency content between 0 and 0.5 Hz. For all $t \in [0, 60]$, the relationship between the subject's control u and the controlled object's position y satisfies the differential equation

$$\dot{x}(t) = Ax(t) + Bu(t), \tag{3.2}$$

$$v(t) = Cx(t), \tag{3.3}$$

$$y(t) = h(v(t)), \tag{3.4}$$

where $x(t) \in \mathbb{R}^n$ is the state, $x(0) = 0$ is the initial condition, $v(t) \in \mathbb{R}$ is the output of the linear dynamics (which is not accessible to the subjects), $y(t) \in \mathbb{R}$ is the output, $A \in \mathbb{R}^{n \times n}$, $B \in \mathbb{R}^{n \times 1}$, $C \in \mathbb{R}^{1 \times n}$, and $h : \mathbb{R} \to \mathbb{R}$ is a continuous and one-to-one function. It follows from (3.2) and (3.3) that the transfer function from u to v is $\mathcal{G}(s) \triangleq C(sI - A)^{-1}B$. The units of r and y are hash marks (hm), which are equally-spaced vertical lines displayed on the computer screen. The distance between hash marks is 2.5 cm, and the range of motion displayed on the computer screen is ± 8 hm.

The 22 subjects were randomly divided into two groups of 11 subjects. Both groups

interacted with the dynamic system (3.2)–(3.4), where A, B, and C are the same for both groups. However, h is different for the two groups. The function h is used to explore the effects of nonlinearity on performance and control strategy. For both groups, the transfer function from u to v is

$$\mathcal{G}(s) = \frac{2s + 4.4}{s^2 + 3.6s + 4},$$

which has a zero at -2.2 and a pair of complex-conjugate poles at $-1.8 \pm j0.872$. For the first group, $h(v)$ is the identity function (i.e., $h(v) = v$), in which case the system (3.2)–(3.4) is LTI. We refer to the first group as the *linear group*. For the second group, $h(v)$ is the unique real root of the polynomial $0.1s^3 - 0.2s^2 + 0.5s - v$. Note that since $y = h(v)$, it follows that

$$h^{-1}(y) = 0.5y - 0.2y^2 + 0.1y^3,$$

which is a cubic nonlinearity. We refer to the second group as the *nonlinear group*.

3.3 Performance Analysis

For all trials, the experimental time signals r, y, and u are recorded with sample time $T_{\mathrm{s}} = 0.02$ s and $N_{\mathrm{s}} = 3001$ samples. The sampled data yield the discrete signals $\{r_k\}_{k=1}^{N_{\mathrm{s}}}$, $\{y_k\}_{k=1}^{N_{\mathrm{s}}}$, and $\{u_k\}_{k=1}^{N_{\mathrm{s}}}$. A *divergent trial* is a trial in which the magnitude of y_k exceeds 8 hm, that is, the controlled object's position exceeds the range of motion displayed on the computer screen. Table 3.1 shows the number of divergent trials for each group. There was only one divergent trial in this study, and it is omitted from the results.

Table 3.1: Number of divergent trials for each group

	Trials 1–10	Trials 11–20	Trials 21–30	Trials 31–40	Total
Linear Group	1	0	0	0	1
Nonlinear Group	0	0	0	0	0

3.3.1 Time-Domain Analysis

The sampled command-following error is $e_k \triangleq r_k - y_k$, and the *time-averaged error* is

$$\|e\| \triangleq \frac{1}{N_s} \sum_{k=1}^{N_s} |e_k|.$$

Figures 3.3 and 3.4 show r_k, y_k, and e_k on the first and last trial for the median performer in the linear and nonlinear groups. The median performer of each group is the subject whose $\|e\|$ on the last trial is the median (i.e., 6th best) of all subjects in their group. The median subject for both groups performs better on the last trial than the first trial. All subjects in both groups exhibit improved performance from their first to last trial. Similar results are observed for all other subjects.

Figure 3.5 shows the mean and standard deviation of $\|e\|$ on each trial. For both the linear and nonlinear group, the mean and standard deviation tend to decrease over the trials. The same results can be seen in Table 3.2, which shows the mean $\|e\|$ on 4 different sets of trials for both groups and its percentage change from the first 10 trials to the last 10 trials. The average $\|e\|$ of the linear group is smaller than the average $\|e\|$ of the nonlinear group on 77.5 % of the trials. This suggests that the nonlinear system is more difficult to control than the linear system. However, the linear group exhibits a larger variance in performance on all trials. We note that the variance of the nonlinear group is small compared with the results of several similar experiments [48, 49, 58]. The reason for this small variance is unclear, but it may be a small-sample effect or possibly caused by some feature of the nonlinearity.
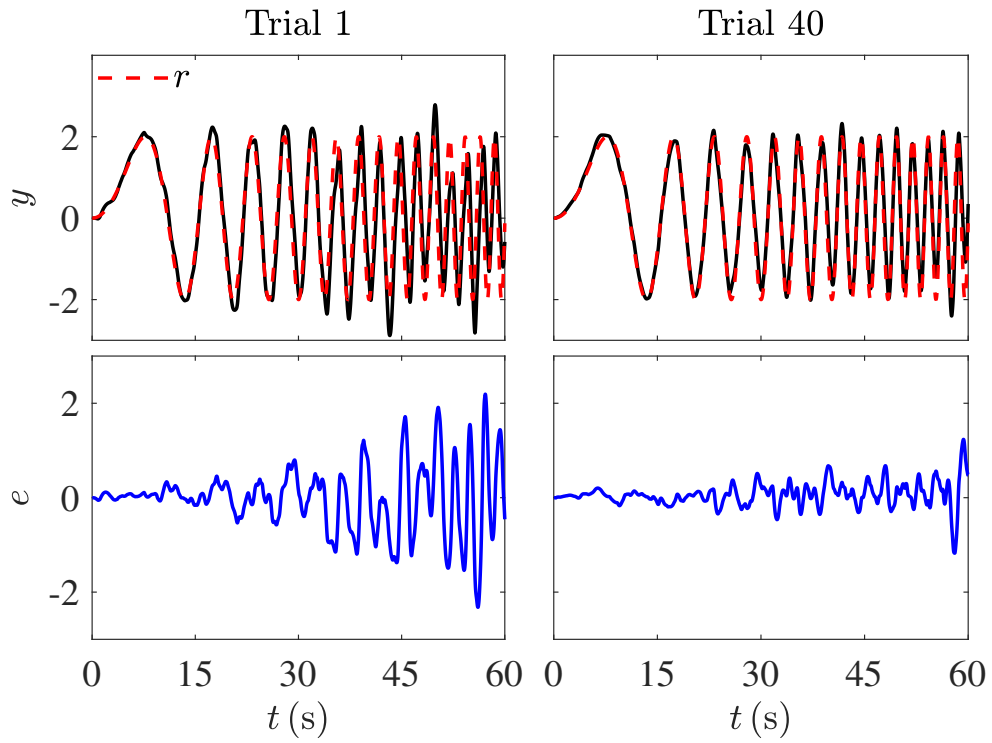
Figure 3.3: The reference r_k, output y_k, and error e_k for the linear group's median subject's 1st and 40th trial.
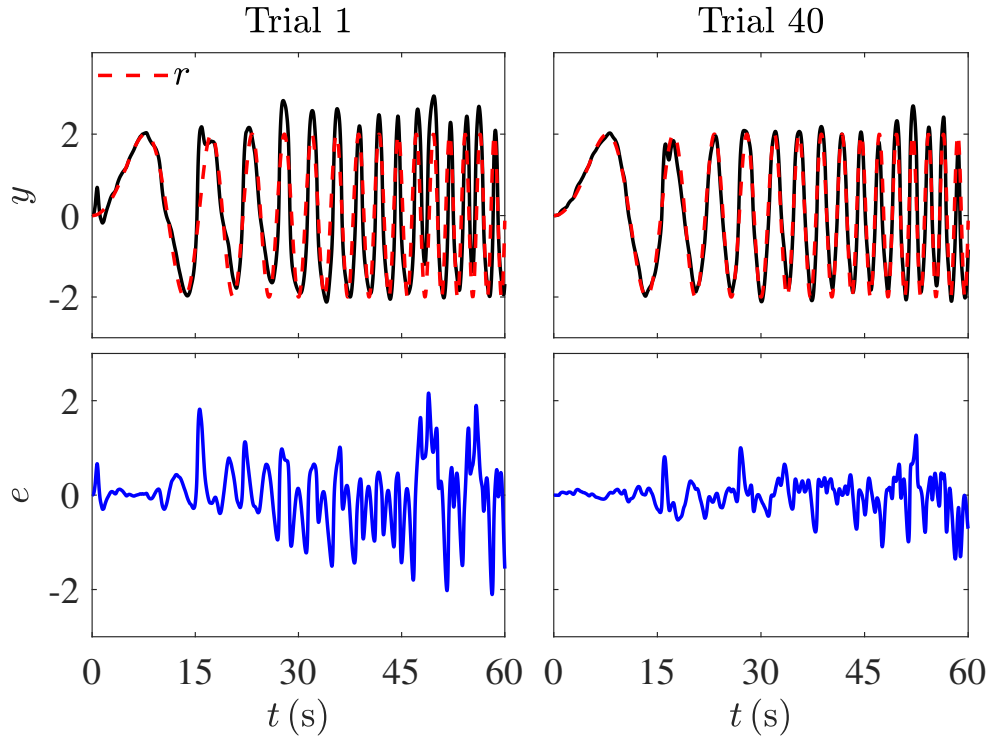
Figure 3.4: The reference r_k, output y_k, and error e_k for the nonlinear group's median subject's 1st and 40th trial.
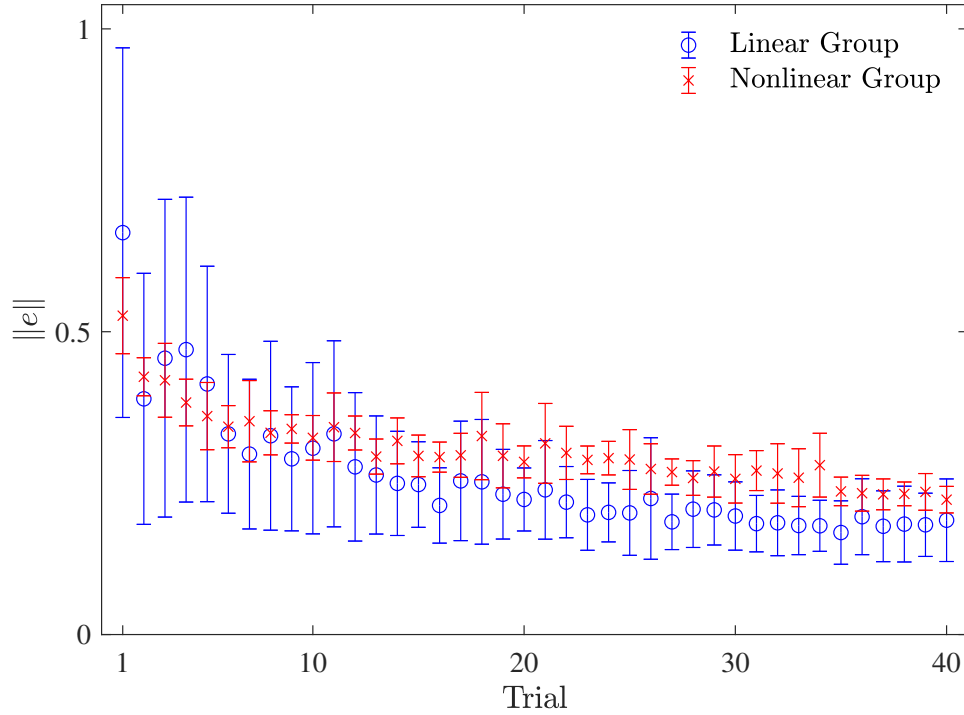
Figure 3.5: The performance of both linear and nonlinear groups improves over 40 trials. The symbols ○ and × indicate the mean of the 11 subjects for linear and nonlinear group respectively and the vertical lines show one standard deviation above and below the mean.

Table 3.2: Mean $\|e\|$ and its percentage change from the first 10 trials to the last 10 trials.

	Trials 1–10	Trials 11–20	Trials 21–30	Trials 31–40	Change (%)
Linear Group	0.395	0.254	0.208	0.182	-53.9
Nonlinear Group	0.381	0.308	0.281	0.247	-35.2

3.3.2 Frequency-Domain Analysis

For all $i = 1, ..., N_f$, let $\omega_i \triangleq (i-1)\pi/30$ rad/s, which are $N_f = 31$ evenly-spaced frequencies over the 0-0.5 Hz range. For each trial, let $r_{dft}(\omega_i)$ and $y_{dft}(\omega_i)$ denote the discrete Fourier transforms (DFT) of the sequences $\{r_k\}_{k=1}^{N_s}$ and $\{y_k\}_{k=1}^{N_s}$ at ω_i, respectively.

For each trial, we define the *frequency-averaged magnitude error* as

$$E_m \triangleq \frac{1}{N_f} \sum_{i=1}^{N_f} \left| |y_{dft}(\omega_i)| e^{\jmath \angle r_{dft}(\omega_i)} - |r_{dft}(\omega_i)| e^{\jmath \angle r_{dft}(\omega_i)} \right|$$

$$= \frac{1}{N_f} \sum_{i=1}^{N_f} \left| |y_{dft}(\omega_i)| - |r_{dft}(\omega_i)| \right|,$$

which is the frequency-averaged magnitude of the difference between y_{dft} and r_{dft}, assuming the phase of y_{dft} is the same as the phase of r_{dft}. Similarly, for each trial, we define the *frequency-averaged phase error* as

$$E_p \triangleq \frac{1}{N_f} \sum_{i=1}^{N_f} \left| |r_{dft}(\omega_i)| e^{\jmath \angle y_{dft}(\omega_i)} - |r_{dft}(\omega_i)| e^{\jmath \angle r_{dft}(\omega_i)} \right|$$

$$= \frac{1}{N_f} \sum_{i=1}^{N_f} |r_{dft}(\omega_i)| \left| e^{\jmath \angle y_{dft}(\omega_i)} - e^{\jmath \angle r_{dft}(\omega_i)} \right|,$$

which is the frequency-averaged magnitude of the difference between y_{dft} and r_{dft}, assuming the magnitude of y_{dft} is the same as the magnitude of r_{dft}.

Figure 3.6 shows the mean and standard deviation of E_m and E_p for subjects in the linear and nonlinear group on each trial. These results are similar to what we had previously seen in our time-domain analysis. For subjects in both groups, the mean and standard deviation of frequency-averaged magnitude error and frequency-averaged phase error tend to decrease over trials. Moreover, the nonlinear group has a larger mean E_m and mean E_p than the linear group over the later trials.

Tables 3.3 and 3.4 show the mean E_m and E_p on 4 different sets of trials for the
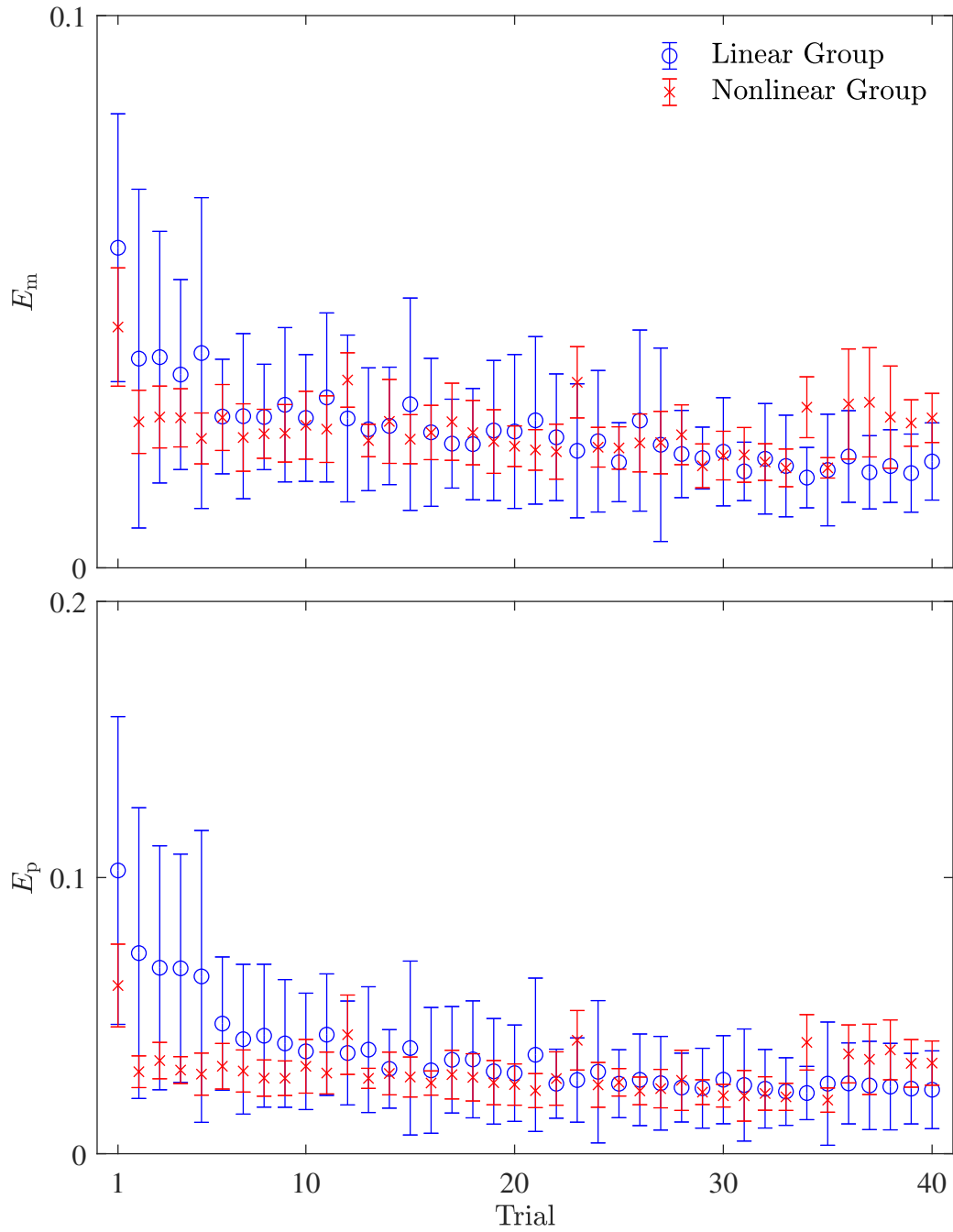
Figure 3.6: The mean E_{m} and the mean E_{p} for both linear and nonlinear group decrease over 40 trials. The symbols ∘ and × indicate the mean of the 11 subjects for linear and nonlinear group respectively and the vertical lines show one standard deviation above and below the mean.

Table 3.3: Mean E_{m} and its percentage change from the first 10 trials to the last 10 trials.

	Trials 1–10	Trials 11–20	Trials 21–30	Trials 31–40	Change (%)
Linear Group	0.035	0.026	0.022	0.018	-47.5
Nonlinear Group	0.027	0.025	0.023	0.024	-10.3

Table 3.4: Mean E_{p} and its percentage change from the first 10 trials to the last 10 trials.

	Trials 1–10	Trials 11–20	Trials 21–30	Trials 31–40	Change (%)
Linear Group	0.058	0.034	0.027	0.024	-58.9
Nonlinear Group	0.033	0.029	0.026	0.030	-10.5

linear group and the nonlinear group. For both groups, the mean E_{m} and mean E_{p} decrease over the trials. This decrease, however, is more evident for subjects in the linear group. These results also suggest that the improvement we had previously seen in the command-following performance of linear group is more a result of their improvement in matching the phase of reference command than their improvement in matching the magnitude. For the nonlinear group, on the other hand, the distribution is relatively even.

3.4 Potential Human Control Strategies

In this section, we consider control strategies that are possible solutions of the SSID algorithm of Chapter 2. We first consider possible control strategies for the linear group. The dynamic system consists of the pair (G, h), where $G(z)$ is the discrete-time transfer function that is obtained by discretizing $\mathcal{G}(s)$ using a zero-order hold on the input with sample time T_{s} and h is the identify function. Let $p = 1$ and $f_1(r_k) = r_k$, then the control (2.2) is

$$\hat{u}(z) = z^{-d}G_{\text{fb}}(z)\hat{e}(z) + G_{\text{ff},1}(z)\hat{r}(z),$$

and it follows that the closed-loop error satisfies

$$\hat{e}(z) = \tilde{G}_{er}(z)\hat{r}(z), \tag{3.5}$$

where

$$\tilde{G}_{er}(z) = \frac{1 - G_{\text{ff},1}(z)G(z)}{1 + z^{-d}G_{\text{fb}}(z)G(z)} \tag{3.6}$$

is the closed-loop transfer function from r_k to e_k. The frequency response of $\tilde{G}_{er}$ is $\tilde{G}_{er}(e^{\jmath\omega T_{\text{s}}})$, where ω is the frequency in radians per second. Good command-following performance is achieved if G_{fb}, $G_{\text{ff},1}$, and d are such that $\tilde{G}_{er}$ is asymptotically stable and $|\tilde{G}_{er}(e^{\jmath\omega T_{\text{s}}})|$ is small at those frequencies coinciding with the frequency content of r_k.

One strategy that can be used to make $|\tilde{G}_{er}(e^{\jmath\omega T_{\text{s}}})|$ small is to make $|G_{\text{fb}}(e^{\jmath\omega T_{\text{s}}})|$ large. It follows from (3.6) that if $|G_{\text{fb}}(e^{\jmath\omega T_{\text{s}}})|$ is large at the frequencies of r_k, then $|\tilde{G}_{er}(e^{\jmath\omega T_{\text{s}}})|$ is small at those frequencies, in which case (3.5) implies that e_k is small, provided that $\tilde{G}_{er}$ is asymptotically stable. However, there are some practical limitations for using high-gain feedback for manual command-following tasks. Humans cannot use arbitrarily high gain due to physical limitations in speed and range of motion. Moreover, a human's ability to use high gain in feedback is limited by their feedback time delay, which can cause closed-loop instability if the gain in feedback is too large.

Consider the high-gain controller $G_{\text{fb}} = k_{\text{p}}$, where $k_{\text{p}} > 0$ is a proportional gain. Assume that the feedback time delay is 100 ms (i.e., $d = 5$) and that there is no feedforward control (i.e., $G_{\text{ff}} = 0$). For this case, the largest stabilizing feedback gain is approximately 8.5. Figure 3.7 shows the closed-loop output y_k and error e_k for the case that $k_{\text{p}} = 8.4$. We note that this proportional feedback controller yields a better performance than the median-performer's 40th-trial results shown in Fig. 3.3.

41
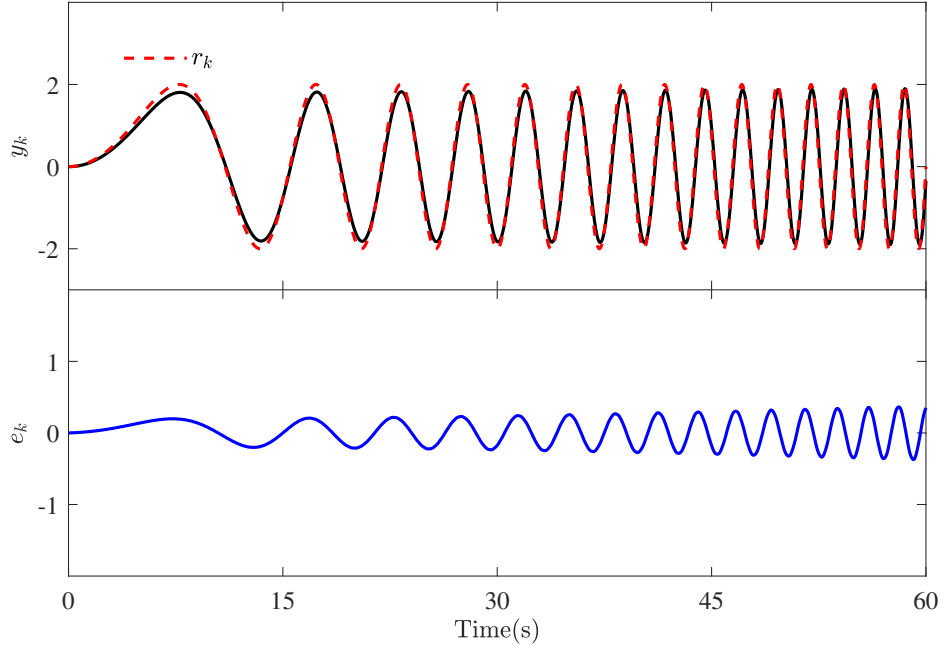
Figure 3.7: A feedback control strategy that makes the magnitude of the error small for the linear plant is high gain in feedback: The feedback controller is a proportional controller where $G_{\text{fb}} = 8.4$, the feedback time delay is 100 ms (i.e., $d = 5$), and there is no feedforward controller (i.e., $G_{\text{ff}} = 0$). (b) Approximate inverse dynamics in feedforward: $p = 1$, the feedforward controller is a fifth-order FIR approximation of G^{-1} across the 0-to-0.5 Hz range, f_1 is the identity function, and there is no feedback controller (i.e., $G_{\text{fb}} = 0$).

Moreover, the time-averaged error corresponding to Fig. 3.7 is approximately 0.16, which is smaller than the mean-averaged error for all trials of the linear group (cf. Fig. 3.5).

Another possible control strategy for the linear plant is approximate feedforward plant inversion. Specifically, if the feedforward controller G_{ff} approximates G^{-1}, then it follows from (3.6) that $\tilde{G}_{er}$ is approximately 0. If in addition G_{fb} and d are such that $\tilde{G}_{\text{er}}$ is asymptotically stable, then it follows from (3.5) that the magnitude of e_k is small. As with high-gain feedback control, there may also be practical limitations with feedforward plant inversion. In particular, a human's ability to approximate the plant inverse may be limited by the plant's complexity. Features that contribute to plant complexity include high order, high relative degree, time delays, and nonminimum-phase zeros [58].
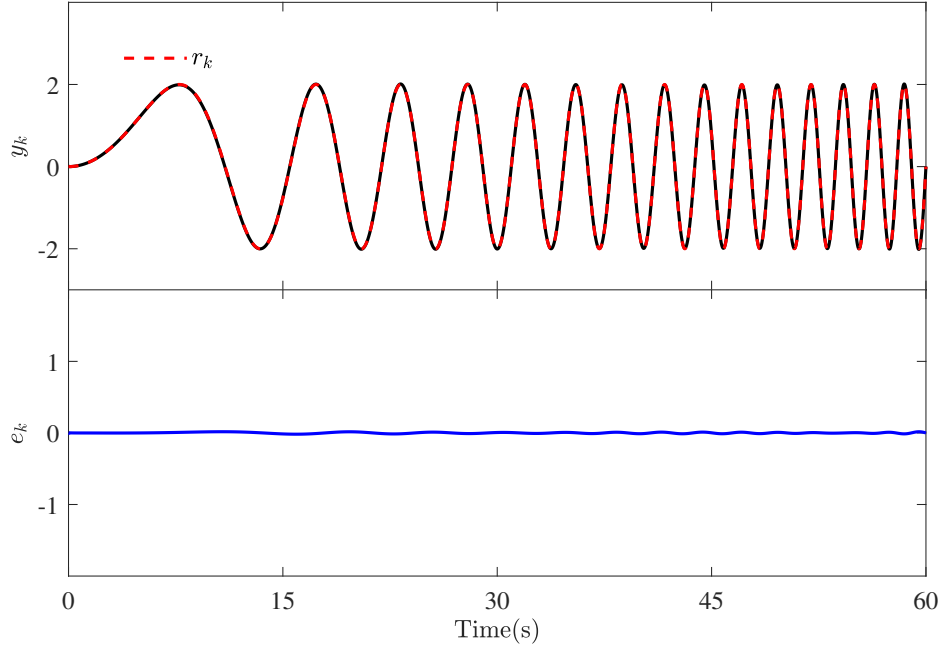
Figure 3.8: A feedforward control strategy that makes the magnitude of the error small for the linear plant is approximate inverse dynamics in feedforward: $p = 1$, the feedforward controller is a fifth-order FIR approximation of G^{-1} across the 0-to-0.5 Hz range, f_1 is the identity function, and there is no feedback controller (i.e., $G_{\mathrm{fb}} = 0$).

Consider the case that $G_{\mathrm{ff},1}$ is the best-fit 5th-order FIR approximation of G^{-1} over the 0-to-0.5 Hz frequency range. Specifically, consider $G_{\mathrm{ff}}(z) = 3467.6z^5 - 9280.2z^4 + 2157.3z^3 + 14708.8z^2 - 16081.4z + 5028.7$, which is the best-fit 5th-order FIR approximation of $G^{-1}(z)$ over the 0-to-0.5 Hz frequency range. Figure 3.8 shows the resulting closed-loop output y_k and error e_k for the case $G_{\mathrm{fb}} = 0$. Note that the approximate feedforward plant inversion controller yields a better performance than the median-performer's 40th-trial results shown in Fig. 3.3. Moreover, the time-averaged error corresponding to Fig. 3.8 is approximately 0.01, which is smaller than the mean-averaged error for all trials of linear group (cf. Fig. 3.5).

There are many other control strategies of the form (2.2) that yield good command-following performance for the linear plant. Another possible strategy is a combination of high gain in feedback and feedforward inversion. For example, humans may use high-gain feedback at lower frequencies, where they have more control authority and

the effects of feedback time delay are less pronounced; and then at higher frequencies, humans may utilize their predictive capabilities to implement feedforward inversion to mitigate the effects of reduced control authority and increased phase lag due to time delay.

Next, we consider control strategies for the nonlinear group. The dynamic system consists of the pair (G, h), where $G(z)$ is the discrete-time transfer function that is obtained by discretizing $\mathcal{G}(s)$ using a zero-order hold on the input with sample time T_{s} and h is the unique real root of a 3rd-order polynomial. First, consider a pure feedback control strategy. For all $j \in \{1, ..., p\}$, let $G_{\mathrm{ff},j} = 0$. In this case, the control architecture of Fig. 2.2 reduces to a Lur'e system. One possible control strategy is high gain in feedback, which makes the Bode magnitude large at frequencies of the command r_k. High-gain in feedback yields good command-following performance for LTI systems, provided that the closed-loop is asymptotically stable. Closed-loop stability and performance for the nonlinear system (G, h) is more difficult to evaluate. Since the slope of the magnitude of h is bounded, there are several classical nonlinear stability results that apply [95]. For example, the circle criterion implies that the closed-loop system is absolutely stable if $G_{\mathrm{fb}}G$ is asymptotically stable and its H_∞ norm is sufficiently small [95, Theorem 5.2]. Consider the feedback transfer function $G_{\mathrm{fb}} = 6.67z/(z^2 - 0.07z + 0.8)$. Let the feedback delay be $d = 5$, which corresponds to a feedback time delay of 100 ms. Figure 3.9 shows the resulting closed-loop output y_k and error e_k. The time-averaged error corresponding to Fig. 3.9 is 0.24, which is smaller than time-averaged error for all 40th trial experiments of the nonlinear group (cf. Fig. 3.5).

There are some practical limitations for using high-gain in feedback for manual command-following tasks. Humans cannot use arbitrarily high gain due to physical limitations in speed and range of motion. Moreover, a human's ability to use high gain in feedback is limited by their feedback time delay, which can cause closed-loop

44
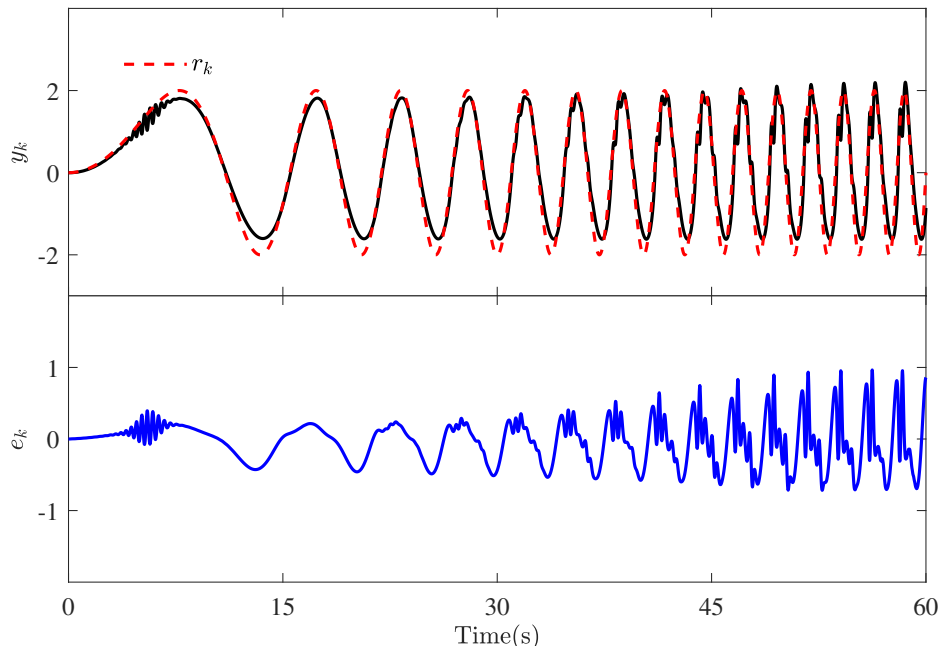
Figure 3.9: A feedback control strategy that makes the magnitude of the error small for the nonlinear plant is high gain in feedback.

instability if the gain in feedback is too large.

Another possible control strategy is feedforward inversion. Let $p = 3$, $f_1(r_k) = 0.5r_k$, $f_2(r_k) = -0.2r_k^2$, $f_3(r_k) = 0.1r_k^3$, and $G_{\mathrm{ff},j} = G^{-1}$ for all $j \in \{1, 2, 3\}$. If in addition $G_{\mathrm{fb}} = 0$, then the closed-loop response is $\hat{e} = [1 - G^{-1}G]\hat{r} = 0$, which implies that the command-following error is zero. Similar performance results can also be obtained by approximate feedforward inversion, where the feedforward controllers are approximations of G^{-1}. Figure 3.7 shows the resulting closed-loop output y_k and error e_k for the case that for all $j \in \{1, 2, 3\}$, $G_{\mathrm{ff},j}$ is the matched z-transform mapping of $22\,G^{-1}(s)/(s + 22)$, which is a proper approximation of G^{-1}. We note that the approximate feedforward inversion controller yields a better performance than the median-performer's 40th-trial results shown in Fig. 3.3. The time-averaged error corresponding to Fig. 3.7 is 0.09, which is smaller than time-averaged error for all 40th trial experiments of the nonlinear group (cf. Fig. 3.5).

As with high gain in feedback, there may also be practical limitations with feedfor-
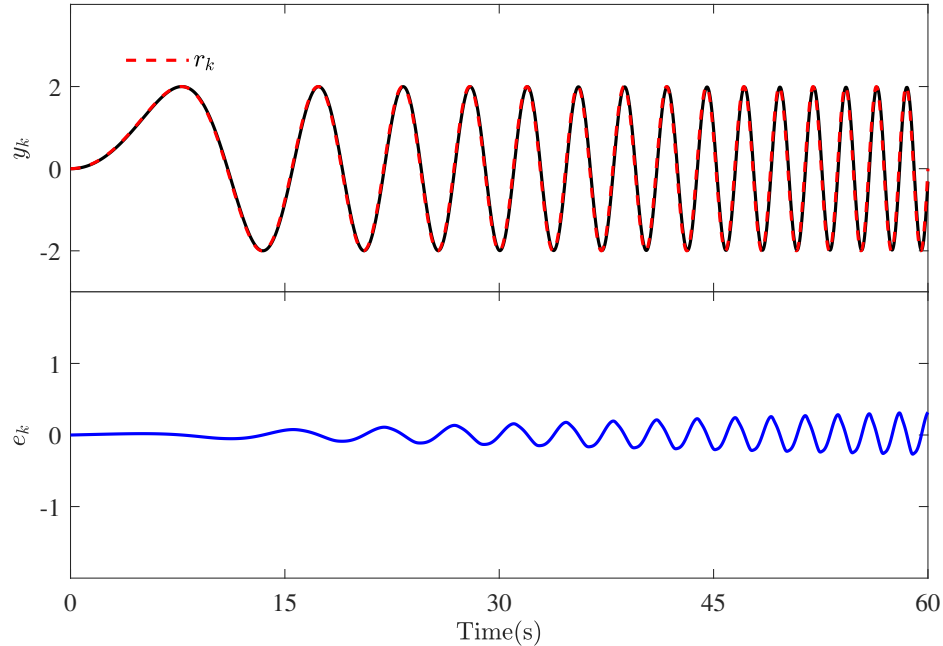
Figure 3.10: A feedforward control strategy that makes the magnitude of the error small for the nonlinear plant is approximate inverse dynamics in feedforward.

ward inversion. In particular, a human's ability to approximate the dynamic-system inverse may be limited by various features, such as relative degree, time delays, and nonminimum-phase zeros [58]. Nonlinearities may also inhibit accurate approximation of the dynamic-system inverse.

There are many other control strategies of the form (2.2) that yield good command-following performance for the nonlinear plant. As with the linear plant, another possible strategy is a combination of high gain in feedback and feedforward inversion. For example, similar to the linear plant, humans may use high-gain feedback at lower frequencies, where they have more control authority and the effects of feedback time delay are less pronounced; and then at higher frequencies, humans may utilize their predictive capabilities to implement feedforward inversion to mitigate the effects of reduced control authority and increased phase lag due to time delay.

3.5 Subsystem Identification Results and Discussion

The time-domain SSID method described in Chapter 2 is applied to the experimental data of the linear and nonlinear groups. For each subject and each trial, we identify a feedback transfer function G_{fb}, feedback delay d, and feedforward transfer functions $G_{\mathrm{ff},1}, ..., G_{\mathrm{ff},p}$. The candidate pool Γ contains approximately 50 million candidate pairs (d, G_{fb}) and captures a wide range control behavior over the 0-to-0.5 Hz frequency range of the command (3.1). Since sensory feedback time delay for humans is in the range 80 ms to 500 ms [33, 41, 96, 97], and the sampling rate for the experiments is 20 ms, the candidate pool includes all $\delta \in \{4, 5, \cdots, 25\}$. The candidate feedback transfer functions G_{fb} are second order relative degree one with monic denominator (i.e., $n_{\mathrm{fb}} = 1$, and $d_{\mathrm{fb}} = 2$). The parameters of candidate feedback controller are designed such that the zero and poles of the candidate feedback transfer functions G_{fb} lie inside the unit circle. More specific details on the candidate pool are provided in Appendix A. The feedforward transfer functions $G_{\mathrm{ff},1}, ..., G_{\mathrm{ff},p}$ are each 5th-order FIR, and for $i \in \{1, ..., 5\}$, $f_i(r_k) = r_k^i$. These orders allow the identified feedforward system to approximate the plant pair (h^{-1}, G^{-1}) with approximately 0.1% error over the 0-to-0.5 Hz frequency range of the command (3.1). The SSID algorithm is implemented using parallel computation on a supercomputer. A validation analysis of the identification results is presented in Appendix B.1.

We first present identification results of the feedback pair (d, G_{fb}). For each identified feedback transfer function, we define

$$\|G_{\mathrm{fb}}\| \triangleq \max_{\omega \in [0,\pi]} \left| G_{\mathrm{fb}}(e^{\jmath \omega T_{\mathrm{s}}}) \right|,$$

which is the peak magnitude of the feedback transfer function over the 0-to-0.5 Hz range of the command r. For each trial, we compute the average $\|G_{\mathrm{fb}}\|$ and average time delay d of all 11 subjects in each group. Figures 3.11 and 3.12 show the trial-by-
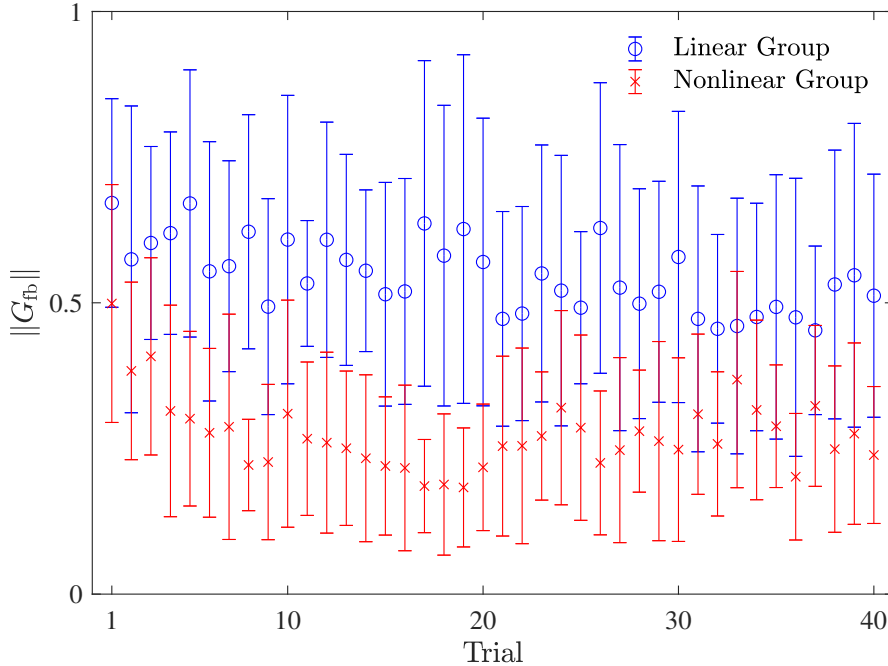
Figure 3.11: The feedback controller's peak magnitude for the nonlinear group is smaller than that of the linear group over all 40 trials. The symbols ○ and × indicate the mean of the 11 subjects for linear and nonlinear group respectively and the vertical lines show one standard deviation above and below the mean.

trial averages for the linear and nonlinear groups. The subjects in the nonlinear group consistently use a lower feedback gain and a larger time delay than the subjects in the linear group. The larger time delay suggests that the nonlinear-group subjects are more hesitant to react to command-following errors than the linear-group subjects. The larger time delay for the nonlinear subjects limits the amount of gain they can use in feedback to maintain a stable closed-loop response. In contrast, the linear-group subjects have a smaller time delay and are thus able to use larger feedback gain.

Next, identification results are presented for the feedforward controllers. For all $k \in \{1, ..., N_s\}$, define the identified feedforward control signal $u_{\mathrm{ff},k}^+ \triangleq \sum_{j=1}^{p} N_{\mathrm{ff},j}(\mathrm{q}) f_j(r_k)$. We compare $u_{\mathrm{ff},k}^+$ with the feedforward-inversion control signal $u_{\mathrm{ff},k}^*$, which is the zero-initial-condition solution of $u_{\mathrm{ff},k}^* \triangleq G^{-1}(\mathrm{q}) h^{-1}(r_k)$. Note that $u_{\mathrm{ff},k}^+$ is the feedforward control signal using the identified feedforward controller G_{ff}^+ and the identified feedforward nonlinear function f^+, and $u_{\mathrm{ff},k}^*$ is the feedforward control signal assuming
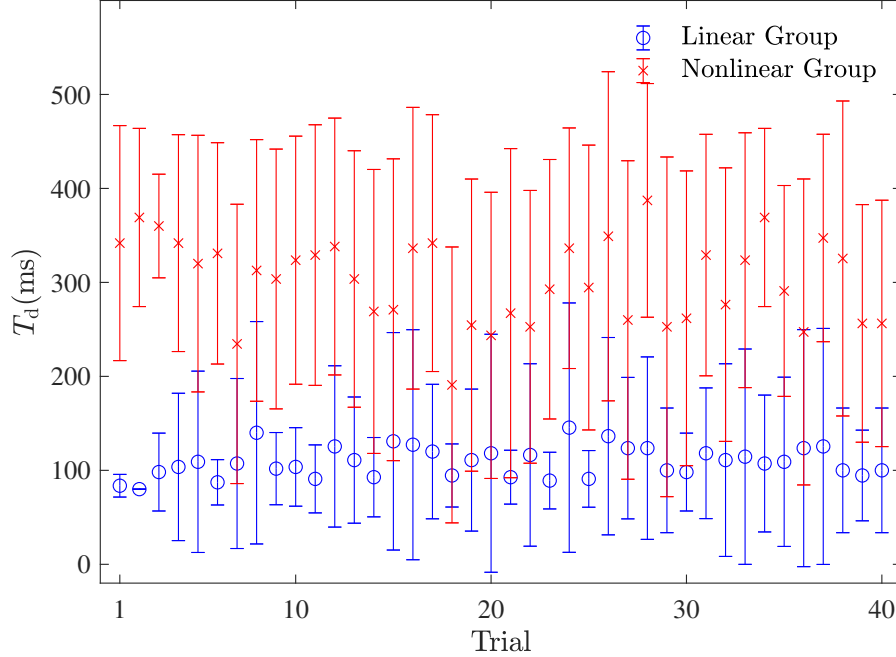
Figure 3.12: Subjects in the nonlinear group have more feedback delay over the 40 trials compared to subjects in the linear group. The symbols ∘ and × indicate the mean of the 11 subjects for linear and nonlinear group respectively and the vertical lines show one standard deviation above and below the mean.

there is plant inversion in feedforward. For each identified feedback controller, the average difference between $u_{\mathrm{ff},k}^+$ and $u_{\mathrm{ff},k}^*$ is defined as

$$\left\| u_{\mathrm{ff}}^+ - u_{\mathrm{ff}}^* \right\| \triangleq \frac{1}{N_{\mathrm{s}}} \sum_{k=1}^{N_{\mathrm{s}}} \left| u_{\mathrm{ff},k}^+ - u_{\mathrm{ff},k}^* \right| .$$

A smaller $\left\| u_{\mathrm{ff}}^+ - u_{\mathrm{ff}}^* \right\|$ indicates that the feedforward controller more closely approximates feedforward inversion. Figure 3.13 shows the average $\left\| u_{\mathrm{ff}}^+ - u_{\mathrm{ff}}^* \right\|$ of the 11 subjects in the linear and nonlinear groups for each trial. For both groups, the average of $\left\| u_{\mathrm{ff}}^+ - u_{\mathrm{ff}}^* \right\|$ decreases over the 40 trials. The linear group's feedforward control is on average a better approximation of feedforward inversion than the nonlinear group. This difference may account for some of the difference in performance between the two groups (see Fig. 3.5). Specifically, the dynamic system's static output nonlinearity may make it more difficult for the subjects to accurately invert the dynamics in
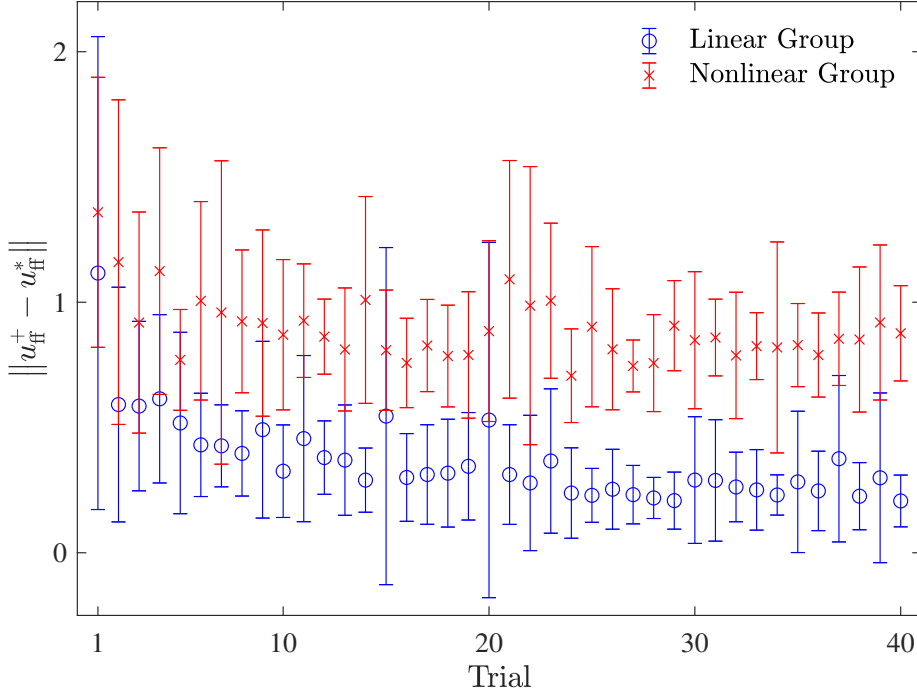
Figure 3.13: The time-averaged difference between $u_{\text{ff},k}$ and $u^*_{\text{ff},k}$ for the linear and nonlinear group decreases over 40 trials. The symbols $\circ$ and $\times$ indicate the mean of the 11 subjects for linear and nonlinear group respectively and the vertical lines show one standard deviation above and below the mean.

feedforward, thus yielding decreased performance.

The results in Fig. 3.13 suggest that both groups of subjects learn to approximate the dynamic system's inverse in feedforward. To distinguish between the learning of G^{-1} and h^{-1} for the nonlinear group, we use each subject's identified controller to derive a Hammerstein-model approximation of their feedforward controller. Specifically, we compute a pair (f, G_{ff}) where $f : \mathbb{R} \to \mathbb{R}$ is an input nonlinearity, G_{ff} is a FIR transfer function, and $G_{\text{ff}}(\text{q})f(r_k)$ is the Hammerstein-model approximation. Note that the identified feedforward control $\sum_{j=1}^{p} G_{\text{ff},j}(\text{q})f_j(r_k)$ is a Hammerstein model if for all $j \in \{1, ..., p\}$, there exists scalar c_j such that $G_{\text{ff},j} = c_j G_{\text{ff}}$. The Hammerstein model structure is more restrictive feedforward control model than that of Fig. 2.2. However, when the feedforward controller approximates feedforward inversion, then a Hammerstein model pair (f, G_{ff}) can approximate this behavior and provide a direct comparison with the components of the exact feedfoward inversion pair (h^{-1}, G^{-1}).

Replacing the feedforward controller in (2.13) with the Hammerstein model (f, G_{ff}) yields

$$D(z)D_{\text{fb}}(z)z^{d+n_{\text{ff}}}\hat{v}(z) = N(z)N_{\text{fb}}(z)z^{n_{\text{ff}}}\hat{e}(z) + N(z)D_{\text{fb}}(z)z^d G_{\text{ff}}(z)\hat{s}(z), \qquad (3.7)$$

where $\hat{s}(z)$ is the z-transform of $f(r_k)$. Let f be defined by $f(r_k) \triangleq \sum_{j=1}^p \alpha_j f_j(r_k)$, where $\alpha_1, ..., \alpha_p \in \mathbb{R}$ are unknown coefficients. We assume that the linear behavior of the identified feedforward controller is primarily captured by its linear component $G_{\text{ff},1}(\text{q})f_1(r_k)$, and we let $G_{\text{ff}} = \frac{1}{\alpha_1}G_{\text{ff},1}$. Thus, the Hammerstein model can be expressed as $G_{\text{ff}}(\text{q})f(r_k) = G_{\text{ff},1}(\text{q})\bar{f}(r_k)$, where

$$\bar{f}(r_k) \triangleq f_1(r_k) + [f_2(r_k) \quad \cdots \quad f_p(r_k)]\bar{\alpha},$$

and $\bar{\alpha} \triangleq [\frac{\alpha_2}{\alpha_1} \quad \cdots \quad \frac{\alpha_p}{\alpha_1}]^{\text{T}}$. We use (3.7) along with the identified control components d, G_{fb}, and $G_{\text{ff},1}$ to find a best-fit $\bar{\alpha}$. For all $k \in \{1 - \ell_d, ..., N_{\text{s}} - \ell_d\}$, define

$$m_k \triangleq N(\text{q})D_{\text{fb}}(\text{q})N_{\text{ff},1}(\text{q})\text{q}^d[f_2(r_k) \quad \cdots \quad f_p(r_k)],$$

$$n_k \triangleq D(\text{q})D_{\text{fb}}(\text{q})\text{q}^{d+n_{\text{ff}}}v_k - N(\text{q})N_{\text{fb}}(\text{q})\text{q}^{n_{\text{ff}}}e_k - N(\text{q})D_{\text{fb}}(\text{q})N_{\text{ff},1}(\text{q})\text{q}^d f_1(r_k),$$

where d, N_{fb}, D_{fb}, and $N_{\text{ff},1}$ are identified parameters. For all $k = 1, ..., N_{\text{f}}$, let $\omega_k \triangleq (k-1)\pi/30$ rad/s, which are $N_{\text{f}} = 31$ evenly-spaced frequencies over the 0-0.5 Hz range. Let $m_{\text{dft}}(\omega_k)$ and $n_{\text{dft}}(\omega_k)$ denote the discrete Fourier transforms of the sequences $\{m_{k-\ell_d}\}_{k=1}^{N_{\text{s}}}$ and $\{n_{k-\ell_d}\}_{k=1}^{N_{\text{s}}}$. We seek $\bar{\alpha}$ that minimizes the cost function

$$\mathcal{J}_{\text{H}}(\bar{\alpha}) \triangleq \sum_{\omega_k \in [\omega_1, \omega_{N_{\text{f}}}]} |m_{\text{dft}}(\omega_k)\bar{\alpha} - n_{\text{dft}}(\omega_k)|^2 .$$

The cost $\mathcal{J}_{\text{H}}$ is convex in the elements of $\bar{\alpha}$. The method of least squares is used to determine the best-fit $\bar{\alpha}$ that minimizes $\mathcal{J}_{\text{H}}$.

The Hammerstein-model pair is $(\alpha_1 \bar{f}, G_{\text{ff},1}/\alpha_1)$, where α_1 is unknown. Note that for any nonzero α_1, $\frac{1}{\alpha_1}G_{\text{ff},1}(\text{q})\alpha_1\bar{f}(r_k) = G_{\text{ff},1}(\text{q})\bar{f}(r_k)$. Thus, α_1 is an arbitrary with regards to the input-output response. To compare (f, G_{ff}) with (h^{-1}, G^{-1}), we let

$$\alpha_1 \triangleq \frac{\sqrt{\sum_{k=1}^{N_s} |h^{-1}(r_k)|^2}}{\sqrt{\sum_{k=1}^{N_s} |\bar{f}(r_k)|^2}}, \tag{3.8}$$

which enforces the condition that $\{f(r_k)\}_{k=1}^{N_s}$ and $\{h^{-1}(r_k)\}_{k=1}^{N_s}$ have the same ℓ_2 norm.

For each subject and each trial, we identify a best-fit Hammerstein model pair (f, G_{ff}). The following discussion compares the subjects' identified feedforward components f and G_{ff} with the ideal feedforward inversion components h^{-1} and G^{-1}.

First, we compare f with h^{-1}. Figures 3.14 and 3.15 show the average f for all subjects on the first and last trials of the linear and nonlinear groups. For both groups, the average f is a better approximation of h^{-1} on the last trial than on the first trial. The nonlinear group has a more significant change in f from the first to the last trial.

To further compare f with h^{-1}, define

$$\|f - h^{-1}\| \triangleq \frac{1}{2} \sum_{k=1}^{N_s} \frac{|f(r_k) - h^{-1}(r_k)|}{|h^{-1}(r_k)|},$$

which is a measure of the difference between f and h^{-1}. Figure 3.16 shows the mean and standard deviation of $\|f - h^{-1}\|$ on each trial of the linear and nonlinear group. The average of $\|f - h^{-1}\|$ is smaller for the linear group than the nonlinear group on all trials. For both groups, the average of $\|f - h^{-1}\|$ is smaller on the last trial compared to the first trial. However, the nonlinear group exhibits a more significant decreasing trend over the 40 trials. These results suggest that the nonlinear subjects learn to approximate h^{-1} in feedforward, whereas there is less learning for the linear group. We also note that the average of $\|f - h^{-1}\|$ for the nonlinear group continues to
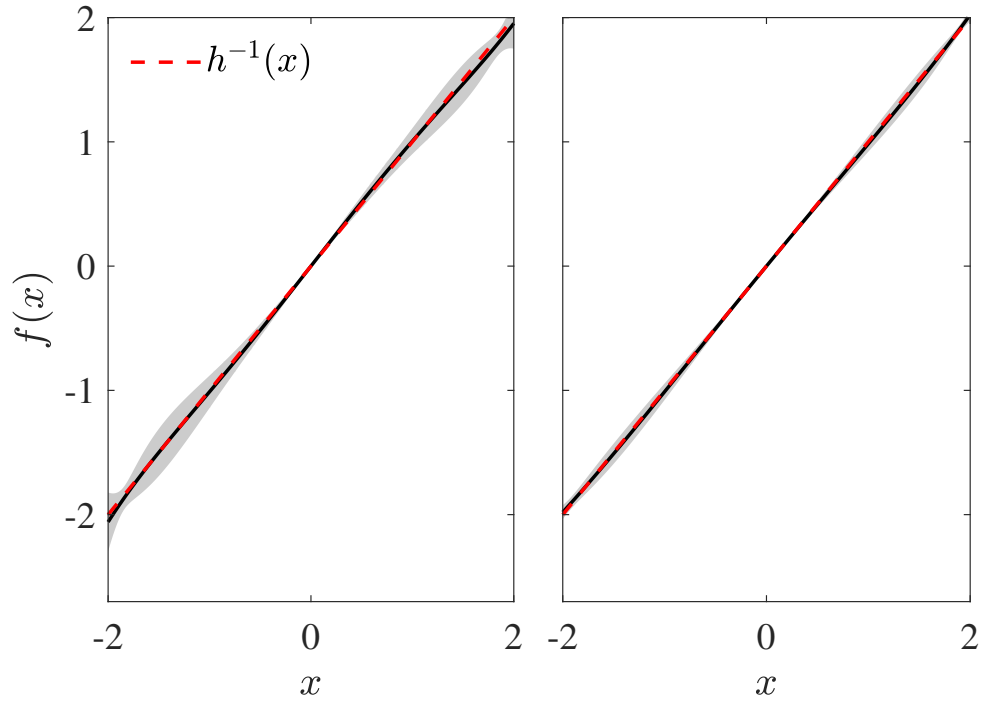
Figure 3.14: The average basis function f is a better approximation of h^{-1} on the last trial than the first trial of the linear group. The shaded region shows one standard deviation above and below the mean.
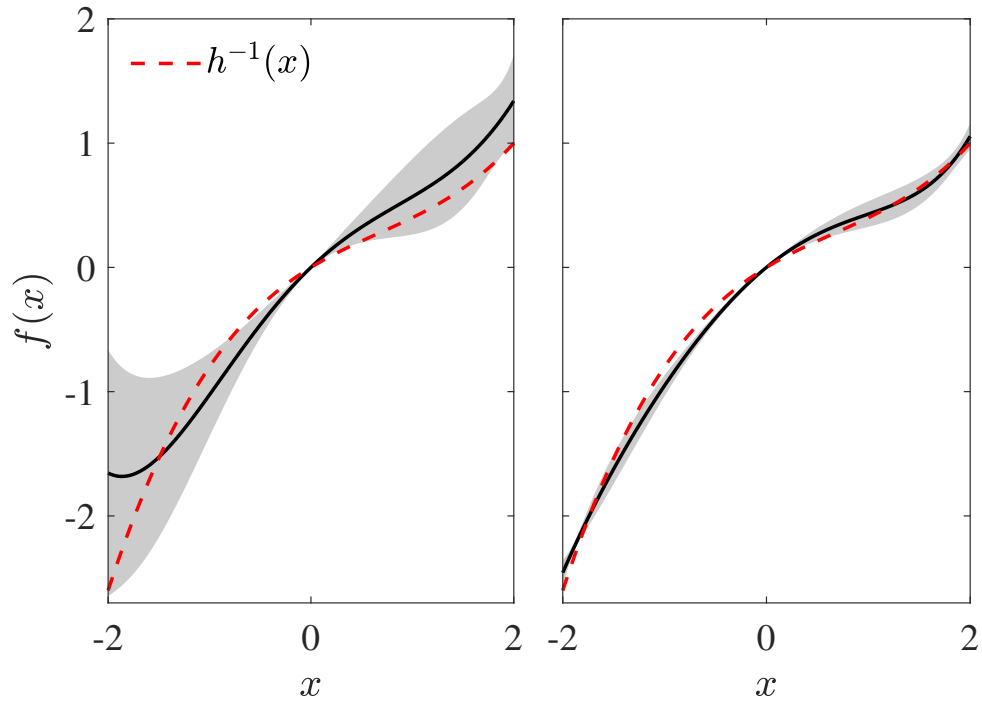
Figure 3.15: The average basis function f is a better approximation of h^{-1} on the last trial than the first trial of the nonlinear group. The shaded region shows one standard deviation above and below the mean.
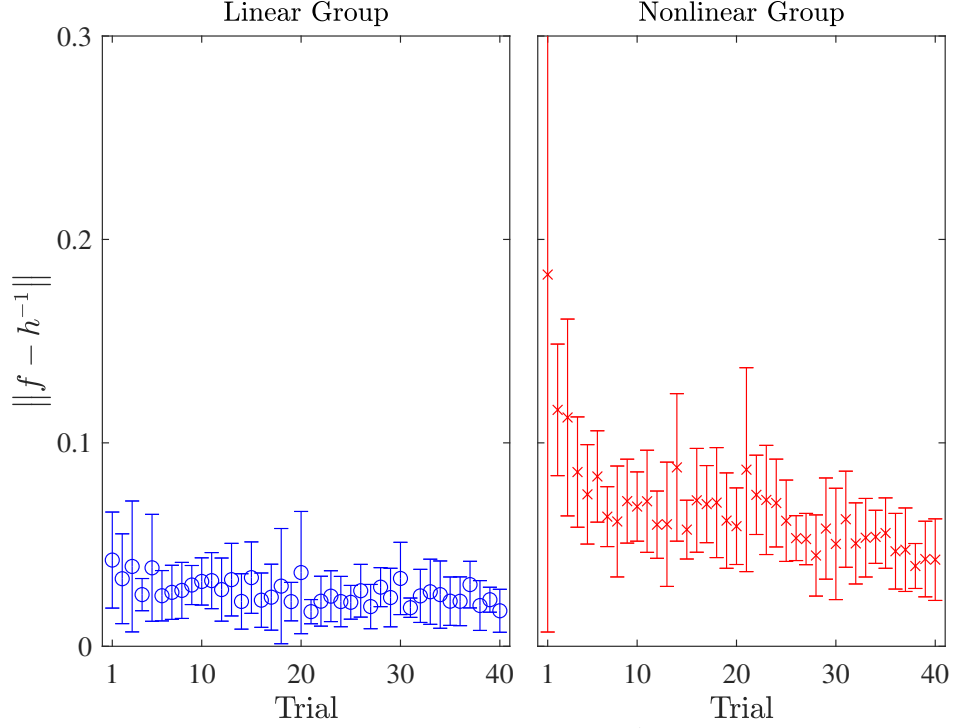
Figure 3.16: Mean and standard deviation of $\|f - h^{-1}\|$ on each trial. The difference between f and h^{-1} for the nonlinear group has a more significant decreases over the 40 trials. The symbols $\circ$ and $\times$ indicate the mean of 11 subjects for the linear and nonlinear group respectively and the vertical lines show one standard deviation above and below the mean.

decrease over the last 10 trials, suggesting that the subjects may continue to improve their approximation of h^{-1} if given more trials.

Next, we compare G_{ff} with G^{-1}. Figures 3.17 and 3.18 show the average Bode plot over the frequency range of 0-to-0.5 Hz of the identified G_{ff} for all 11 subjects on the first and last trials of the linear and nonlinear group. For both groups, the average feedforward transfer function more closely approximates G^{-1} on the last trial compared to the first trial. To further compare G_{ff} with G^{-1}, define

$$\|G_{\text{ff}}G - 1\| \triangleq \frac{1}{\pi} \int_0^\pi \left| G_{\text{ff}}(e^{j\omega T_{\text{s}}})G(e^{j\omega T_{\text{s}}}) - 1 \right| \mathrm{d}\omega,$$

which is a frequency-domain measure of the difference between G_{ff} and G^{-1}. Figure 3.19 shows the mean and standard deviation of $\|G_{\text{ff}}G - 1\|$ for each trial of the
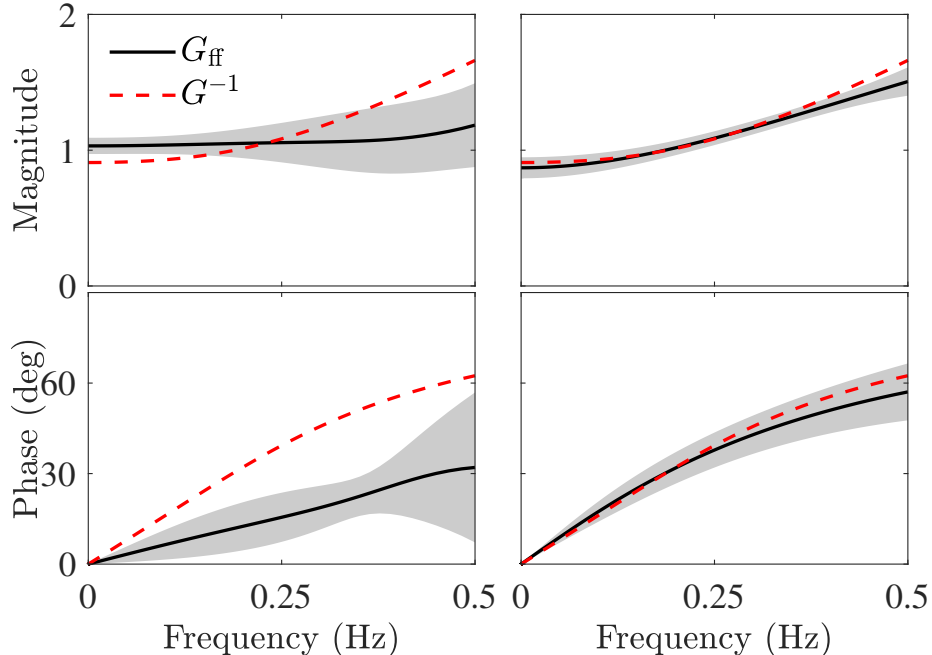
Figure 3.17: The average feedforward transfer function G_{ff} approximates G^{-1} after 40 trials of linear group. The shaded region shows one standard deviation above and below the average identified feedforward transfer function.

linear and nonlinear group. We note that the trends for the linear group are comparable to those in [48], which applies a frequency-domain SSID method to the same experimental data.

The average of $\|G_{\text{ff}}G - 1\|$ for the two groups have a similar trend over the 40 trials. Over the first 10 trials, there is a decreasing trend for both groups; and over the last 10 trials, the trend is relatively flat for both groups. The linear group achieves a better approximation of G^{-1} than the nonlinear group. These results suggest that the subjects of both groups learn to approximate the inverse of G in feedforward over the 40 trials.

3.6 Summary and Conclusions

We now discuss the impact of system nonlinearities on the contol strategies used by humans. In this chapter, we presented the results of a HITL experiment, which was designed to investigate the control strategies that humans use to interact with
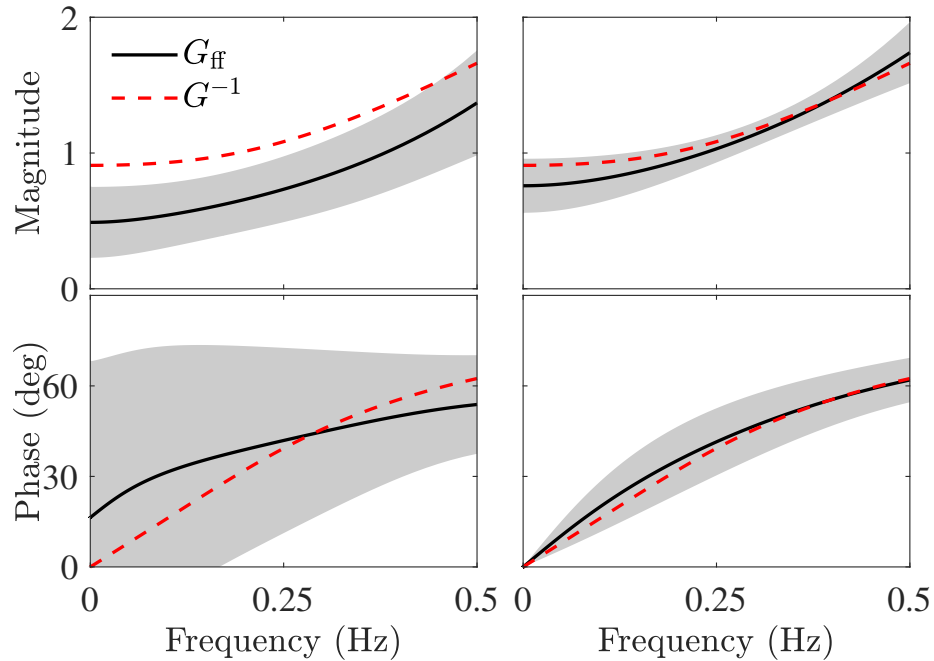
Figure 3.18: The average feedforward transfer function G_{ff} approximates G^{-1} after 40 trials of nonlinear group. The shaded region shows one standard deviation above and below the average identified feedforward transfer function.
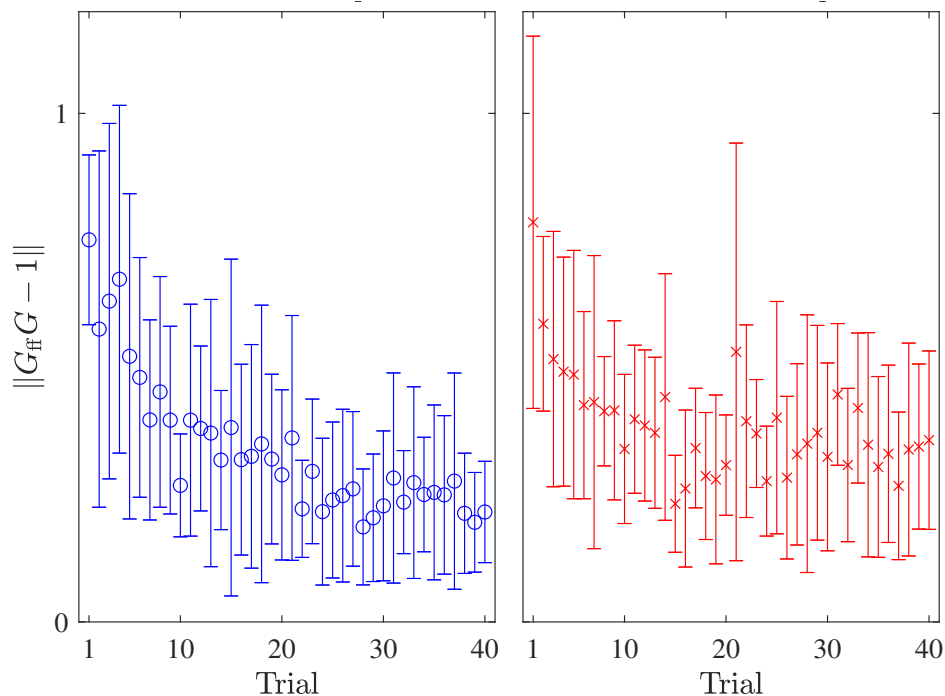
Figure 3.19: Mean and standard deviation of $\|G_{\text{ff}}G - 1\|$ on each trial. For both groups, the difference between G_{ff} and G^{-1} decreases over the 40 trials. The symbols $\circ$ and $\times$ indicate the mean of the 11 subjects for linear and nonlinear group respectively and the vertical lines show one standard deviation above and below the mean.

nonlinear dynamic systems. In this experiment, 22 human subjects interacted with a dynamic system and performed a command-following task. One group interacted with an LTI dynamic system, while the other group interacted with a Wiener system, which consisted of the same LTI dynamics cascaded with a static output nonlinearity.

This chapter presented new results on the impact of nonlinearities on HITL control behavior. The experimental results indicate that static output nonlinearities can make a dynamic system more difficult for humans to control. The average command-following performance of the linear group is better on 77.5% of trials than the nonlinear group (see Fig. 3.5). To investigate the control strategies of both groups, a nonlinear SSID algorithm is used to identify best-fit feedback and feedforward controllers for each subject and on each trial. The SSID results reveal several differences between the linear and nonlinear groups. The linear group tends to use more feedback-control authority. Specifically, the linear group has a smaller feedback time delay and uses a larger feedback gain than the nonlinear group (see Figs. 3.11 and 3.12).

The main finding of this chapter addresses feedforward behavior. Prior HITL studies suggest that adaptive feedforward inversion is a primary command-following control strategy for many linear systems. The results in this chapter provide supporting evidence that humans also adopt this control strategy for some nonlinear systems. For both the linear and nonlinear groups, the identified feedforward controllers approximate the dynamic system's inverse better on the last trial than on the first trial (see Figs. 3.14, 3.15, 3.17, and 3.18). However, the linear group achieves better approximation of the dynamic system's inverse (see Figs. 3.16 and 3.19). This difference in approximating the inverse is a possible explanation for the difference in performance between the two groups. Finally, the SSID results suggest that the nonlinear subjects learn the linear part of the dynamic system more quickly than they learn the static output nonlinearity. Over the latter half of the trials, the nonlinear subjects' feedforward transfer function does not change significantly (see Fig. 3.19), whereas

they continue to learn the output nonlinearity (see Fig. 3.16). Given more trials, the nonlinear subjects may continue to learn a better approximation of the dynamic system's inverse and perform as well as the linear subjects.

Chapter 4   The Impact of Relaxed Command-Following Objectives on Human Control Strategies

In this chapter, we present the results of a human-in-the-loop experiment which is designed to investigate the effects of relaxing the control objectives on the control strategies used by humans in command-following tasks. In this experiment, 22 human subjects each interact with a dynamic system 40 times over a one-week period. The subjects are divided into 2 groups of 11 subjects. Each group interacts with the same dynamic system and performs a command-following task; however, the groups have different control objectives. One group's control objective is to follow the reference command as closely as possible at all instants in time. In contrast, the other group's control objective is to follow the reference command with some allowable error. A preliminary analysis of the experimental results appears in [98]. We expand on that analysis to examine the effects of a relaxed command-following control objective. We also use the frequency-domain subsystem identification (SSID) algorithm presented in Chapter 2 to model the control strategies (feedforward, feedback, and feedback time delay) that each subject uses on each trial. We use the identification results of this chapter's experiment to improve our understanding of the effects that relaxing the control objectives has on control strategies used by humans.

4.1   Introduction

In human-in-the-loop (HITL) manual tasks, humans manipulate a system, which could be unknown to them, in order to accomplish a certain task that has been given

to them. For instance, a human driver utilizes steering and braking to drive a vehicle along a road path. The control strategies used by humans to accomplish these tasks depend on many factors. One of the most significant factors influencing the human control strategy is the nature of the task that is being accomplished. In the human driver example, the control strategy adopted by the driver depends on the control task in hand; a control strategy employed for a path-following task cannot succeed in an obstacle-avoidance task and vice versa.

There have been many studies investigating a variety of manual tasks, including reaching tasks [7–11,99,100] and grasping tasks [12,13,101–107]. These studies suggest that humans form internal models of the body and the physical world as they learn to accomplish the instructed tasks. Similar results have been suggested by studies that investigate command-following tasks, including compensatory tracking tasks [32, 33, 37, 40, 77, 108–110], pursuit tracking tasks [38, 41, 111–116], and tracking tasks with preview [117–121].

In multiple studies, data from HITL experiments are used to model human control behavior in command-following tasks using SSID techniques [47–49, 71]. The SSID results of those studies suggest that a primary command-following strategy used by humans is adaptive *feedforward inversion*. Specifically, if the LTI system is represented by the transfer function G, then over repeated interactions the human updates its feedforward controller until it approximates G^{-1}. SSID results suggest that feedforward inversion is used for many LTI systems, provided that the command is predictable or a preview of the command is available [93, 94].

Some studies have investigated the impact of changes in the reference command on the control strategies adopted by humans in a command-following task. The results in [58,59] suggest that certain reference commands are more difficult for humans to follow than others. Moreover, these results suggest that as long as the reference command is predictable, adaptive feedforward inversion remains as their primary control strategy,

even after the reference command has changed. However, to the best of our knowledge, so far no study has been conducted to investigate the possible impacts of relaxing the command-following control objectives on human control behavior in a pursuit tracking task. Many real-world human-machine interactions do not require a human operator to strictly follow a reference command, but rather a relaxed command-following is required. For example, the control objective of a human driver usually is not to keep the vehicle on an exact path trajectory along the road at all time, but rather to maintain the vehicle within the boundaries of a certain lane on the road. Therefore, achieving a better understanding of human control behavior when performing a relaxed command-following task could have applications in many real-world HITL technologies.

The main motivation of this chapter is to investigate the effects that relaxing the command-following control objectives potentially has on the control strategies that humans learn to use when interacting with a dynamic system. We present the results of an experiment with 2 groups of 11 subjects, where all subjects interact with the same dynamic system and have the same reference command, but each group has a different control objective. For one group, the control objective is to follow the reference command perfectly, that is, to make a controlled object follow a reference object as closely as possible at all instants in time. For the other group, the control objective is to follow the reference command with some allowable error. Each subject's command-following behavior is modeled by a discrete-time control architecture consisting of a feedback time delay, a linear feedback controller, and a linear feedforward controller. We compare the time-domain performance, frequency-domain performance, and control behavior of these two groups. By comparing the time-domain performance, frequency-domain performance, and control behavior of these two groups, we investigate the effects of relaxing the command-following control objective on control strategies used by human subjects.

4.2 Experimental Methods

Twenty-two volunteers participated in this study. The subjects were 18 to 35 years old and had no known neurological disorder. This study satisfies the U.S. Department of Health and Human Services Code of Federal Regulation for human subject research (45 CFR 46) and was approved by the University of Kentucky Institutional Review Board (IRB number 14-0526-P4K).

The experimental setup is shown in Fig. 4.1. The subjects used a rotational joystick (Teledyne Gurley model 8225-6000-DQSD) to control the motion of an object that is displayed on a computer screen. The computer monitor displays two rectangular markers, one above the other. The top rectangular marker is called the *reference object*, and its horizontal position is denoted r. The bottom rectangular marker is called the *control object*, and its horizontal position is denoted y. The reference object follows a predetermined path, which is the same for all subjects and all trials. The control object's position y is controlled by the joystick's angular position u. The relationship between u and y is governed by a dynamic system, which is numerically simulated by a computer. Prior to performing the experiment, the subjects have no knowledge of the reference object's motion r or the dynamic system relating u and y. The subject's objective is to manipulate the joystick in a manner that makes the control object follow the reference object.

Each subject performes 40 trials of the experiment. A *trial* is a 60-s time period during which a subject operates the joystick, and a *session* consists of 10 consecutive trials completed within a period of 20 minutes. Subjects completed 4 sessions over a 7-day period, but no more than one session in a 12-hour period. For each session, a subjects is placed in an isolated area free from distraction. The subject sits in a chair facing a computer screen, which is located approximately 60 cm from the subject's eyes and measures 47.6 cm high by 26.8 cm wide. The subject's dominant hand is
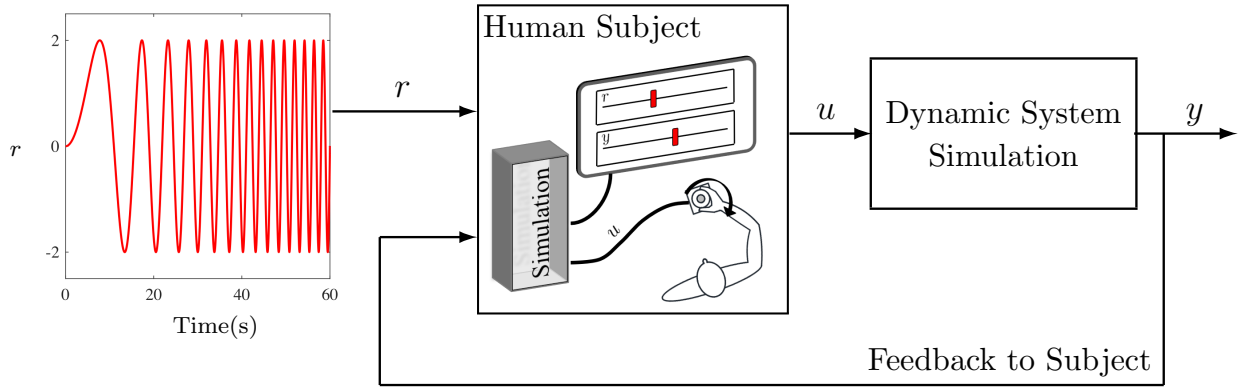
Figure 4.1: Subjects use a rotational joystick to control the position y of the bottom marker displayed on the computer screen. The joystick's angular position u is the control input of an unknown dynamic system, which is simulated by a computer, and the the dynamic system's output is y.

used to manipulate the rotational joystick.

The reference object's position r is a 60-second chirp signal with frequency content between 0 and 0.5 Hz. Specifically, for all $t \in [0, 60]$,

$$r(t) \triangleq 2 \sin\left(\frac{\pi}{120} t^2\right).$$

The control object's position y satisfies the differential equation

$$\dddot{y}(t) + a_2 \ddot{y}(t) + a_1 \dot{y}(t) + a_0 y(t) = b_1 \dot{u}(t) + b_0 u(t),$$

where $a_0 = 6.4$, $a_1 = 9.76$, $a_2 = 5.2$, $b_0 = 7.04$, and $b_1 = 3.2$. Thus, the transfer function from u to y is given by

$$\mathcal{G}(s) \triangleq \frac{3.2(s + 2.2)}{(s + 1.6)(s^2 + 3.6s + 4)},$$

which has poles at -1.6 and $-1.8 \pm j0.87$, and a zero at -2.2. The units of r and y are hash marks (hm), which are equally-spaced vertical lines displayed on the computer screen. The distance between hash marks is 2.5 cm, and the range of motion displayed
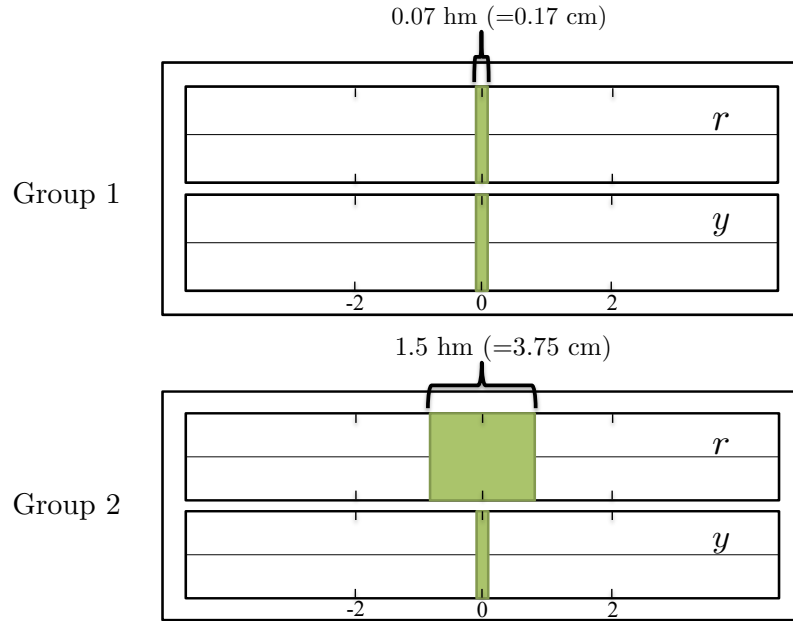
Figure 4.2: Subjects in group 1 have a reference object with width 0.07 hm, while subjects in group 2 have a reference object with width 1.5 hm.

on the computer screen is ± 8 hm.

The 22 subjects were randomly divided into two groups, where each group had 11 subjects. To examine the effects of relaxing the command-following control objective, the reference object is different for the two groups. The width of the reference object for *group 1* is 0.07 hm (i.e., 0.17 cm), and the width of the reference object for *group 2* is 1.5 hm (i.e., 3.75 cm). Figure 4.2 depicts the computer screen interface for both groups.

Subjects in group 1 were instructed to manipulate the joystick such that the control object and the reference object maintain the same position. Subjects in group 2 were instructed to manipulate the joystick such that the control object remains between the boundaries of the reference object. Thus, group 1 subjects have a command-following control objective, whereas group 2 subjects have a relaxed command-following control objective.

Table 4.1: Number of divergent trials for each group

	Trials 1–10	Trials 11–20	Trials 21–30	Trials 31–40	Total
Group 1	0	1	0	0	1
Group 2	6	4	0	0	10

4.3 Performance Analysis

A *divergent trial* is defined as a trial in which the magnitude of y_k exceeds 8 hm, that is, the controlled object's position exceeds the range of motion displayed on the computer screen. Table 4.1 shows the number of divergent trials for each group. There was only one divergent trial among 440 trials of group 1. In 440 trials of group 2, there were 10 divergent trials. All divergent trials occurred before trial 20 and are omitted from the results.

The time signals r, y, and u are sampled for all subjects and all trials with sample time $T_{\mathrm{s}} = 0.02$ s and number of samples $N_{\mathrm{s}} = 3001$. The sampled data obtained from r, u, and y yield the discrete signals $\{r_k\}_{k=1}^{N_{\mathrm{s}}}$, $\{y_k\}_{k=1}^{N_{\mathrm{s}}}$, and $\{u_k\}_{k=1}^{N_{\mathrm{s}}}$.

4.3.1 Time-Domain Analysis

The *command-following performance* is for $k = 1, \ldots, N_{\mathrm{s}}$,

$$z_{1,k} \triangleq r_k - y_k.$$

The objective of group 1 subjects is to make $z_{1,k} = 0$. The *relaxed command-following performance* is for $k = 1, \ldots, N_{\mathrm{s}}$,

$$
z_{2,k} \triangleq \begin{cases}
z_{1,k} - 0.75, & \text{if } z_{1,k} \in (0.75, \infty) \\
0, & \text{if } z_{1,k} \in [-0.75, 0.75] \\
z_{1,k} + 0.75, & \text{if } z_{1,k} \in (-\infty, -0.75)
\end{cases},
$$

65

Table 4.2: Mean $\|z_1\|$ and its percentage change from the first 10 trials to the last 10 trials.

	Trials 1–10	Trials 11–20	Trials 21–30	Trials 31–40	Change (%)
Group 1	0.646	0.454	0.406	0.346	-46.5
Group 2	0.857	0.667	0.600	0.545	-36.4

which is the value obtained by passing the error $z_{1,k}$ through a deadzone function that has a deadzone on the interval $[-0.75,\, 0.75]$. This deadzone corresponds to the width of the reference object for group 2. The objective of group 2 subjects is to make $z_{2,k} = 0$.

We define for each trial the *time-averaged performance*

$$\|z_1\| \triangleq \frac{1}{N_s} \sum_{k=1}^{N_s} |z_{1,k}|,$$

which is the time average of the signal $z_{1,k}$. Table 4.2 shows the mean $\|z_1\|$ on 4 different sets of trials for group 1 and group 2 and its percentage change from the first 10 trials to the last 10 trials. For both groups the mean $\|z_1\|$ decreases over the trials. This decrease, however, is more evident for subjects in group 1 than subjects in group 2. Figure 4.3 shows group statistical properties of $\|z_1\|$ for all trials. For both groups, the mean and median $\|z_1\|$ decrease over the 40 trials. The mean $\|z_1\|$ of group 1 is smaller than the mean $\|z_1\|$ of group 2 on every trial. Thus, as expected, group 1 outperforms group 2 in the non-relaxed command-following objective.

We define for each trial the *time-averaged relaxed performance*

$$\|z_2\| \triangleq \frac{1}{N_s} \sum_{k=1}^{N_s} |z_{2,k}|,$$

which is the time average of the signal $z_{2,k}$. Table 4.3 shows the mean $\|z_2\|$ on 4 different sets of trials for group 1 and group 2 and its percentage change from the first 10 trials to the last 10 trials. For both groups the mean $\|z_2\|$ decreases over the

Figure 4.3: Mean, median, first quartile, and third quartile of $\|z_1\|$ on each trial. For both groups, the mean and median $\|z_1\|$ improve over the 40 trials. The mean $\|z_1\|$ for group 1 is smaller than that of group 2 over all trials. $\bullet$ is the mean, and the boxplot shows the median, first quartile, and third quartile.

Table 4.3: Mean $\|z_2\|$ and its percentage change from the first 10 trials to the last 10 trials.

	Trials 1–10	Trials 11–20	Trials 21–30	Trials 31–40	Change (%)
Group 1	0.235	0.110	0.086	0.055	-76.8
Group 2	0.391	0.244	0.207	0.165	-57.8

trials. However, this decrease is more evident for subjects in group 1 than subjects in group 2. Figure 4.4 shows group statistical properties of $\|z_2\|$ on each trial. The mean and median $\|z_2\|$ decrease over the 40 trials for both groups. The mean $\|z_2\|$ of subjects in group 1 is smaller than that of subjects in group 2 on every trial. The mean $\|z_2\|$ can be considered as a measure of group 2's performance of keeping the controlled object between the outer edges of the reference object. Thus, group 1 also outperforms group 2 in the relaxed command-following objective.

Figure 4.5 shows r_k, y_k, and $z_{1,k}$ on the first and last trial for the median performer

Figure 4.4: Mean, median, first quartile, and third quartile of $\|z_2\|$ on each trial. For both groups, the mean and median $\|z_2\|$ improve over the 40 trials. The mean $\|z_2\|$ for group 1 is smaller than that of group 2 over all trials. $\bullet$ is the mean, and the boxplot shows the median, first quartile, and third quartile.

in group 1. The median performer of group 1 is the subject whose $\|z_1\|$ on the last trial is the median (i.e., 6th best) of all subjects in their group. Similarly, Fig. 4.6 shows r_k, y_k, and $z_{2,k}$ on the first and last trial for the median performer in group 2. The median performer of group 2 is the subject whose $\|z_2\|$ on the last trial is the median (i.e., 6th best) of all subjects in their group. The median subject for both groups performs better on the last trial than the first trial. All subjects in both groups exhibit improved performance from their first to last trial. Similar results are observed for all other subjects.

Next, we define for each trial the *control effort*

$$\|u\| \triangleq \frac{1}{N_{\mathrm{s}}} \sum_{k=1}^{N_{\mathrm{s}}} |u_k|,$$

which is the time average of the control signal u_k. A subject's *steady-state control*
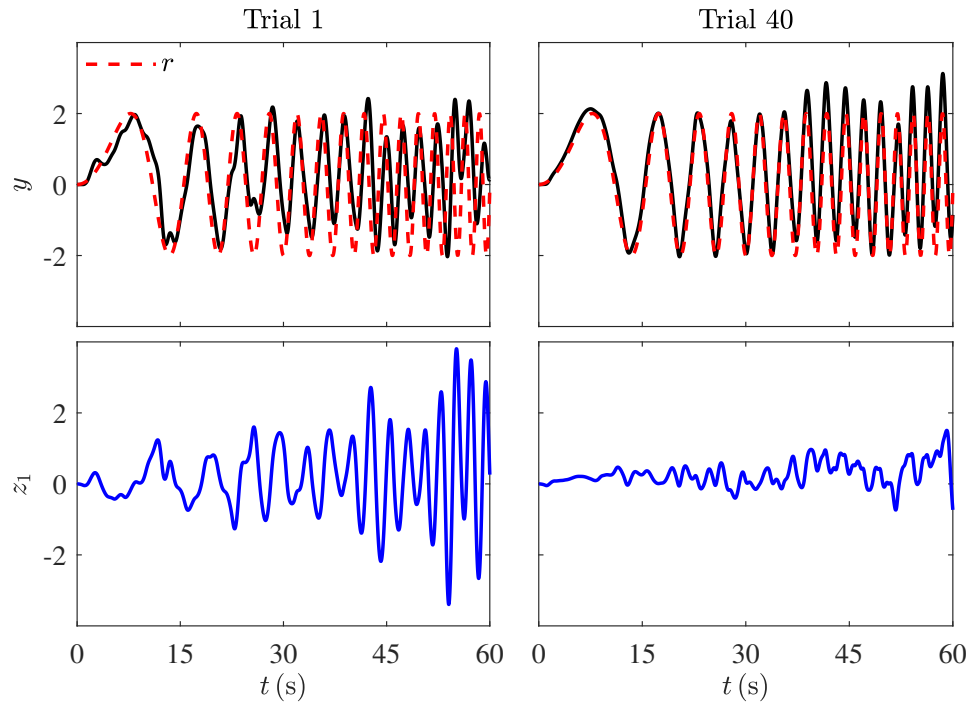
Figure 4.5: The reference r_k, output y_k, and command-following error $z_{1,k}$ for the group 1's median subject's 1st and 40th trial.
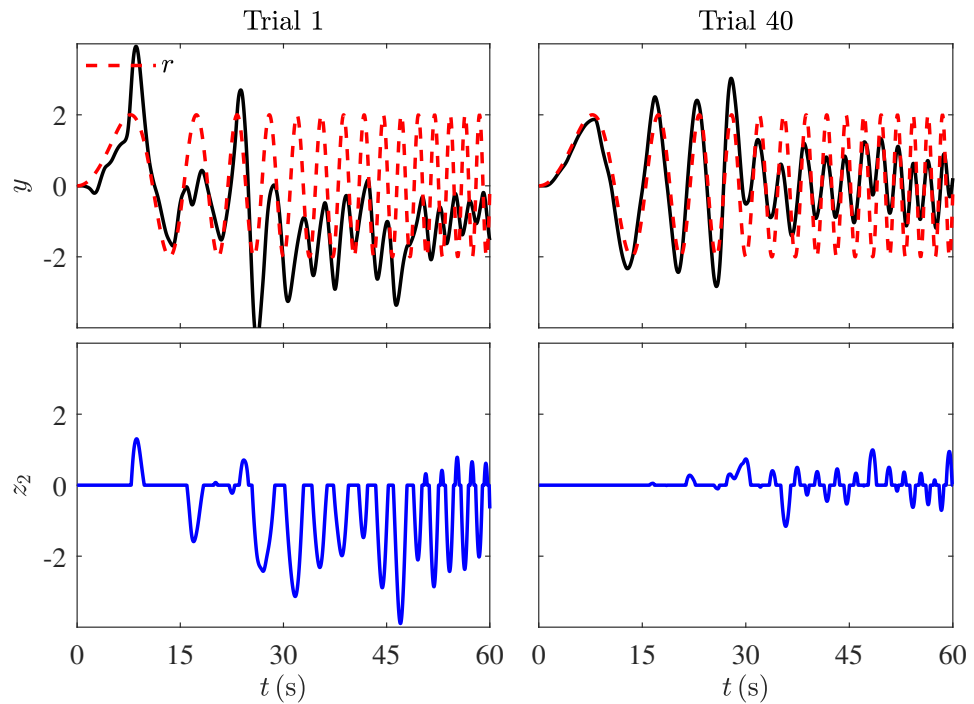
Figure 4.6: The reference r_k, output y_k, and relaxed command-following error $z_{2,k}$ for group 2's median subject's 1st and 40th trial.
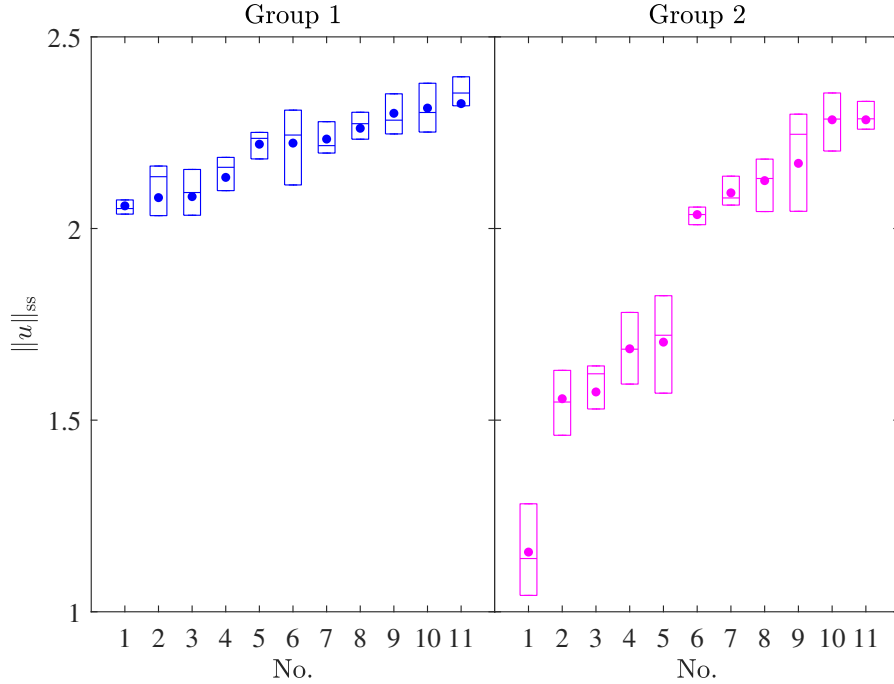
Figure 4.7: Mean, median, first quartile, and third quartile of $\|u\|$ for each subject over the last 10 trials. The mean $\|u\|$ over the last 10 trials for 5 subjects in group 2 fall below that of all subjects in group 1 and the rest of subjects in group 2. $\bullet$ is the mean, the boxplot shows the median, first quartile and third quartile, and the whiskers show the minimum and maximum.

effort $\|u\|_{\mathrm{ss}}$ is defined as their mean $\|u\|$ over their last 10 trials. Note from Fig. 4.3 and Fig. 4.4 that for both groups the mean $\|z_1\|$ and $\|z_2\|$ do not change significantly over the last 10 trials, suggesting that the subjects reach near-steady-state performance. Thus, $\|u\|_{\mathrm{ss}}$ is a measure of a subject's control effort upon learning to control the dynamic system.

Figure 4.7 shows statistical properties of $\|u\|_{\mathrm{ss}}$ for each subject in ascending order. Of the 11 subjects within group 2, 5 have a significantly smaller steady-state control effort compared to other subjects in group 2, as well as all 11 subjects in group 1. For the rest of this chapter, we refer to those 5 subjects as group 2b, and the remaining 6 subjects in group 2 are referred to as group 2a.

Figure 4.8 shows group 1, group 2a, and group 2b statistical properties of $\|z_1\|$ on each trial. For all three groups, the mean and median $\|z_1\|$ decrease over the 40 trials.

70
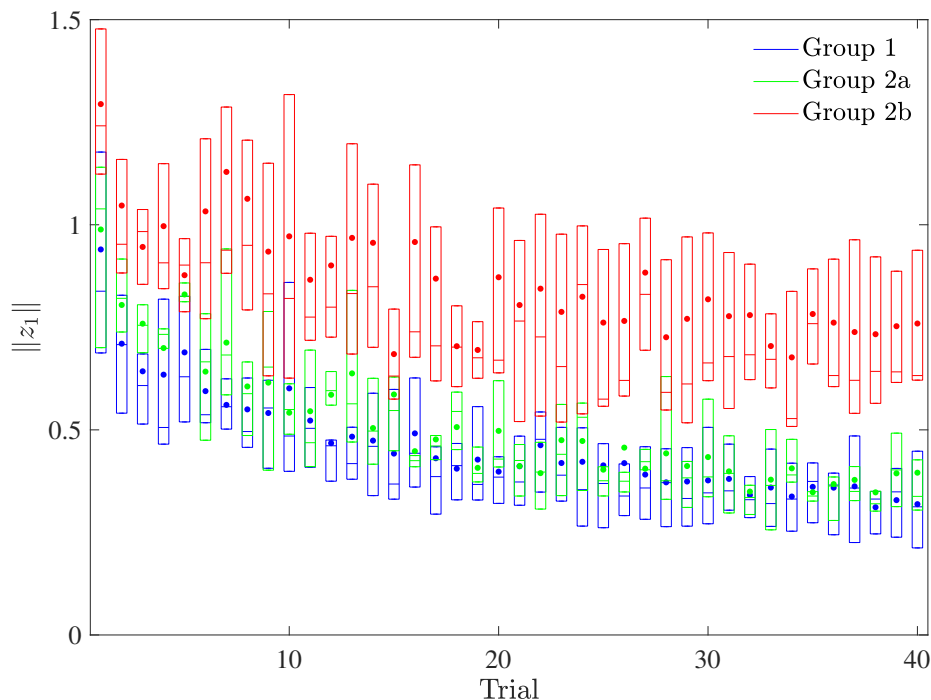
Figure 4.8: Mean, median, first quartile, and third quartile of $\|z_1\|$ on each trial. For all groups, the mean and median $\|z_1\|$ improve over the 40 trials. The mean $\|z_1\|$ for groups 1 and 2a are smaller than that of group 2b. ● is the mean, and the boxplot shows the median, first quartile, and third quartile.

The mean $\|z_1\|$ for groups 1 and 2a are smaller than the mean $\|z_1\|$ of group 2b on every trial. Moreover, the group 2a mean and interquartile range are more similar to those of group 1 than group 2b. For groups 1 and 2a, the interquartile range (i.e., the difference between third and first quartile) decreases from trial 1 to trial 40. In contrast, the interquartile range for group 2b is relatively constant over the trials. This result suggests that, in contrast to group 2b subjects, group 2a subjects attempt to follow the center of the reference object and thus adopt the same non-relaxed command-following objective as group 1 subjects. Group 2b also shows a larger variance in $\|z_1\|$ on 92.5 % of the trials compared to group 1 and on 97.5 % of the trials compared to group 2a. The same results can be seen in Table 4.4, which shows the mean $\|z_1\|$ on 4 different sets of trials for group 1, group 2a, and group 2b and its percentage change from the first 10 trials to the last 10 trials.

A one-way ANOVA on mean $\|z_1\|$ over all trials for subjects in groups 1, 2a, and 2b

Table 4.4: Mean $\|z_1\|$ and its percentage change from the first 10 trials to the last 10 trials.

	Trials 1–10	Trials 11–20	Trials 21–30	Trials 31–40	Change (%)
Group 1	0.646	0.454	0.406	0.346	-46.5
Group 2a	0.720	0.520	0.431	0.376	-47.7
Group 2b	1.030	0.847	0.799	0.747	-27.5

shows a significant difference at the $p < 0.01$ level ($F_{2,19} = 9.17$, $p = 1.63 \times 10^{-3}$). Post hoc comparisons between group 2b and group 1 and between group 2b and group 2a using the Tukey HSD test yield $p = 1.42 \times 10^{-3}$ and $p = 9.87 \times 10^{-3}$, respectively. Thus, the mean time-averaged error over all trials for subjects in group 2b ($M = 0.87$, $SD = 0.32$) is significantly different than that of subjects in group 1 ($M = 0.46$, $SD = 0.13$) and group 2a ($M = 0.51$, $SD = 0.09$) at the $p < 0.01$ level. However, the post hoc comparison between group 1 and group 2a yields $p = 0.88$, which shows that there is no significant statistical difference between the two groups.

Figure 4.9 demonstrates the mean, median, first quartile, and third quartile of $\|z_2\|$ for subjects in group 1, group 2a, and group 2b on each trial. The mean and median $\|z_2\|$ improve over the 40 trials for all three groups. The average $\|z_2\|$ of subjects in groups 1 and 2a are better than that of subjects in group 2b on every trial. For groups 1 and 2a, the interquartile range decreases from trial 1 to trial 40. However, the interquartile range for group 2b is relatively constant over the trials. The same results can be seen in Table 4.5, which shows the mean $\|z_2\|$ on 4 different sets of trials for group 1, group 2a, and group 2b and its percentage change from the first 10 trials to the last 10 trials. These results provide more evidence in support of the idea that subjects in group 2a adopt the same non-relaxed command-following objective as group 1 subjects.

A one-way ANOVA on mean $\|z_2\|$ over all trials for subjects in groups 1, 2a, and 2b shows a significant difference at the $p < 0.01$ level ($F_{2,19} = 7.16$, $p = 4.80 \times 10^{-3}$). Post hoc comparisons between group 2b and group 1 and between group 2b and group 2a
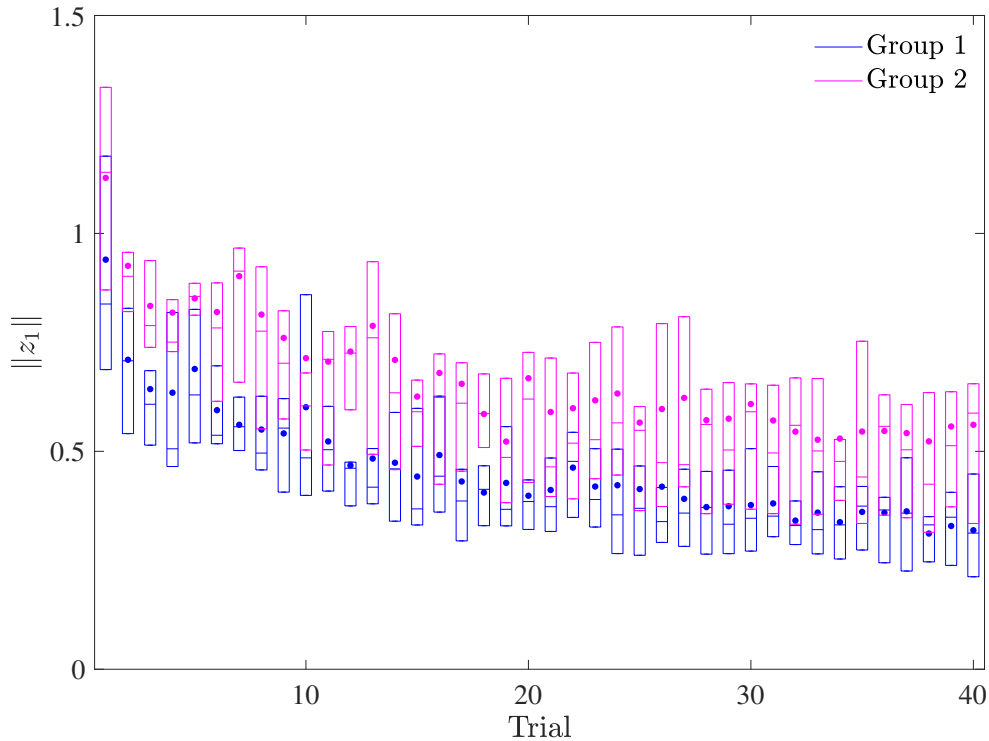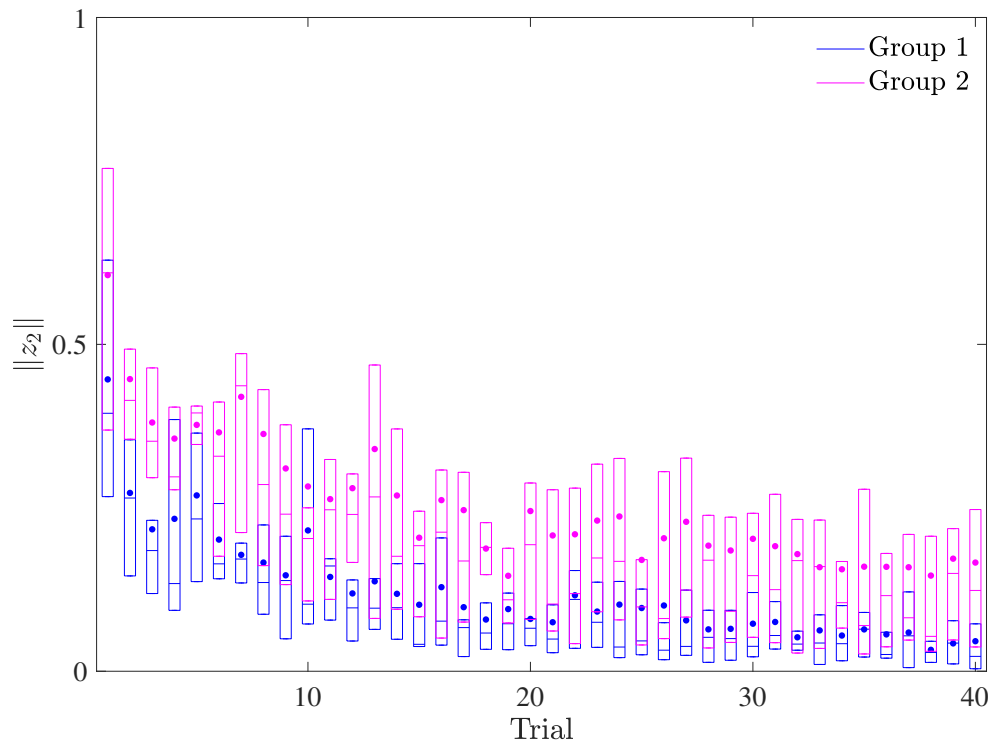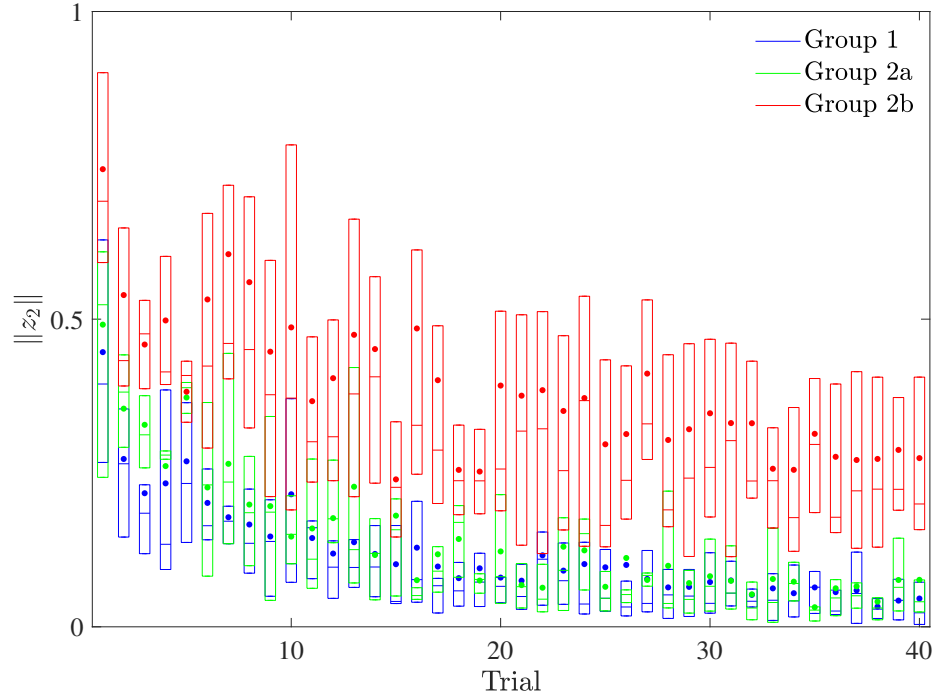
Figure 4.9: Mean, median, first quartile, and third quartile of $\|z_2\|$ on each trial. For all groups, the mean and median $\|z_2\|$ improve over the 40 trials. The mean $\|z_2\|$ for groups 1 and 2a are smaller than that of group 2b. $\bullet$ is the mean, and the boxplot shows the median, first quartile, and third quartile.

Table 4.5: Mean $\|z_2\|$ and its percentage change from the first 10 trials to the last 10 trials.

	Trials 1–10	Trials 11–20	Trials 21–30	Trials 31–40	Change (%)
Group 1	0.235	0.110	0.086	0.055	-76.8
Group 2a	0.284	0.140	0.090	0.063	-77.8
Group 2b	0.525	0.372	0.348	0.287	-45.4
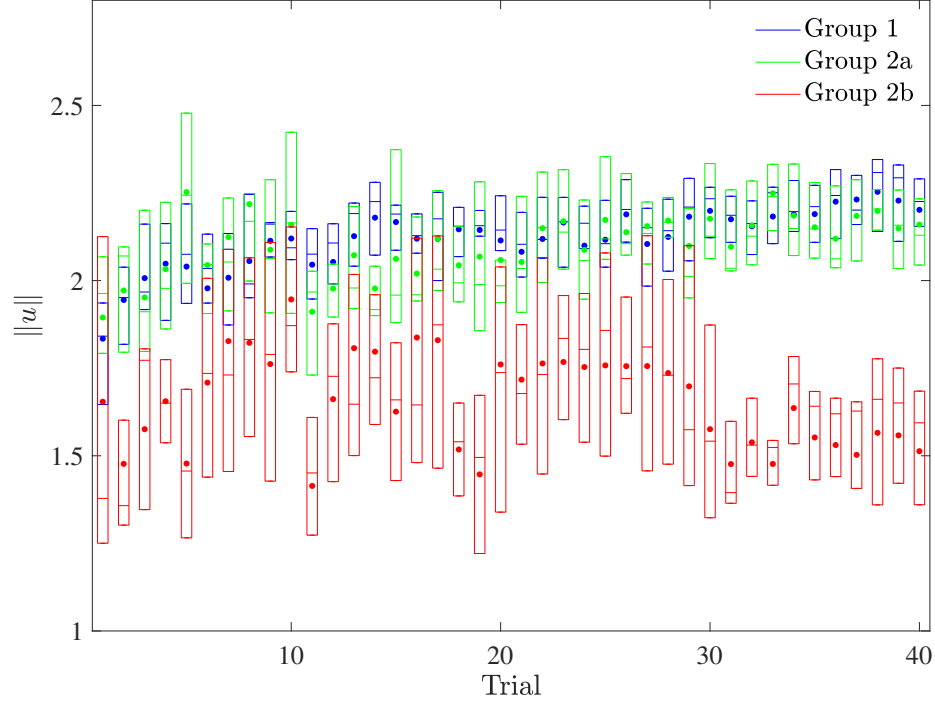
Figure 4.10: Mean, median, first quartile, and third quartile of $\|u\|$ on each trial. The mean and median $\|u\|$ for groups 1, 2a, and 2b suggest that subjects in group 2b learn to use less control effort over the 40 trials compared to subjects in groups 1 and 2a. • is the mean, and the boxplot shows the median, first quartile, and third quartile.

using the Tukey HSD test yield $p = 4.56 \times 10^{-3}$ and $p = 1.87 \times 10^{-2}$, respectively. Thus, the mean time-averaged relaxed error over all trials for subjects in group 2b ($M = 0.40$, $SD = 0.27$) is significantly different than that of subjects in group 1 ($M = 0.12$, $SD = 0.08$) and group 2a ($M = 0.14$, $SD = 0.06$) at the $p < 0.02$ level. However, the post hoc comparison between group 1 and group 2a yields $p = 0.95$, which shows that there is no significant statistical difference between the two groups.

The mean, median, first quartile, and third quartile of $\|u\|$ for subjects in group 1, group 2a, and group 2b on each trial are shown in Fig. 4.10. The mean and median control effort used by subjects in groups 1 and 2a increase over the trials. The subjects in group 2b consistently use a lower control effort than the subjects in the other two groups. Moreover, their control effort decreases as they continue to learn to control the dynamic system and reaches a steady state over the last 10 trials.

A one-way analysis of variance (ANOVA) was performed on mean $\|u\|$ over all

40 trials for subjects in groups 1, 2a, and 2b. This analysis indicates a significant difference at the $p < 0.01$ level ($F_{2,19} = 11.67$, $p = 4.94 \times 10^{-4}$). Post hoc comparisons between group 2b and group 1 and between group 2b and group 2a using the Tukey HSD test yield $p = 5.27 \times 10^{-4}$ and $p = 2.35 \times 10^{-3}$, respectively. Thus, the mean control effort over all trials for subjects in group 2b ($M = 1.67$, $SD = 0.34$) is significantly different than the mean control effort over all trials for subjects in group 1 ($M = 2.12$, $SD = 0.11$) and group 2a ($M = 2.10$, $SD = 0.10$) at the $p < 0.01$ level. In contrast, the post hoc comparison between group 1 and group 2a yields $p = 0.98$, which indicates that there is no significant statistical difference between the two groups.

4.3.2 Frequency-Domain Analysis

For all $i = 1, ..., N_f$, let $\omega_i \triangleq (i - 1)\pi/30$ rad/s, which are $N_f = 31$ evenly-spaced frequencies over the 0-0.5 Hz range. For each trial, let $r_{\mathrm{dft}}(\omega_i)$ and $y_{\mathrm{dft}}(\omega_i)$ denote the discrete Fourier transforms (DFT) of the sequences $\{r_k\}_{k=1}^{N_s}$ and $\{y_k\}_{k=1}^{N_s}$ at ω_i, respectively.

For each trial, we define the *frequency-averaged magnitude error* as

$$
\begin{aligned}
E_{\mathrm{m}} &\triangleq \frac{1}{N_f} \sum_{i=1}^{N_f} \left| |y_{\mathrm{dft}}(\omega_i)| e^{\jmath \angle r_{\mathrm{dft}}(\omega_i)} - |r_{\mathrm{dft}}(\omega_i)| e^{\jmath \angle r_{\mathrm{dft}}(\omega_i)} \right| \\
&= \frac{1}{N_f} \sum_{i=1}^{N_f} \left| |y_{\mathrm{dft}}(\omega_i)| - |r_{\mathrm{dft}}(\omega_i)| \right|,
\end{aligned}
$$

which is the frequency-averaged magnitude of the difference between y_{dft} and r_{dft}, assuming the phase of y_{dft} is the same as the phase of r_{dft}. Similarly, for each trial, we define the *frequency-averaged phase error* as

$$
E_{\mathrm{p}} \triangleq \frac{1}{N_f} \sum_{i=1}^{N_f} \left| |r_{\mathrm{dft}}(\omega_i)| e^{\jmath \angle y_{\mathrm{dft}}(\omega_i)} - |r_{\mathrm{dft}}(\omega_i)| e^{\jmath \angle r_{\mathrm{dft}}(\omega_i)} \right|
$$

$$= \frac{1}{N_{\mathrm{f}}} \sum_{i=1}^{N_{\mathrm{f}}} |r_{\mathrm{dft}}(\omega_i)| \left| e^{\jmath \angle y_{\mathrm{dft}}(\omega_i)} - e^{\jmath \angle r_{\mathrm{dft}}(\omega_i)} \right|,$$

which is the frequency-averaged magnitude of the difference between y_{dft} and r_{dft}, assuming the magnitude of y_{dft} is the same as the magnitude of r_{dft}.

Figure 4.11 shows the mean, median, first quartile, and third quartile of E_{m} and E_{p} for subjects in group 1, group 2a, and group 2b on each trial. These results support what we had previously seen in our time-domain analysis. Subjects in group 1 and group 2a show similar trends in both frequency-averaged magnitude error and frequency-averaged phase error. For both these groups, the mean E_{m} and the mean E_{p} decrease over 40 trials. While the same decreasing trend can be seen in group 2b, their mean E_{m} and mean E_{p} are much larger compared to the other groups. Moreover, E_{p} for group 2b has a large interquartile range which does not get smaller over the trials.

Tables 4.6 and 4.7 show the mean E_{m} and E_{p} on 4 different sets of trials for group 1, group 2a, and group 2b. For all three groups, the mean E_{m} and mean E_{p} decrease over the trials. This means that subjects in all three groups match the magnitude and the phase of reference command better on the later trials compared to the earlier trials. This decrease, however, is more evident for subjects in group 1 and group 2a. These results also suggest that the improvement we had previously seen in the command-following performance of the subjects in group 1 and group 2a is more a result of their improvement in matching the phase of reference command than their improvement in matching the magnitude. For group 2b, on the other hand, the distribution is relatively even.

4.4 Subsystem Identification Results and Discussion

We apply the frequency-domain SSID algorithm described in Chapter 2 to the time-domain data obtained from the subjects in all three groups. Each subject's control
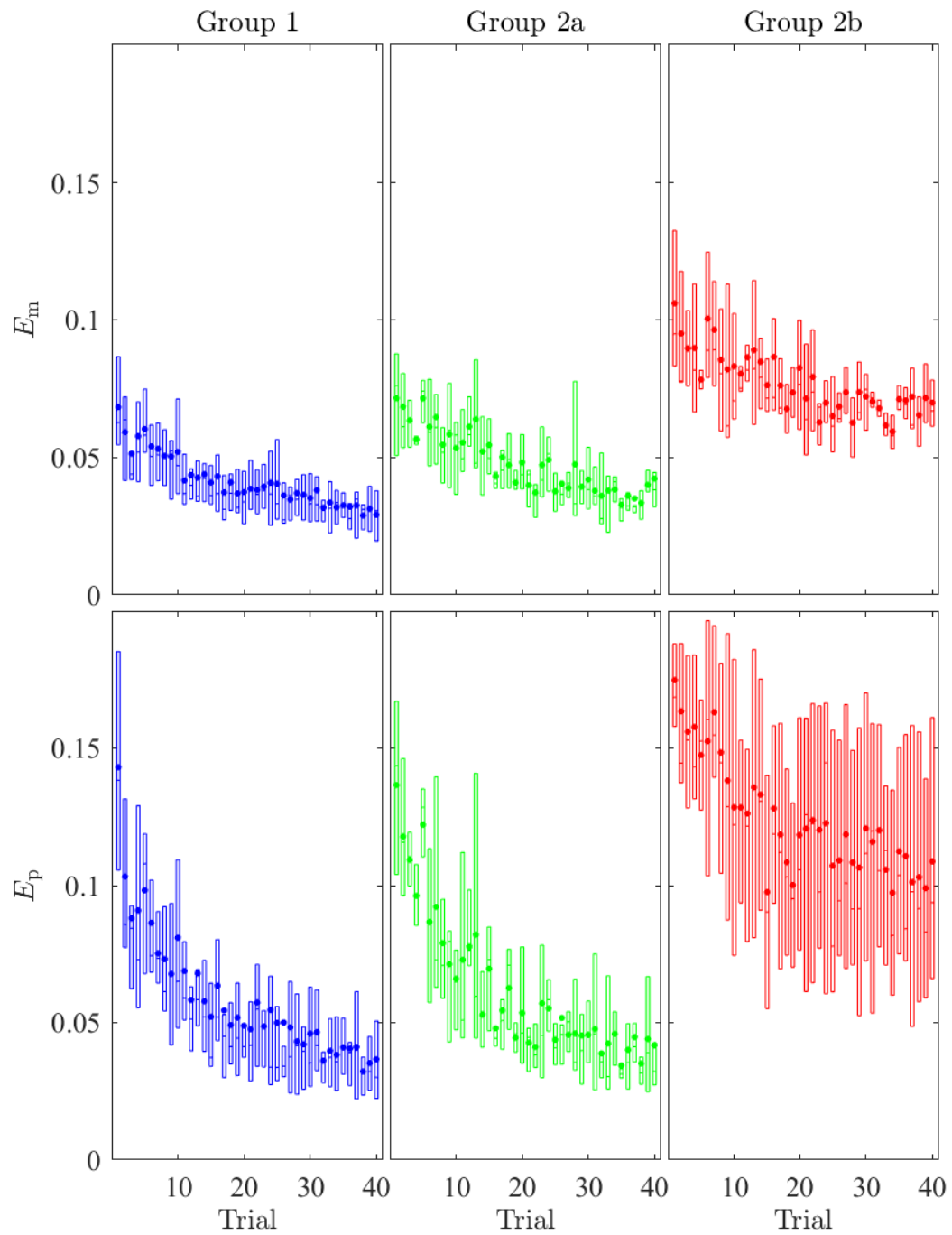
Figure 4.11: Mean, median, first quartile, and third quartile of E_m and E_p. ● is the mean, and the boxplot shows the median, first quartile, and third quartile.

Table 4.6: Mean E_m and its percentage change from the first 10 trials to the last 10 trials.

	Trials 1–10	Trials 11–20	Trials 21–30	Trials 31–40	Change (%)
Group 1	0.056	0.041	0.038	0.032	-42.2
Group 2a	0.062	0.052	0.042	0.037	-40.7
Group 2b	0.091	0.080	0.070	0.068	-25.0

Table 4.7: Mean E_p and its percentage change from the first 10 trials to the last 10 trials.

	Trials 1–10	Trials 11–20	Trials 21–30	Trials 31–40	Change (%)
Group 1	0.091	0.057	0.049	0.039	-57.3
Group 2a	0.098	0.062	0.047	0.041	-57.5
Group 2b	0.153	0.119	0.116	0.107	-29.8
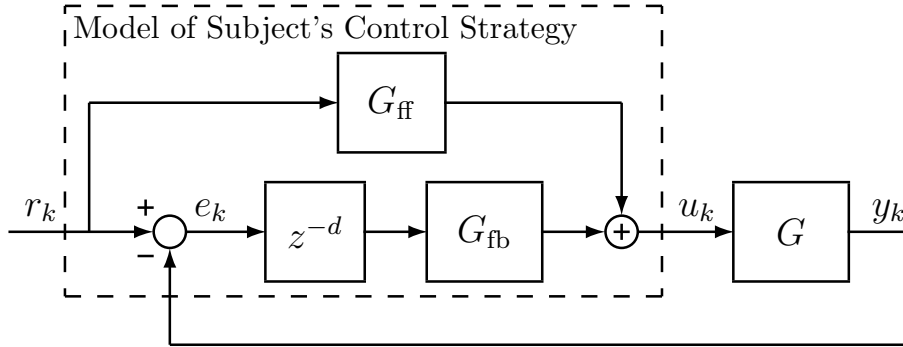
Figure 4.12: A time-invariant system, where the input r_k, the output y_k, and the signals v_k and u_k are accessible, but all internal signals are inaccessible.

strategy is modeled by the linear time-invariant (LTI) control structure shown in Fig. 4.12, where $G(z)$ is the discrete-time transfer function obtained by discretizing $\mathcal{G}(s)$ using a zero-order hold on the input with sample time $T_\mathrm{s} = 0.02\,\mathrm{s}$.

For each subject on each trial (880 trials in total) we identify the feedback time delay T_d, the feedback transfer function G_fb, and the feeforward transfer function G_ff. The candidate pool Γ contains approximately 50 million candidate pairs (d, G_fb) and captures a wide range control behavior over the 0-to-0.5 Hz frequency range of the

command (3.1). Since sensory feedback time delay for humans is in the range 80 ms to 500 ms [33,41,96,97], and the sampling rate for the experiments is 20 ms, the candidate pool includes all $\delta \in \{4, 5, \cdots, 25\}$. The candidate feedback transfer functions G_{fb} are second order relative degree one with monic denominator (i.e., $n_{\mathrm{fb}} = 1$, and $d_{\mathrm{fb}} = 2$). The parameters of candidate feedback controller are designed such that the zero and poles of the candidate feedback transfer functions G_{fb} lie inside the unit circle. More specific details on the candidate pool are provided in Appendix A. The feedforward transfer function G_{ff} is a 2nd-order FIR. These orders are selected to allow for large range of control behavior, including high gain in feedback and dynamic inversion in feedforward. The SSID algorithm is implemented using parallel computation on a supercomputer. A validation analysis of the identification results is presented in Appendix B.2.

4.4.1 Discussion of Group 1 and Group 2a Results

For each identified feedback transfer function, we define

$$\|G_{\mathrm{fb}}\| \triangleq \frac{1}{\pi} \int_0^{\pi} \left| G_{\mathrm{fb}}(e^{\omega T_{\mathrm{s}}}) \right| \, \mathrm{d}\omega,$$

which is the frequency-averaged magnitude of the feedback transfer function over the 0-to-0.5 Hz range of the command r. Figure 4.13 shows the trial-by-trial mean, median, first quartile, and third quartile of $\|G_{\mathrm{fb}}\|$ for subjects in group 1 and group 2a. For both groups, the frequency-averaged feedback gain used by subjects tends to increase over the first 10 trials. These results may indicate that over the first 10 trials, subjects in both groups learn to use a higher feedback gain without causing closed-loop system instability.

Figure 4.14 shows mean, median, first quartile, and third quartile of the identified feedback time delay T_{d} on each trial for all subjects in group 1 and group 2a. The
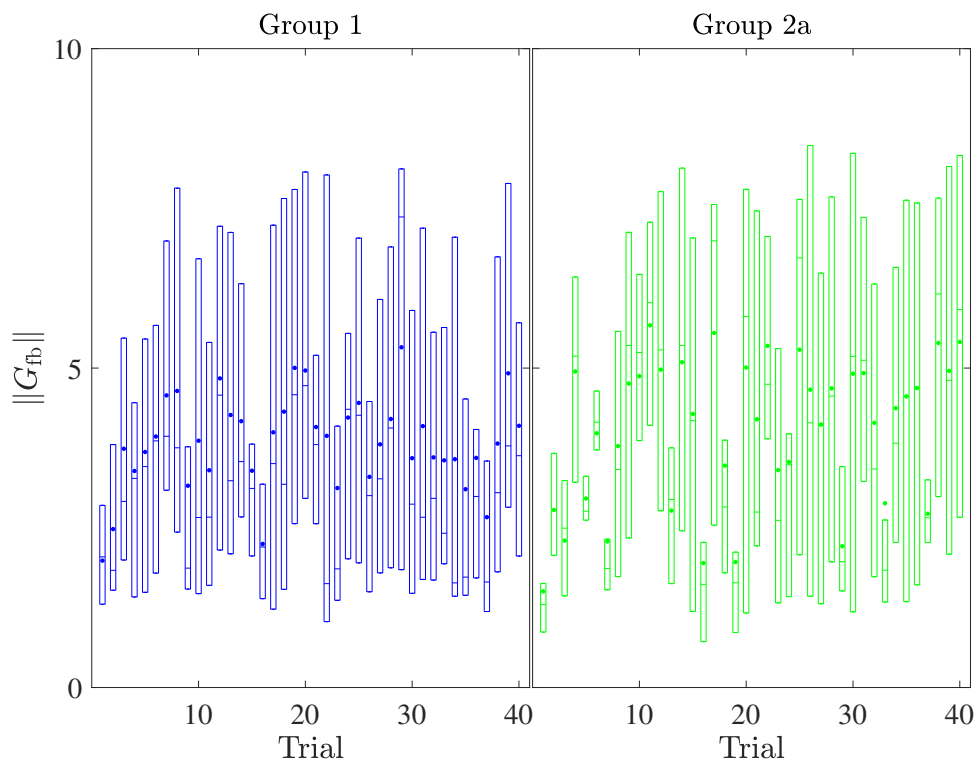
Figure 4.13: Mean, median, first quartile, and third quartile of $\|G_{\text{fb}}\|$ on each trial of subjects in group 1 and group 2a. The mean $\|G_{\text{fb}}\|$ tends to increase over the first 10 trials. ● is the mean, and the boxplot shows the median, first quartile, and third quartile.

mean identified feedback time delay for both groups remains relatively constant. The average identified feedback time delay T_{d} over all 40 trials for subjects in groups 1 and 2a are 241 and 221 ms, respectively.

Next, for each identified feedforward transfer function, we define

$$\|G_{\text{ff}}G - 1\| \triangleq \frac{1}{\pi} \int_0^\pi \left| G_{\text{ff}}(e^{\jmath \omega T_{\text{s}}}) G(e^{\jmath \omega T_{\text{s}}}) - 1 \right| \mathrm{d}\omega,$$

which the frequency-averaged magnitude of the difference between G_{ff} and G^{-1} over the 0-to-0.5 Hz frequency range. Figure 4.15 shows the trial-by-trial mean, median, first quartile, and third quartile of $\|G_{\text{ff}}G - 1\|$ of group 1 and group 2a. The average of $\|G_{\text{ff}}G - 1\|$ for both groups have a similar trend and decrease over the 40 trials.

Figures 4.16 and 4.17 demonstrate the average Bode plot over the 0-to-0.5 Hz frequency range of the identified feedforward transfer function on the first and last
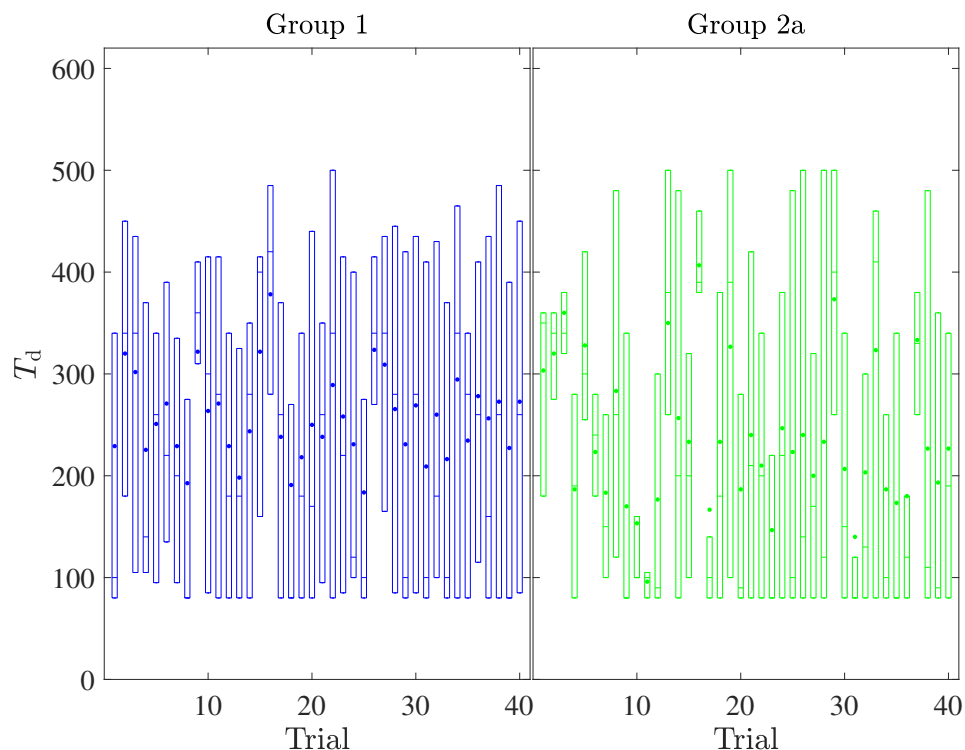
Figure 4.14: Mean, median, first quartile, and third quartile of T_d on each trial of subjects in group 1 and group 2a. The mean identified feedback time delay remains relatively constant for both groups. ● is the mean, and the boxplot shows the median, first quartile, and third quartile.

trial of groups 1 and 2a, respectively. For both groups, the identified feedforward controllers better approximate the inverse of dynamic system on the last trial than on the first trial. These results suggest that feedforward dynamic inversion is the primary control strategy that subjects in groups 1 and 2a learn to use after 40 trials.

4.4.2 Discussion of Group 2b Results

As we saw in Figs. 4.7 and 4.10, the control behavior of subjects in group 2b is different than the control behavior of subjects in the other two groups. This difference is also evident in the feedforwad SSID results of the subjects in group 2b. Figure 4.18 demonstrates the average Bode plot over the 0-to-0.5 Hz frequency range of the identified feedforward transfer function G_{ff} on the first and last trial of group 2b. Unlike the other two groups, for subjects in group 2b, the average identified feedforward controller on the last trial does not resemble the inverse of dynamic system. Figure 4.19

81
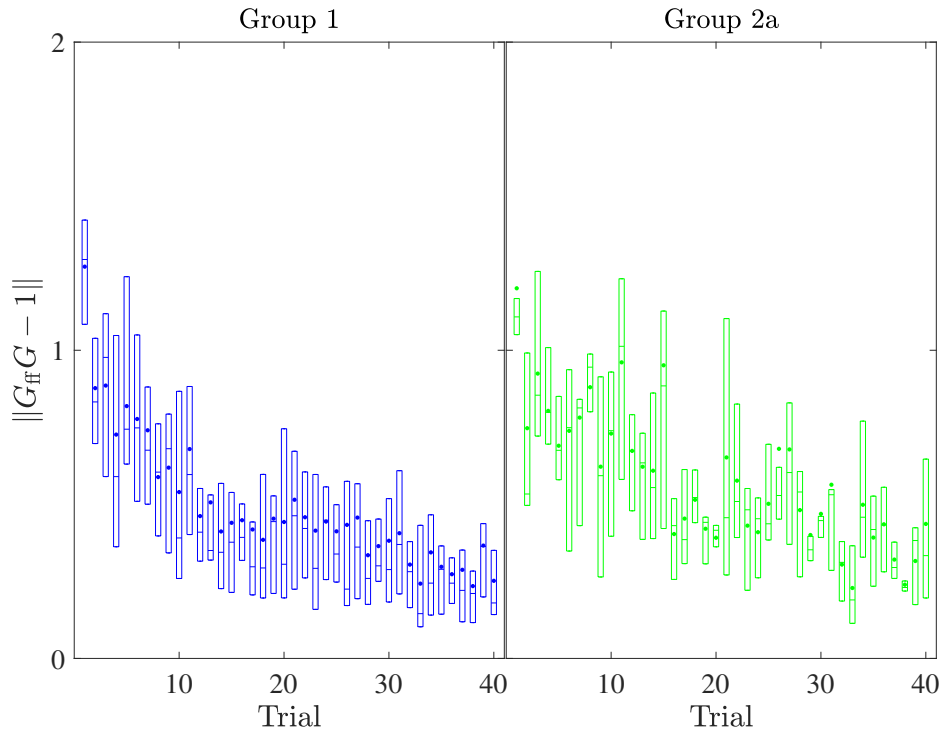
Figure 4.15: Mean, median, first quartile, and third quartile of $\|G_{ff}G-1\|$ on each trial of subjects in group 1 and group 2a. The difference between G_{ff} and G^{-1} decreases over the 40 trials for both groups. $\bullet$ is the mean, and the boxplot shows the median, first quartile, and third quartile.
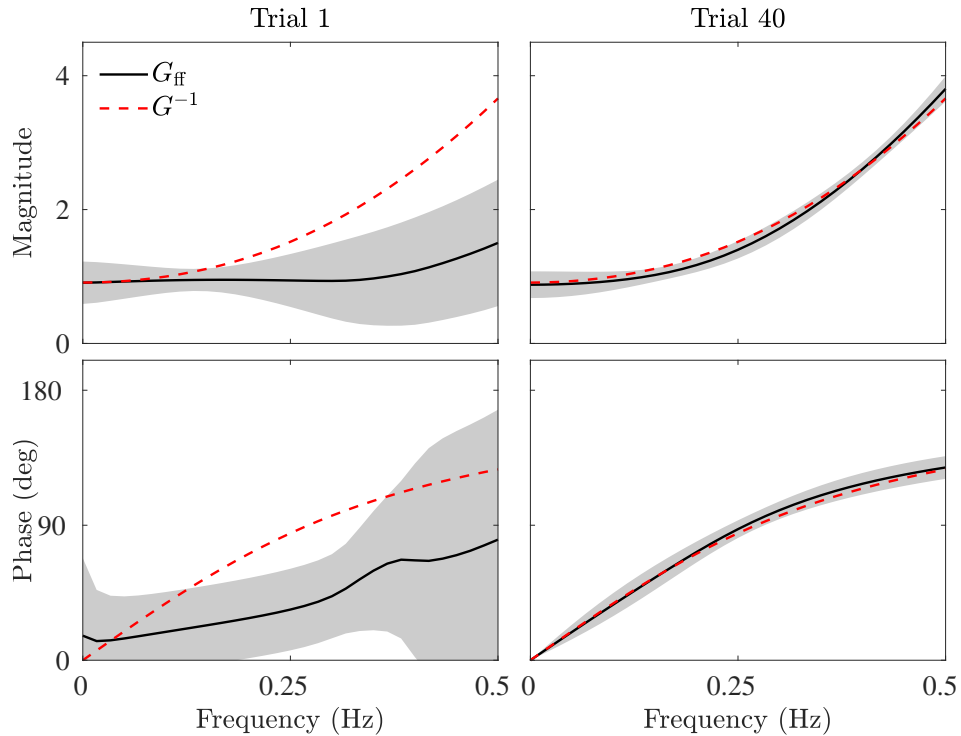
Figure 4.16: The average identified feedforward controller on trials 1 and 40 for group 1. The shaded region shows one standard deviation.
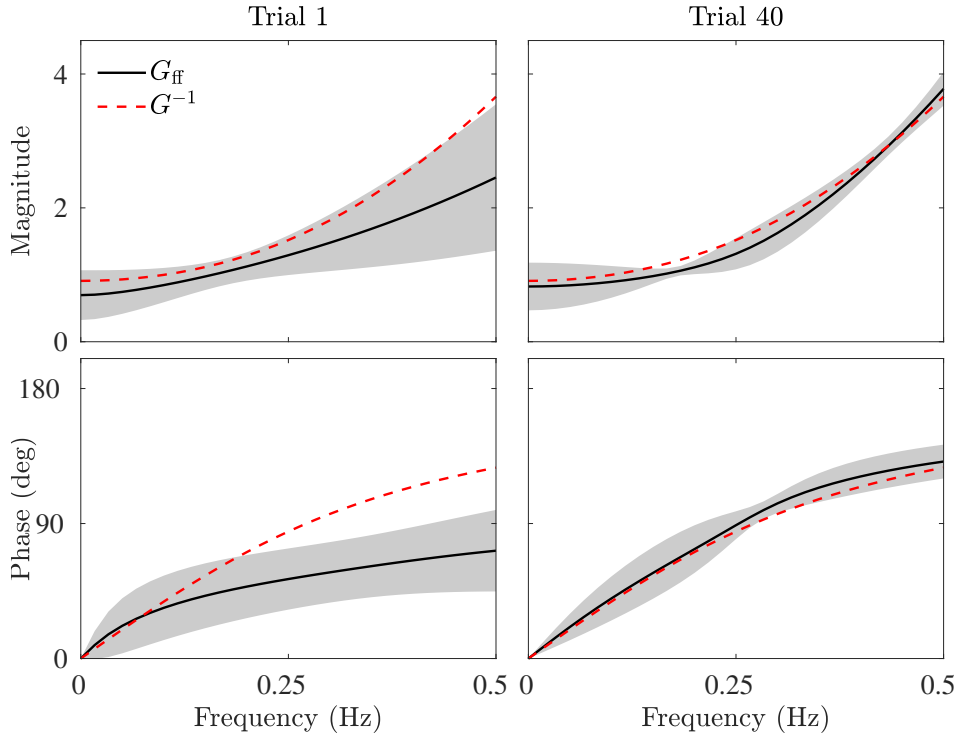
Figure 4.17: The average identified feedforward controller on trials 1 and 40 for group 2a. The shaded region shows one standard deviation.

shows the trial-by-trial mean, median, first quartile, and third quartile of $\|G_{\mathrm{ff}}G - 1\|$ of group 2b. The difference between G_{ff} and G^{-1} stays relatively constant over the 40 trials, which is different than what we saw from SSID results of subjects in group 1 and group 2a.

The validation of SSID results for group 2b (see Fig. B.2) implies that the LTI control structure in 4.12 is not a good representation of the control behavior of the subjects in this group. For group 1 and group 2a, on the other hand, validation of the SSID results suggest that the LTI control structure in 4.12 provides a good representation of the control behavior of the subjects, especially over the later trials. We argue that the control strategy employed by subjects in group 2b contains nonlinear components, which is impossible for the LTI control structure in 4.12 to capture.

In order to better understand the nonlinear components of their control behavior,
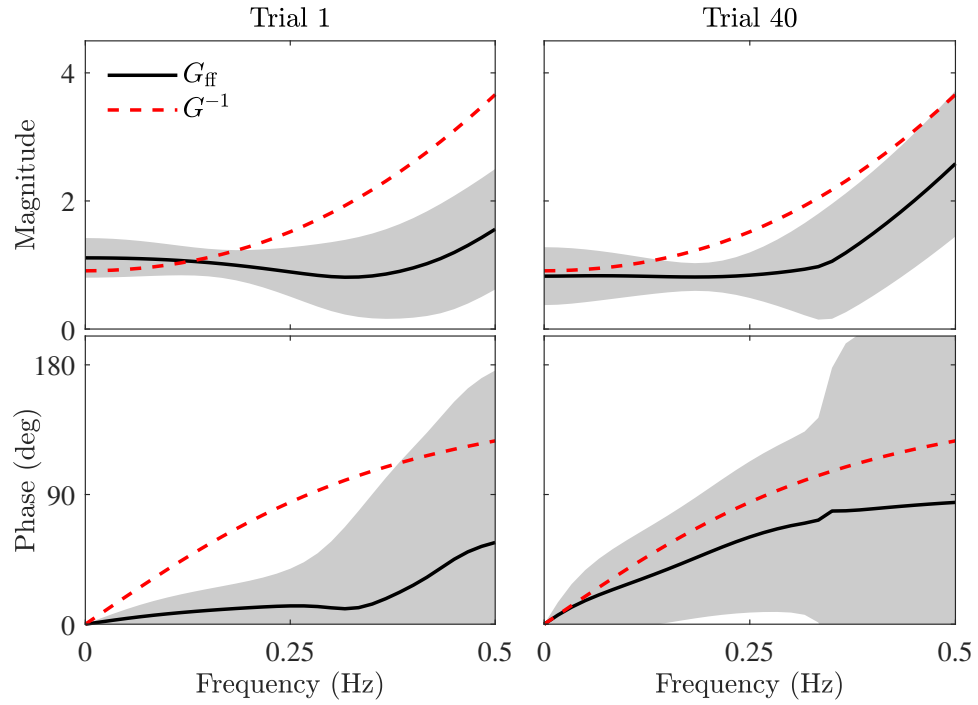
Figure 4.18: The average identified feedforward controller on trials 1 and 40 for group 2b. The shaded region shows one standard deviation.
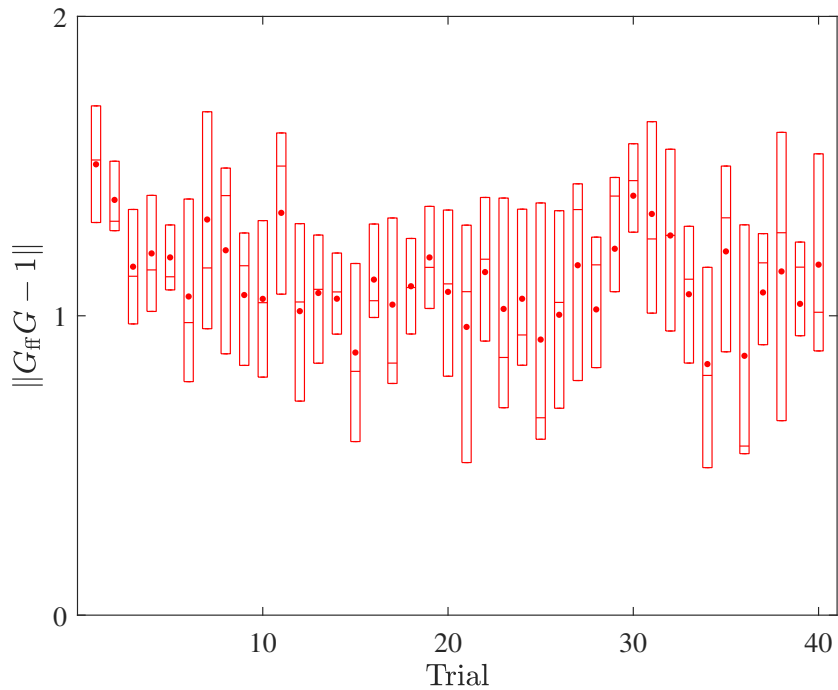
Figure 4.19: Mean, median, first quartile, and third quartile of $\|G_{ff}G - 1\|$ on each trial for group 2b. The difference between G_{ff} and G^{-1} stays relatively constant over the 40 trials. ● is the mean, and the boxplot shows the median, first quartile, and third quartile.

we look at control object's position for subjects in group 2b. For each trial we define

$$\|y\| \triangleq \frac{1}{N_\mathrm{s}} \sum_{k=1}^{N_\mathrm{s}} |y_k|,$$

which is the time average of the control object's position y_k. Note that perfect command-following performance (i.e., $\|z_1\| = 0$) is achieved if and only if $\|y\| = 1.224$, whereas perfect relaxed command-following performance (i.e., $\|z_2\| = 0$) implies $0.584 \leq \|y\| \leq 1.974$. Figure 4.20 shows group 1, group 2a, and group 2b statistical properties of $\|y\|$ on each trial. The mean $\|y\|$ for group 1 and group 2a stay relatively constant over the 40 trials. In contrast, the group 2b mean decreases from trial 1 to trial 40. These results suggest that, in contrast to group 1 and group 2a, subjects in group 2b learn to stay closer to the center of the screen as the experiment goes on. Thus, group 2b learns to use a control that maintains the control object closer to the origin.

Figure 4.21 shows the mean $\|y\|$ over four different phases of each cycle of the reference command r. These 4 phases are defined as following: *phase 1* consists of time steps in which the reference object is outbound to the right side of the screen from the origin (i.e., $r > 0$ and $\dot{r} > 0$); *phase 2* consists of time steps in which the reference object is inbound from the right side of the screen to the origin (i.e., $r > 0$ and $\dot{r} < 0$); *phase 3* consists of time steps in which the reference object is outbound to the left side of the screen from the origin (i.e., $r < 0$ and $\dot{r} < 0$); and *phase 4* consists of time steps in which the reference object is inbound from the left side of the screen to the origin (i.e., $r < 0$ and $\dot{r} > 0$). Results in Fig. 4.21 show that over the last 10 trials, subjects in group 2b learn to stay closer to the origin than subjects in group 1 and group 2a. Specifically, as the reference object moves from 0 hm to 2 hm, subjects in group 2b tend to stay closer to the left side of the reference object and as the reference object moves from 0 hm to -2 hm, subjects in group 2b tend to
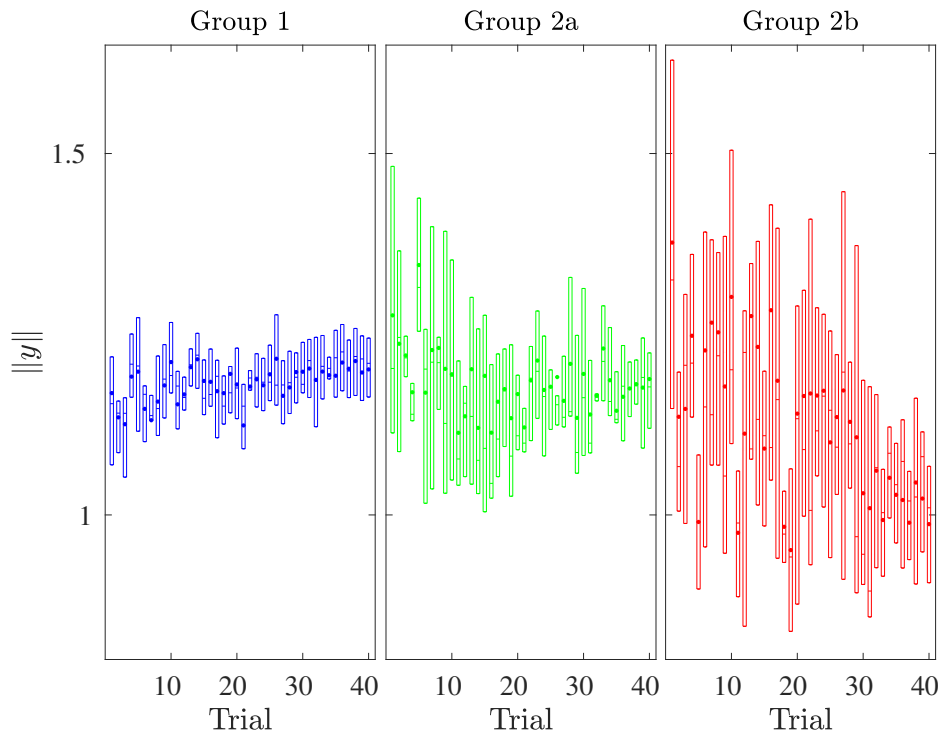
Figure 4.20: Mean, median, first quartile, and third quartile of $\|y\|$ on each trial. Subjects in group 2b learn to stay closer to the center of screen over the 40 trials compared to subjects in groups 1 and 2a. ● is the mean, and the boxplot shows the median, first quartile, and third quartile.

stay closer to the right side of the reference object.

Similar to the steady-state control effort, we define a subject's *steady-state output* $\|y\|_{\text{ss}}$ as their mean $\|y\|$ over their last 10 trials. Note from Fig. 4.20, as well as Figs. 4.3 and 4.4, that for both groups the mean $\|y\|$, $\|z_1\|$, and $\|z_2\|$ do not change significantly over the last 10 trials, suggesting that the subjects reach near-steady-state performance. Thus, $\|y\|_{\text{ss}}$ is a measure of a subject's output signal once they have learned to control the dynamic system. Figure 4.22 shows the discrete Fourier transform (DFT) of average of $\|y\|_{\text{ss}}$ divided by the reference object's position r_k for subjects in group 1, group 2a, and group 2b. As expected, for subjects in group 1 and group 2a, the magnitude stays relatively close to 1 and phase stays relatively close to 0 over the 0-to-0.5 Hz frequency range of the command. This implies that similar to subjects in group 1, subjects in group 2a try to keep the control object's position as close to the position of the reference object's center as possible at all instants in time.

Subjects in group 2b also show similar behavior over the lower frequencies (approximately 0-to-0.2 Hz), both in terms of the magnitude and the phase. However, their behavior changes over the higher frequencies and they attempt to stay closer to the center of screen compared to the subjects in the other two groups. This could also be seen in Fig. 4.23, which shows the average of $\|y\|_{\text{ss}}$ versus the reference object's position r_k for each group. Group 1 and group 2a show an almost linear behavior throughout the 60 seconds of the trial which indicates they are possibly attempting to follow the center of the reference object. Group 2b shows similar behavior for the first part of the trial (approximately the first 20 seconds). However, the behavior of subjects in group 2b changes over the later parts of the trial. This behavior over the higher frequencies of the reference command resembles an approximate hysteresis loop. Thus, the first significant difference between the control behavior of subjects in group 2b and subjects in group 1 and group 2a is the fact that subjects in group 2b
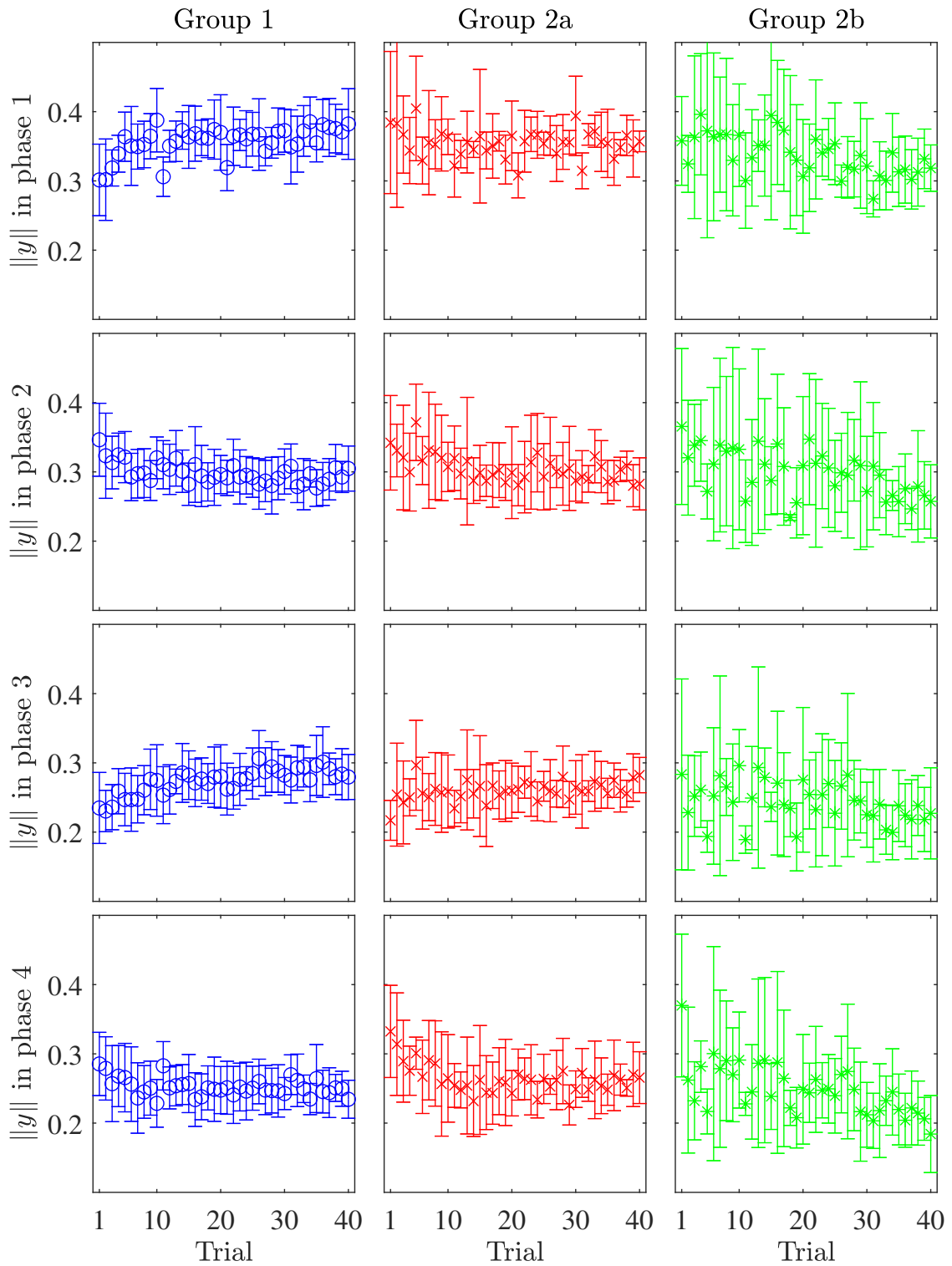
Figure 4.21: The mean $\|y\|$ for groups 1, 2a, and 2b divided into 4 segments based on the position and direction of the reference object. The ∘ indicates the mean of all the subjects in each group and the vertical lines show one standard deviation.
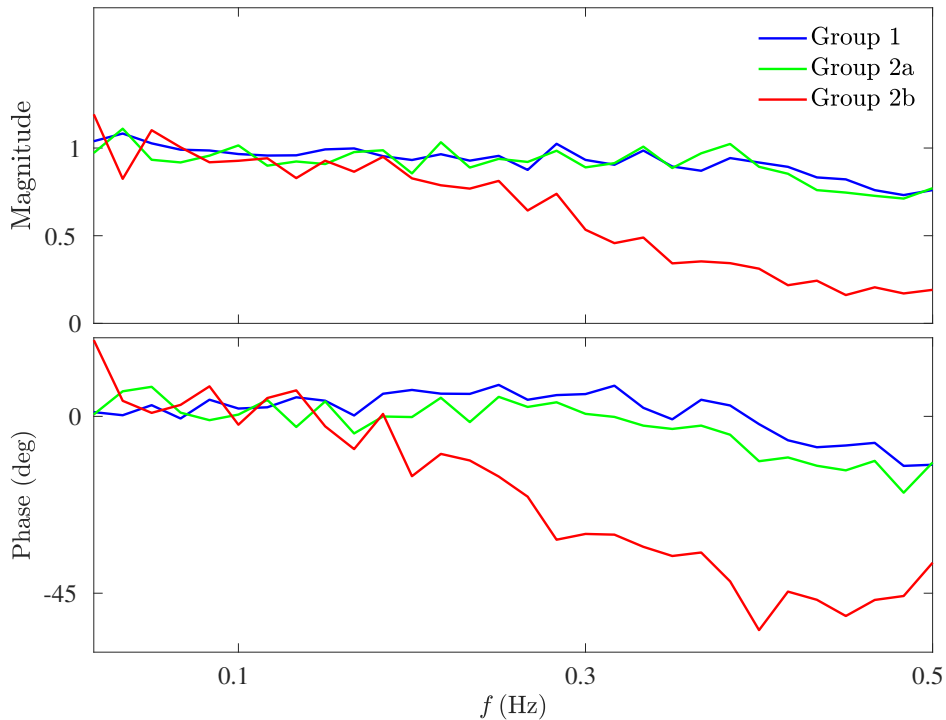
Figure 4.22: Magnitude and phase for the DFT of the average of $\|y\|_{ss}$ divided by the reference object's position r_k for each group over the 0-to-0.5 Hz frequency range of the command.

keep the control object's position closer to the center of the screen at higher frequencies. More specifically, the subjects in group 2b stay as close as possible to the center of the reference object while the reference command's frequency is between 0-to-0.2 Hz. However, once the reference command's frequency increases, they potentially give up on following the center of the reference command, and instead attempt to keep the control object's position within the boundaries of the reference object, while at the same time trying to stay close to the center of the screen. This means that group 2b adopts a combination of nonrelaxed and relaxed command-following objectives. Specifically, group 2b adopts the nonrelaxed command-following objective at lower frequencies (approximately 0-0.2 Hz) and a more relaxed command-following objective at higher frequencies (approximately 0.2-0.5 Hz).

Next, we examine properties of the control signal u for group 2b. Figure 4.24 shows control u on the first and last trial of the median performer of each group. The median performer of group 1 is the subject whose $\|z_1\|$ on the last trial is the median
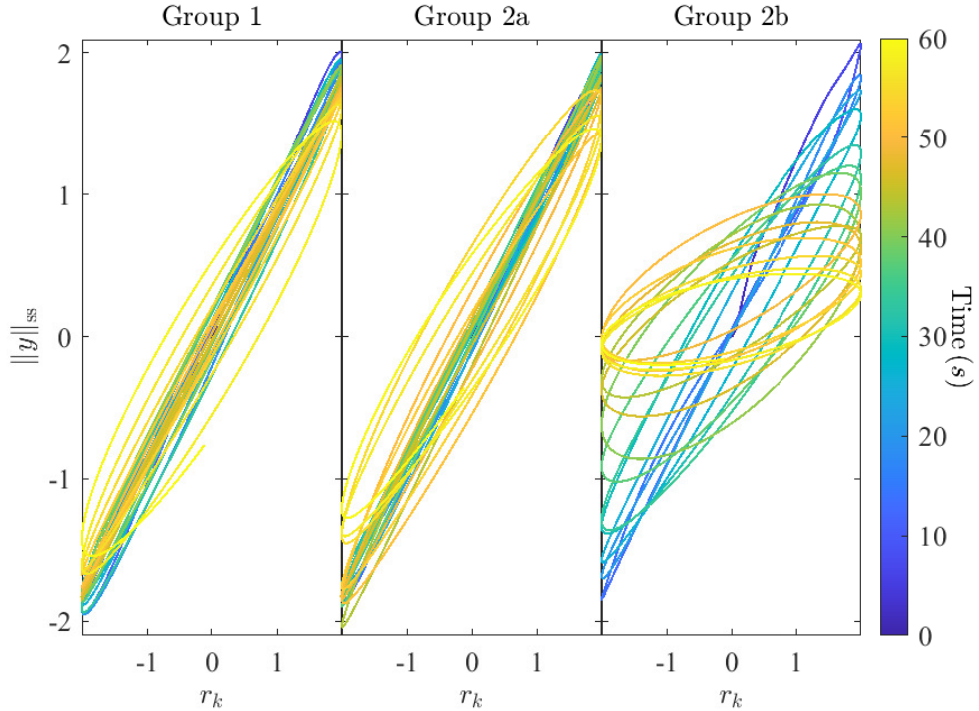
Figure 4.23: Average of $\|y\|_{\mathrm{ss}}$ versus the reference object's position r_k for each group.

(i.e., 6th best) of all subjects in their group. The median performers of group 2a and group 2b are the subjects whose $\|z_2\|$ on the last trial is the median of all subjects in their group. Since there are 6 subjects in group 2a, the median subject of this group is randomly selected from two subjects with the two middlemost value of $\|z_2\|$ on trial 40. As it can be seen in Fig. 4.24, the control signals of the group 1 and 2a median performers are smoother on trial 40 than trial 1; and by trial 40, their control more closely resembles the smoothness of the chirp command r. In contrast, the control signal of median performer of group 2b is less smooth on trial 40 and contains step-like behavior. Figure 4.25 shows control u for all 5 subjects of group 2b on the last trial. The step-like control behavior can be seen in most of the subjects of group 2b.

To investigate this step-like control behavior, we define a metric that captures the
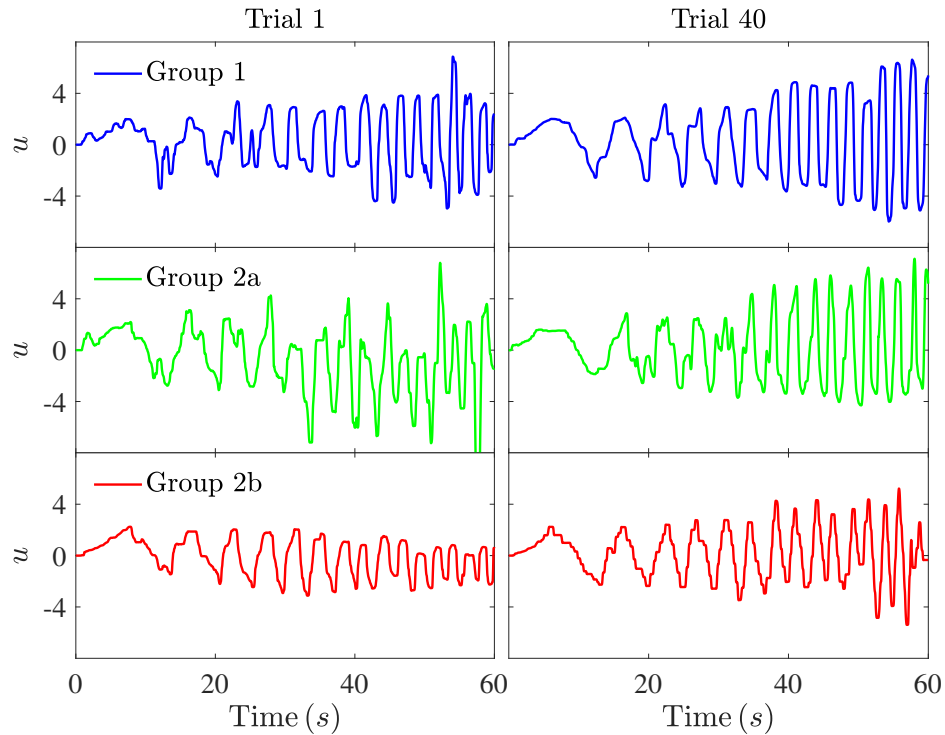
Figure 4.24: Control u on the first and last trial of the median performer of each group. The median performer of group 1 is the subject whose $\|z_1\|$ on the last trial is the median (i.e., 6th best) of all subjects in their group. The median performers of group 2a and group 2b are the subjects whose $\|z_2\|$ on the last trial is the median of all subjects in their group. Since there are 6 subjects in group 2a, the median subject of this group is randomly selected from two subjects with the two middlemost value of $\|z_2\|$ on trial 40.
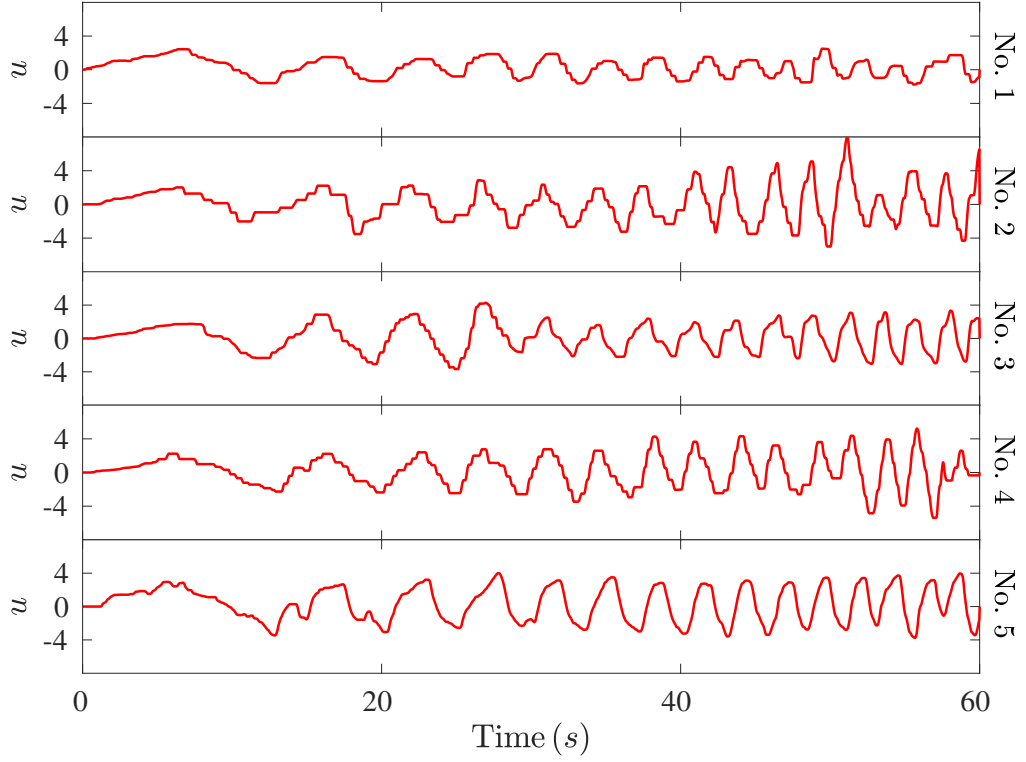
Figure 4.25: Control u on the last trial for all subjects in group 2b.

number of times a step-like control occurs. c

$$|u_k - u_{k-1}| > \delta, \tag{4.1}$$

and

$$\max_{i \in \{1, \cdots, L\}} |u_{k+i} - u_{k+i-1}| < \delta, \tag{4.2}$$

and

$$\max_{i \in \{1, \cdots, L\}} |u_{k-i} - u_{k-i-1}| > 10\delta, \tag{4.3}$$

where $\delta = 0.005$ and $L = 5$. In other words, a step-like behavior at time step kT_{s} has occurred if the following conditions hold:

A1) The slope of the control signal u is greater than $\delta/T_{\mathrm{s}} = 0.25$ per second at

time step kT_s.

A2) The slope of the control signal u is less than $\delta/T_s = 0.25$ per second for $LT_s = 0.1$ seconds after time step kT_s.

A3) The maximum slope of the control signal u is 10 times greater than δ/T_s for LT_s seconds before time step kT_s.

The parameters δ and L were determined by a qualitative analysis of experimental data. The results reported in this section on step-like behavior do not change qualitatively with parameter variations up to $\pm 20\%$. Condition A1) indicates that at the time-step where the step-like behavior occurs, the slope of the control is greater than a certain threshold (δ/T_s). This threshold is determined by finding the maximum no-input control u measured from the joystick. The maximum no-input control u measured from the joystick is found by measuring the control signal coming out of joystick for three minutes while someone holds but does not move the joystick. The maximum measured value for our joystick is 0.004. Thus, we let $\delta = 0.005$ which means $\delta/T_s = 0.25$ per second.

Condition A2) states that for a certain amount of time $(LT_s$ seconds) after the step-like behavior has occurred, the slope of the control does not exceed a certain threshold (δ/T_s). Condition A2) means that the control signal u should be relatively flat for some amount of time after the step-like behavior has occurred. The value of L is determined by examining the experimental data. By looking at Fig. 4.25, we let $L = 5$ which means $LT_s = 0.1$ seconds.

Finally, condition A3) implies that there should be a lower limit on the maximum slope of u over a certain amount of time $(LT_s$ seconds) before the step-like behavior occurs. Condition A3) prevents a step-like control behavior to be detected multiple times.

Figure 4.26 shows control u on the last trial of the median performer of each group. The median performer of group 1 is the subject whose $\|z_1\|$ on the last trial is the

93
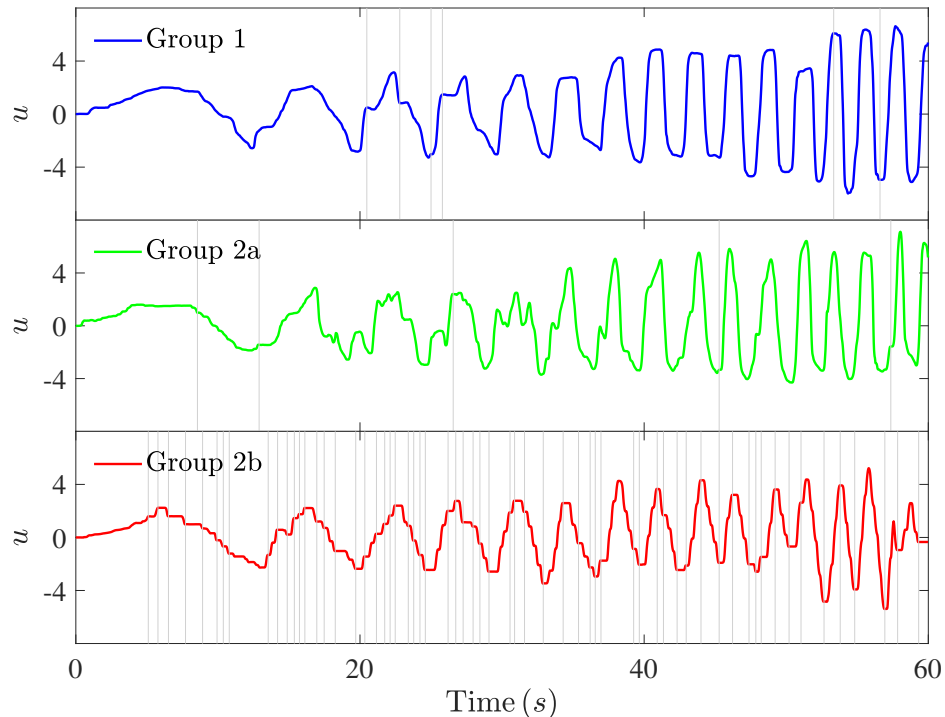
Figure 4.26: Control u on the last trial of the subject from each group who has the median performance on trial 40. The vertical grey lines indicate when a step-like control behavior is detected. The number of step-like controls for the median performer in groups 1, 2a, and 2b is 6, 5, and 63, respectively.

median (i.e., 6th best) of all subjects in their group. The median performer of group 2a and group 2b are the subjects whose $\|z_2\|$ on the last trial is the median of all subjects in their group. Since there are 6 subjects in group 2a, the median subject of this group is randomly selected from two subjects with the two middlemost value of $\|z_2\|$ on trial 40. The vertical gray lines in Fig. 4.26 indicate the time instances where a step-like behavior has been detected. The number of step-like controls detected for the median performer in group 1, group 2a, and group 2b is 6, 5, and 63, respectively.

For each trial, let N_s be the number of times a step-like control behavior is detected. Figure 4.27 shows the mean N_s on each trial for each group. For subjects in group 1 and group 2a, the mean N_s stays relatively small and constant over the 40 trials. There is no significant difference between the number of step-like behavior detected for subjects in group 1 and group 2a. In contrast, for the majority of trials, the group mean of N_s for group 2b is at least 3 times greater than those of groups 1 and 2b.

94
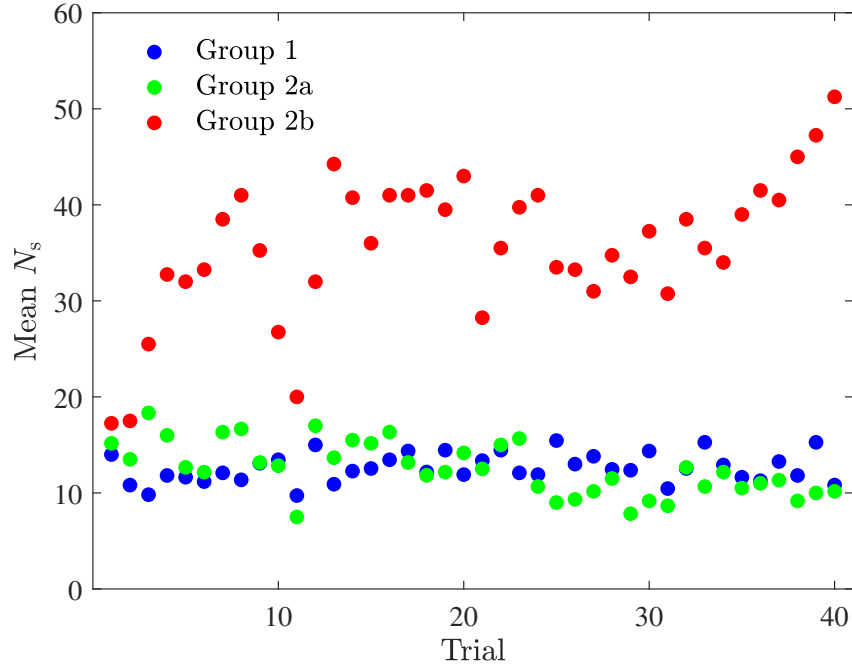
Figure 4.27: Mean, median, first quartile, and third quartile of N_s on each trial. The mean N_s for group 2b is greater than the mean N_s for groups 1 and 2a on all trials.

Moreover, over the 40 trials, the group mean of N_s for group 2b has an increasing trend, whereas those of groups 1 and 2a remain relatively constant. This increasing trend is more significant over the last 10 trials, which corresponds to their control effort reaching a steady state as previously seen in Fig. 4.10. Thus, by the end of the experiment, group 2b adopts a nonlinear control strategy that yields step-like control behavior.

Next, we distinguish between the feedforward and feedback nature of the step-like controls. A step-like control behavior is feedforward, or anticipatory, if control signal u steps in the opposite direction of the reference command r. It is anticipatory behavior because the step anticipate the change of direction in the reference command r. In contrast, a step-like control behavior is feedback, or reactive, if control signal u steps in the same direction of the reference command r. It is reactive behavior because the step reacts to the movement of the reference command r and tries to make y to catch up to r.

Thus, a step-like control at time step kT_s is feedforward if $\dot{u}(kT_s)\dot{r}(kT_s) < 0$, and
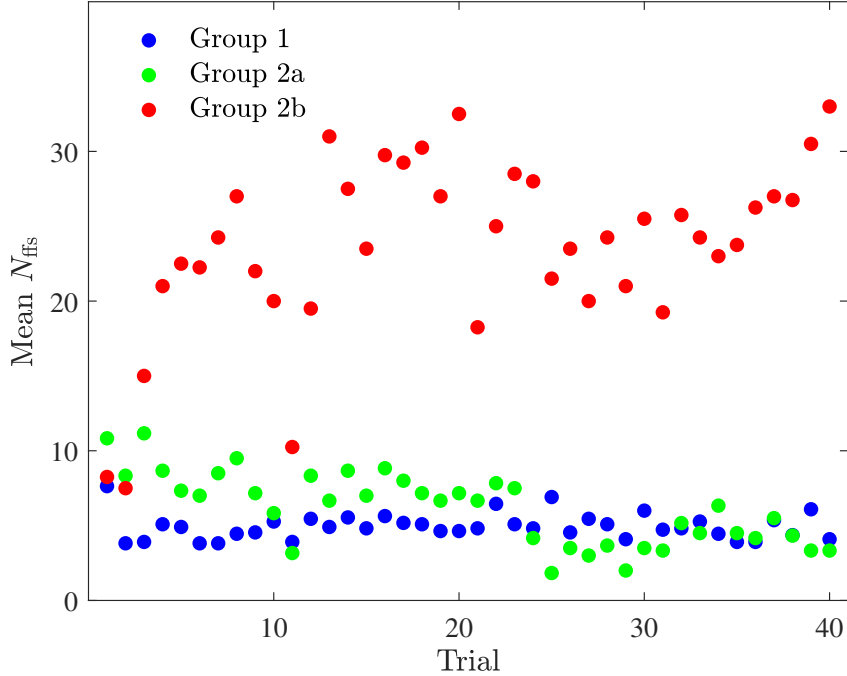
Figure 4.28: Mean of N_{ffs} on each trial. The mean N_{ffs} for group 2b is greater than the mean N_{ffs} for groups 1 and 2a on all trials.

it is feedback if $\dot{u}(kT_s)\dot{r}(kT_s) > 0$. For each trial, let N_{ffs} be the number of times a feedforward step-like control behavior is detected and let N_{fbs} be the number of times a feedback step-like control behavior is detected.

Figures 4.28 and 4.29 show the mean N_{ffs} and the mean N_{fbs} on each trial for each group, respectively. For group 1 and group 2a, the mean N_{ffs} and the mean N_{fbs} are relatively constant over the trials. In contrast, the mean N_{ffs} and the mean N_{fbs} for group 2b tend to increase over the trials. This trend is more visible over the last 10 trials. Moreover, subjects in group 2b have a significantly larger mean N_{ffs} over majority of the trials compared to their mean N_{fbs}. In fact, their mean N_{fbs} is not significantly different from the mean N_{fbs} of the subjects in group 1 and group 2a. One possible explanation for these results is that subjects in group 2b learn to take advantage of the relaxed control objective by exerting a step-like control as part of the feedforward component of their control behavior.

The results in this subsection suggest that the subjects in group 2b use a feedforward

96
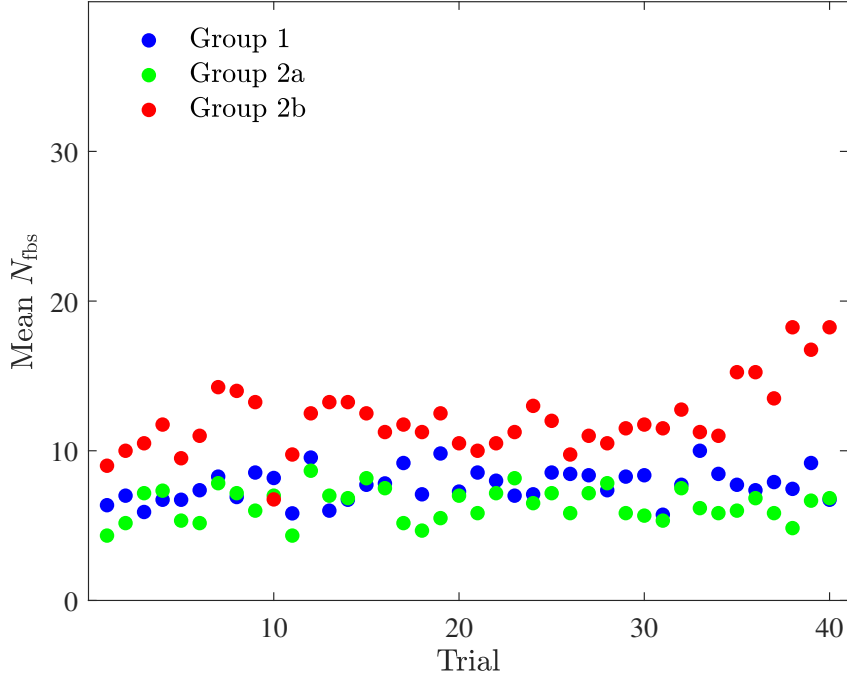
Figure 4.29: Mean of N_{fbs} on each trial. The mean N_{fbs} for group 2b is greater than the mean N_{fbs} for groups 1 and 2a on all trials.

control strategy that generates step-like controls and yields nonrelaxed command following behavior at lower frequencies and more relaxed command following behavior at higher frequencies. We note that feedforward behavior may suggest a predictive control strategy that relies on some knowledge of the dynamic system G. The step-like behavior of group 2b precludes the possibility of feedforward plant inversion (i.e., $G_{\text{ff}} = G^{-1}$), which the SSID results suggest is used by groups 1 and 2a. However, other feedforward model-based nonlinear control strategies are possible.

We now present a possible feedforward control strategy that can model several aspects the group 2b's control behavior. We also show that this potential feedforward control strategy could yield a command-following performance similar to the command-following performance seen in subjects of group 2b.

This control strategy, structure of which is shown in Fig. 4.30, is a relaxed feedforward plant inversion and consists of three components. The first component is a frequency-dependent gain λ, which based on previous observations (see Figs. 4.20,
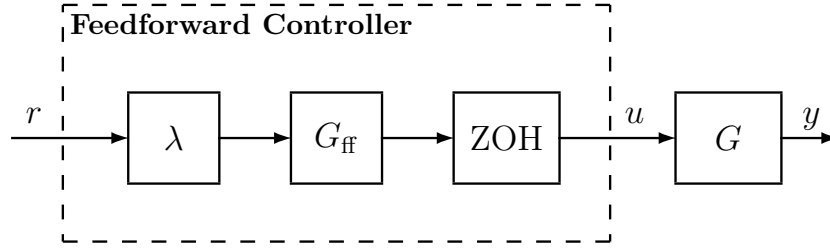
Figure 4.30: A pure feedforward controller consisting of a frequency-dependent gain k cascaded with a feedforward transfer function G_{ff}, and a zero-order hold.

4.22, and 4.23), we define as

$$
\lambda(\omega) \triangleq
\begin{cases}
1, & \text{if} \quad \omega_{\text{i}} \leq \omega \leq \omega_{\text{c}} \\[2mm]
1 - a_0(\omega - \omega_{\text{c}}), & \text{if} \quad \omega_{\text{c}} < \omega \leq \omega_{\text{f}}
\end{cases}
, \tag{4.4}
$$

where ω is the frequency of the reference command r in Hz, ω_{i} and ω_{f} are the initial and final frequencies of the reference command r over a trial, ω_{c} is the cut-off frequency where the gain starts decreasing, and a_0 is the rate at which the gain decreases per Hz. The second component is the feedforward transfer function G_{ff}, which we assume is a 2nd-order FIR transfer function and is an approximation of inverse of the plant or G^{-1}. The third component is a zero-order hold with sampling rate of f_{zoh}, which gives us a step-like behavior in the control signal u. The duration of each step is determined by the value of sampling rate f_{zoh}.

Figure 4.31 shows y and u for a simulation where $\omega_{\text{i}} = 0$ Hz, $\omega_{\text{f}} = 0.5$ Hz, $\omega_{\text{c}} = 0.2$ Hz, $a_0 = 2.7$ per Hz, and $f_{\text{zoh}} = 2$ Hz. These values are determined by examining the experimental data of subjects in group 2b, as seen in Figs. 4.22, 4.23, and 4.26. The time-averaged error for this simulation is $\|z_1\| = 0.60$, and the time-averaged relaxed error for this simulation is $\|z_2\| = 0.15$. Moreover, the control effort for this simulation is $\|u\| = 1.16$. These results are consistent with performance results of subjects in group 2b (see Figs. 4.8, 4.9, 4.10).
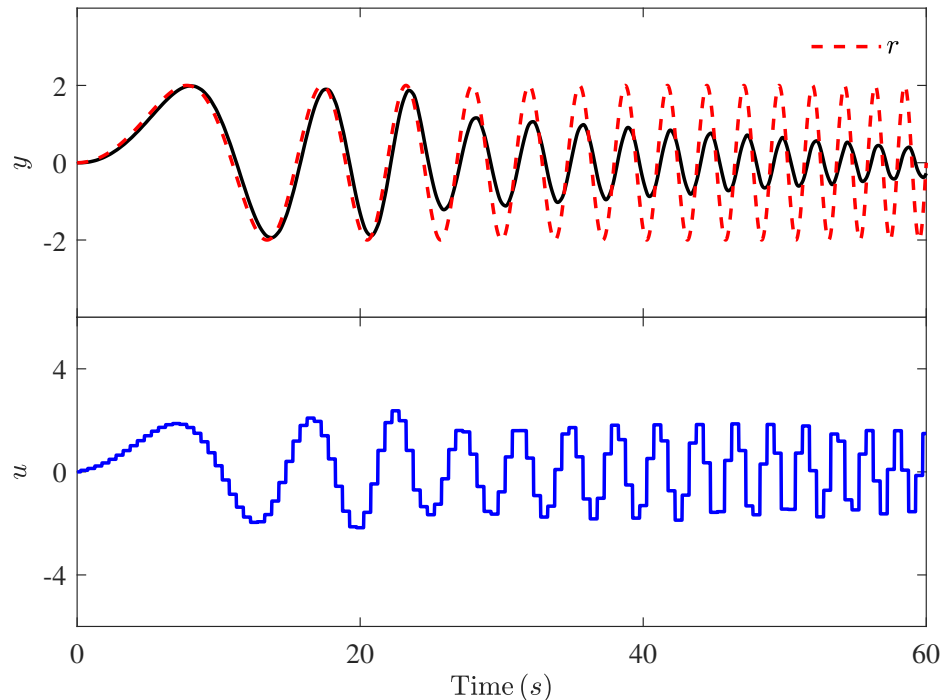
Figure 4.31: Reference command r and simulation results for output y with system G and a pure feedforward control signal u consisting of a frequency-dependent gain cascaded with a second-order FIR approximation of G^{-1} and a zero-order hold. The time-averaged error is $\|z_1\| = 0.60$, the time-averaged relaxed error is $\|z_2\| = 0.15$, and the control effort is $\|u\| = 1.16$.

Figure 4.32 shows simulation results for output y versus the reference command r. These results are also consistent with the hysteresis loop we had previously seen in the control object's position of the subjects in group 2b (see Fig. 4.23).

4.5 Summary and Conclusions

We now discuss the impacts that relaxing the command-following objectives has on the control strategies adopted by humans. This chapter presented the results of a HITL experiment where 22 human subjects interacted with a dynamic system 40 times over a one-week period. The subjects were divided into two groups of 11 subjects. Each group interacted with the same dynamic system performing a command-following task. The only difference between these two groups was their control objectives. Group 1's control objective was to follow the reference command
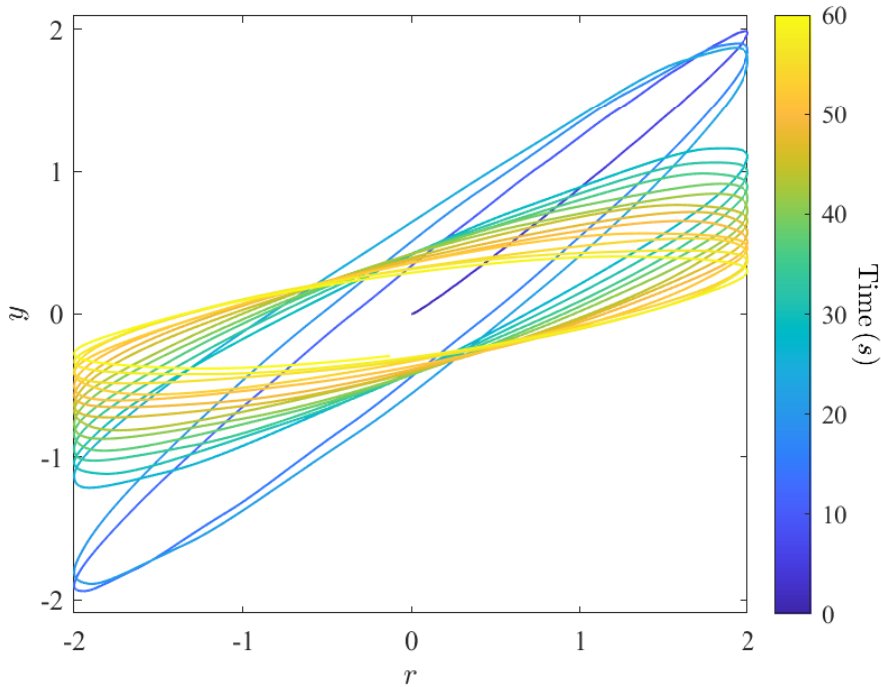
Figure 4.32: Simulation results for output y versus the reference command r with system G and a pure feedforward control signal u consisting of a frequency-dependent gain cascaded with a 2nd-order FIR approximation of G^{-1} and a zero-order hold .

as closely as possible at all instants in time. Group 2's control objective, on the other hand, was to follow the reference command with some allowable error.

This chapter presented new results on the impact of relaxed command-following objectives on HITL control behavior. The experimental results indicate that the average command-following performance of group 1 is better than that of group 2 on all trials (see Fig. 4.3). The same is true about the relaxed command-following performance of group 1 (see Fig. 4.4). This implies that staying as close to the center of the reference object as possible at all instants in time is one possible control strategy that ensures a good result in both performance metrics.

Steady-state control effort results indicate that out of 11 subjects of group 2, 5 exert a significantly smaller control effort compared to the other 6 subjects in the same group and all 11 subjects of group 1 (see Fig. 4.7). This observation was the basis for breaking up group 2 into group 2a and group 2b. The command-following performance results and the control effort results over all trials provide

further supporting evidence that subjects in group 1 and group 2a employ similar control strategies, while subjects in group 2b adopt a different approach (see Figs. 4.8, 4.9, and 4.10).

To investigate the control strategies of all three groups, a linear SSID algorithm is used to identify best-fit feedback and feedforward controllers for each subject and on each trial. Prior HITL studies suggest that adaptive feedforward inversion is a primary control strategy for many command-following tasks. The SSID results of group 1 provide supporting evidence that humans use adaptive feedforward inversion as their primary control strategy when instructed to perform a non-relaxed command-following task. Moreover, the SSID results of group 2a show that even when instructed to perform a relaxed command-following task, some humans use the same control strategy as the non-relaxed group. The identified feedforward controllers for these two groups approximate the dynamic system's inverse better on the last trial than on the first trial (see Figs. 4.16, 4.17, and 4.15). They also use approximately the same amount of feedback gain and have similar feedback time delay (see Figs. 4.13 and 4.14).

The SSID results of group 2b, however, show that not all the human subjects who are instructed to perform a relaxed command-following task adopt adaptive feedforward inversion as their primary control strategy (see Figs. 4.18 and 4.19). In fact, the validation of SSID results for this group reveals that their control behavior cannot be modeled by the LTI control structure used for other groups (see Fig. B.2). This could be because of nonlinear components that potentially exist in their control strategy. The experimental data of these subjects provide further evidence in support of existence of some nonlinear components in their control behavior. One observation taken from comparing the experimental data of group 2b's subjects with the other two groups is that subjects in group 2b try to follow the center of the reference object at lower frequencies. But, at higher frequencies they potentially attempt to keep

the control object's position within the boundaries of the reference object, while at the same time staying close to the center of the screen (see Figs. 4.20, 4.22, and 4.23). This behavior, which could be modeled by a frequency-dependent gain, is the first potential nonlinear component of the control behavior of subjects in group 2b. Another observation comes from comparing the control signal of subjects in each group. We show that subjects in group 2b have a step-like control behavior, which corresponds to their significantly lower control effort over the later trials (see Figs. 4.25, 4.26, and 4.27). This step-like behavior, which has an anticipatory nature (see Fig. 4.28), is the second potential nonlinear component of the control behavior of subjects in group 2b.

Finally, we propose one possible control strategy that contains the observed nonlinear components of group 2b's control behavior. This control strategy, which is assumed to be purely feedforward, includes a frequency-dependent gain cascaded with a second-order FIR approximation of G^{-1} and a zero-order hold. Using simulation results, we show that this control strategy could lead to similar command-following performance and control effort (see Figs. 4.31 and 4.32).

Chapter 5 Summary and Conclusion

In this dissertation, we investigated the effects of system output nonlinearities and relaxed command-following control objectives on the human-in-the-loop (HITL) control behavior by using different subsystem identification (SSID) algorithms as well as other analytical methods. These SSID algorithms were developed and presented both in frequency-domain and time-domain, and use the input and output measurements of the closed-loop system to identify feedback and feedforward components of human control behavior.

We conducted two HITL experiments in order to explore the impacts of system output nonlinearities and relaxed command-following control objectives on HITL control behavior. The frequency-domain and time-domain SSID algorithms presented in this dissertation were applied to the time-domain data obtained from these two experiments to model the human control behavior. Using the SSID results as well as the experimental data, we sought insight into the effects that system output nonlinearities and relaxed command-following control objectives have on the human learning and HITL control behavior.

The results of these analyses suggest that similar to many linear systems, humans also adopt adaptive feedforward inversion as their primary command-following control strategy for some nonlinear systems. They also suggest that once the control objectives of a command-following task has been relaxed, some humans choose to use a step-like control behavior that results in minimum control effort.

Summary of Results from Chapter 2

In this chapter, we presented a frequency-domain and a time-domain SSID algorithm that could be used to identify best-fit feedback and feedforward controllers of a closed-loop system where these controllers are connected to a known plant. These SSID algorithms use a candidate pool to search among all the candidate feedback controllers. Then, a convex optimization problem is solved to determine the best-fit feedforward controller. The frequency-domain algorithm is applicable to a closed-loop system where the plant and the controllers are linear while the time-domain algorithm is also applicable to a closed-loop system where the plant and/or the feedforward controller contain nonlinear components.

Summary of Results from Chapter 3

In this chapter, new results on the impact of nonlinearities on HITL control behavior were presented. We presented the results of a HITL experiment, which was designed to investigate the control strategies that humans use to interact with nonlinear dynamic systems. In this experiment, 22 human subjects interacted with a dynamic system and performed a command-following task. One group interacted with an LTI dynamic system, while the other group interacted with a Wiener system, which consisted of the same LTI dynamics cascaded with a static output nonlinearity.

The experimental results indicate that static output nonlinearities can make a dynamic system more difficult for humans to control. The average command-following performance of the linear group, who interacted with the linear plant G, is better on majority of trials than the nonlinear group (see Fig. 3.5).

The SSID results suggest several differences between the linear and nonlinear groups. The linear group tends to use more feedback-control authority. Specifically, the linear group has a smaller feedback time delay and uses a larger feedback gain than the

nonlinear group (see Figs. 3.11 and 3.12). One possible explanation is that the introduction of output nonlinearity adds to the systems's uncertainty and this uncertainty results in a more conservative approach by subjects in feedback.

Moreover, the feeforward part of the SSID results suggest that humans use adaptive feedforward inversion as their main control strategy for both linear and nonlinear plant. For both the linear and nonlinear groups, the identified feedforward controllers approximate the dynamic system's inverse better on the last trial than on the first trial (see Figs. 3.14, 3.15, 3.17, and 3.18). However, the linear group achieves better approximation of the dynamic system's inverse (see Figs. 3.16 and 3.19). This difference in approximating the inverse is a possible explanation for the difference in performance between the two groups. The SSID results suggest that the nonlinear subjects learn the linear part of the dynamic system more quickly than they learn the static output nonlinearity. Over the latter half of the trials, the nonlinear subjects' feedforward transfer function does not change significantly (see Fig. 3.19), whereas they continue to learn the output nonlinearity (see Fig. 3.16).

The results from this study provide some insight into human-control strategies for nonlinear systems. However, many open questions remain. Further investigation is needed into whether these results extend to dynamic systems with more complex transfer functions (e.g., higher order, higher relative degree, nonminimum phase, etc.) and more complex output nonlinearities. The control strategies that humans use for systems with dynamic nonlinearities is also a significant open question.

Summary of Results from Chapter 4

In this chapter, new results on the impact of relaxed command-following objectives on HITL control behavior were presented. We presented the results of a HITL experiment where 22 human subjects interacted with a dynamic system 40 times over a one-week period. The subjects were divided into two groups of 11 subjects. Each

group interacted with the same dynamic system performing a command-following task. The only difference between these two groups was their control objectives. Group 1's control objective was to follow the reference command as closely as possible at all instants in time. Group 2's control objective, on the other hand, was to follow the reference command with some allowable error.

The experimental results indicate that the average command-following performance of group 1 is better than that of group 2 on all trials (see Fig. 4.3). The same is true about the relaxed command-following performance of group 1 (see Fig. 4.4). This implies that staying as close to the center of the reference object as possible at all instants in time is one possible control strategy that ensures a good result in both performance metrics.

Steady-state control effort results indicate that out of 11 subjects of group 2, 5 exert a significantly smaller control effort compared to the other 6 subjects in the same group and all 11 subjects of group 1 (see Fig. 4.7). This observation was the basis for breaking up group 2 into group 2a and group 2b. The command-following performance results and the control effort results over all trials provide further supporting evidence that subjects in group 1 and group 2a employ similar control strategies, while subjects in group 2b adopt a different approach (see Figs. 4.8, 4.9, and 4.10).

To investigate the control strategies of all three groups, a linear SSID algorithm is used to identify best-fit feedback and feedforward controllers for each subject and on each trial. Prior HITL studies suggest that adaptive feedforward inversion is a primary control strategy for many command-following tasks. The SSID results of group 1 provide supporting evidence that humans use adaptive feedforward inversion as their primary control strategy when instructed to perform a non-relaxed command-following task. Moreover, the SSID results of group 2a show that even when instructed to perform a relaxed command-following task, some humans use the same control

strategy as the non-relaxed group. The identified feedforward controllers for these two groups approximate the dynamic system's inverse better on the last trial than on the first trial (see Figs. 4.16, 4.17, and 4.15). They also use approximately the same amount of feedback gain and have similar feedback time delay (see Figs. 4.13 and 4.14).

The SSID results of group 2b, however, show that not all the human subjects who are instructed to perform a relaxed command-following task adopt adaptive feedforward inversion as their primary control strategy (see Figs. 4.18 and 4.19). In fact, the validation of SSID results for this group reveals that their control behavior cannot be modeled by the LTI control structure used for other groups (see Fig. B.2). This could be because of nonlinear components that potentially exist in their control strategy. The experimental data of these subjects provide further evidence in support of existence of some nonlinear components in their control behavior. One observation taken from comparing the experimental data of group 2b's subjects with the other two groups is that subjects in group 2b try to follow the center of the reference object at lower frequencies. But, at higher frequencies they potentially attempt to keep the control object's position within the boundaries of the reference object, while at the same time staying close to the center of the screen (see Figs. 4.20, 4.22), and 4.23). This behavior, which could be modeled by a frequency-dependent gain, is the first potential nonlinear component of the control behavior of subjects in group 2b. Another observation comes from comparing the control signal of subjects in each group. We show that subjects in group 2b have a step-like control behavior, which corresponds to their significantly lower control effort over the later trials (see Figs. 4.25, 4.26, and 4.27). This step-like behavior, which has a predictive nature (see Fig. 4.28), is the second potential nonlinear component of the control behavior of subjects in group 2b.

Finally, we propose one possible control strategy that contains the observed non-

linear components of group 2b's control behavior. This control strategy, which is assumed to be purely feedforward, includes a frequency-dependent gain cascaded with a second-order FIR approximation of G^{-1} and a zero-order hold. Using simulation results, we show that this control strategy could lead to similar command-following performance and control effort (see Figs. 4.31 and 4.32).

The results from this study provide some insight into the impacts of relaxing the control objectives on the human control strategies in command-following tasks. In this study, the control objective was relaxed in a pursuit tracking command-following task. However, further investigation is needed into whether these results extend to other tasks. Moreover, further experiments are needed to examine the extent to which the proposed possible control strategy for subjects in group 2b is valid.

Appendices

A Candidate Pool

The candidate pool Γ is a set that contains approximately 50 million elements and is designed to capture a wide range of possible human control behavior over the 0-to-0.5 Hz frequency range. Candidate feedback transfer functions are second-order IIR with monic denominator and relative degree one, that is, $n_{\text{fb}} = 1$, and $d_{\text{fb}} = 2$. For each $\gamma \in \Gamma$, the following conditions hold:

B1) If $\lambda \in \mathbb{C}$ is a root of the candidate polynomial $\mathcal{N}_{\text{fb}}$, then $|\lambda| < 1$.

B2) If $\lambda \in \mathbb{C}$ is a root of the candidate polynomial $\mathcal{D}_{\text{fb}}$, then $|\lambda| < 1$.

B3) $\max_{\omega \in [0, \pi]} \left| \frac{\mathcal{N}_{\text{fb}}(e^{\jmath \omega T_{\text{s}}})}{\mathcal{D}_{\text{fb}}(e^{\jmath \omega T_{\text{s}}})} \right| \le 30.5$.

B4) $\delta \in \{4, 5, 6, \ldots, 25\}$.

Conditions B1) and B2) indicate that the parameters of candidate feedback controller are designed such that the zero and poles of G_{fb} lie inside the unit circle. Thus, the candidate pool assumes that the feedback control behavior of the subjects is stable. Condition B3) states that the peak magnitude of the feedback controller over the frequency range $[0, \pi]$ rad/s is no more than 30.5 (or approximately 30 dB). Thus, B3) imposes an upper limit on the magnitude of the feedback controller. The 30 dB upper limit is based on a separate experiment with 10 subjects, where each subject was asked to follow a single-frequency sinusoid using only error feedback (i.e., feedforward of the reference signal was not available). In this experiment, the peak magnitude of the feedback controller used by the subjects is approximately 30 dB,

suggesting that 30 dB is the peak gain that a human can use in feedback. Condition B4) implies that the human's sensory feedback time delay is in the range of 80 ms to 500 ms. This is consistent with [33, 41, 96, 97]. Since the sampling rate in this experiment for both groups is 20 ms, we assume that $\delta \in \{4, 5, \cdots, 25\}$.

B   Validation of SSID Results

B.1   Experiment on System Output Nonlinearities

To validate the SSID results, for each trial we use the identified control pairs (d^+, G_{fb}^+) and (f^+, G_{ff}^+) to simulate the closed-loop system, where the input to the simulation is $\{r_k\}_{k=1}^{N_\text{s}}$, the output of the simulation is the validation data $\{y_k^+\}_{k=1}^{N_\text{s}}$, and all initial conditions are zero. We then use the experimental data $\{y_k\}_{k=1}^{N_\text{s}}$ and validation data $\{y_k^+\}_{k=1}^{N_\text{s}}$ to calculate the variance accounted for (VAF) for each trial. VAF is a measure of the accuracy of the identified controllers and is given by

$$\text{VAF} \triangleq 1 - \frac{\sum_{k=1}^{N_\text{s}} \left| y_k - y_k^+ \right|^2}{\sum_{k=1}^{N_\text{s}} \left| y_k \right|^2}. \tag{B.1}$$

Table B.1 shows the mean VAF on 4 different sets of trials for the linear group and the nonlinear group. Figure B.1 shows the mean, median, first quartile, and third quartile of VAF on each trial. For both groups, the mean and median VAF increase over the 40 trials. The increase in the VAF suggests that the identified models obtained for the later trials are a more accurate representation of the data than the models obtained for the earlier trials. This means that as the subjects learn, their control behavior can be better modeled by the control structure used in this dissertation.

Table B.1: Mean VAF and its percentage change from the first 10 trials to the last 10 trials.

	Trials 1–10	Trials 11–20	Trials 21–30	Trials 31–40	Change (%)
Linear Group	0.875	0.924	0.943	0.961	+9.8
Nonlinear Group	0.887	0.927	0.938	0.951	+7.2
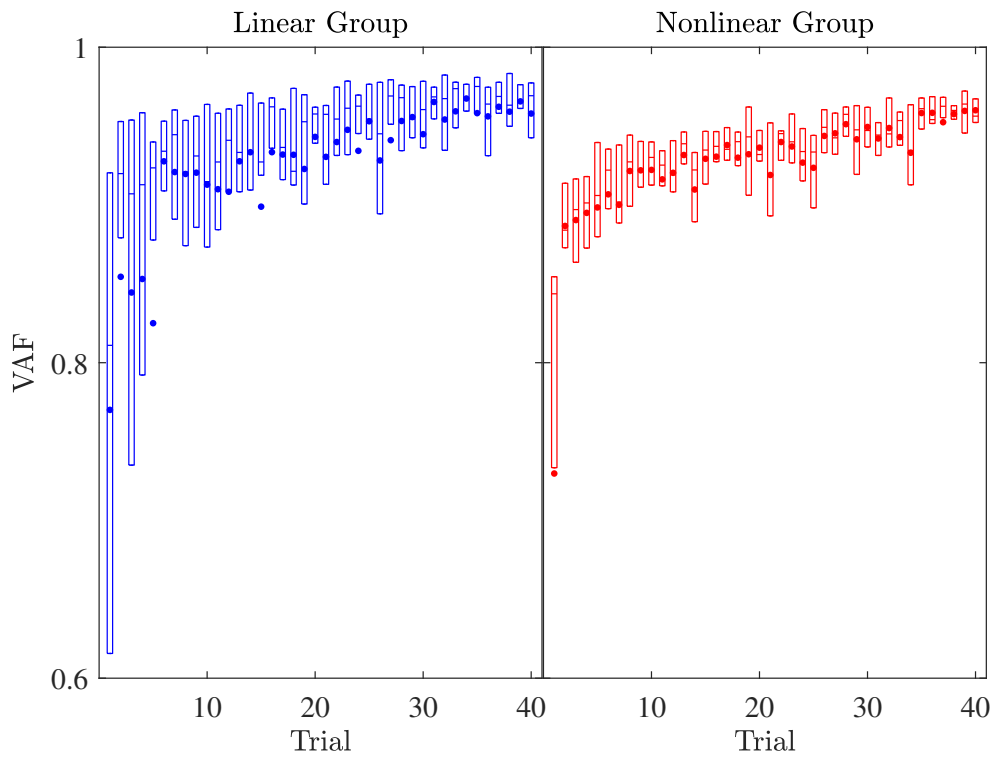
Figure B.1: Mean, median, first quartile, and third quartile of VAF on each trial. For both groups, the mean and median VAF increase over the 40 trials. ● is the mean, and the boxplot shows the median, first quartile, and third quartile.

B.2 Experiment on Relaxed Command-following Control Objectives

To validate the SSID results, for each trial we use the identified feedback control pair (d^+, G_{fb}^+) and the identified feedforward transfer function G_{ff}^+ to simulate the closed-loop system, where the input to the simulation is $\{r_k\}_{k=1}^{N_s}$, the output of the simulation is the validation data $\{y_k^+\}_{k=1}^{N_s}$, and all initial conditions are zero. We then use the experimental data $\{y_k\}_{k=1}^{N_s}$ and validation data $\{y_k^+\}_{k=1}^{N_s}$ to calculate the variance accounted for (VAF) for each trial using (B.1).

Table B.2 shows the mean VAF on 4 different sets of trials for all three groups. Figure B.2 shows the mean, median, first quartile, and third quartile of VAF on each trial. For all three groups, the mean and median VAF increase over the 40 trials. The increase in the VAF suggests that the identified models obtained for the later trials are a more accurate representation of the data than the models obtained for the earlier trials. This means that as the subjects learn, their control behavior can be better modeled by the control structure used in this dissertation. However, even over the later trials, the mean VAF for group 2b is not close to 1. This implies that the control structure used in this dissertation is not a good representation of the control behavior of subjects in group 2b.

Table B.2: Mean VAF and its percentage change from the first 10 trials to the last 10 trials.

|	Trials 1–10	Trials 11–20	Trials 21–30	Trials 31–40	Change (%)
Group 1	0.740	0.823	0.853	0.889	+20.1
Group 2a	0.684	0.765	0.864	0.875	+27.9
Group 2b	0.548	0.649	0.713	0.737	+34.6
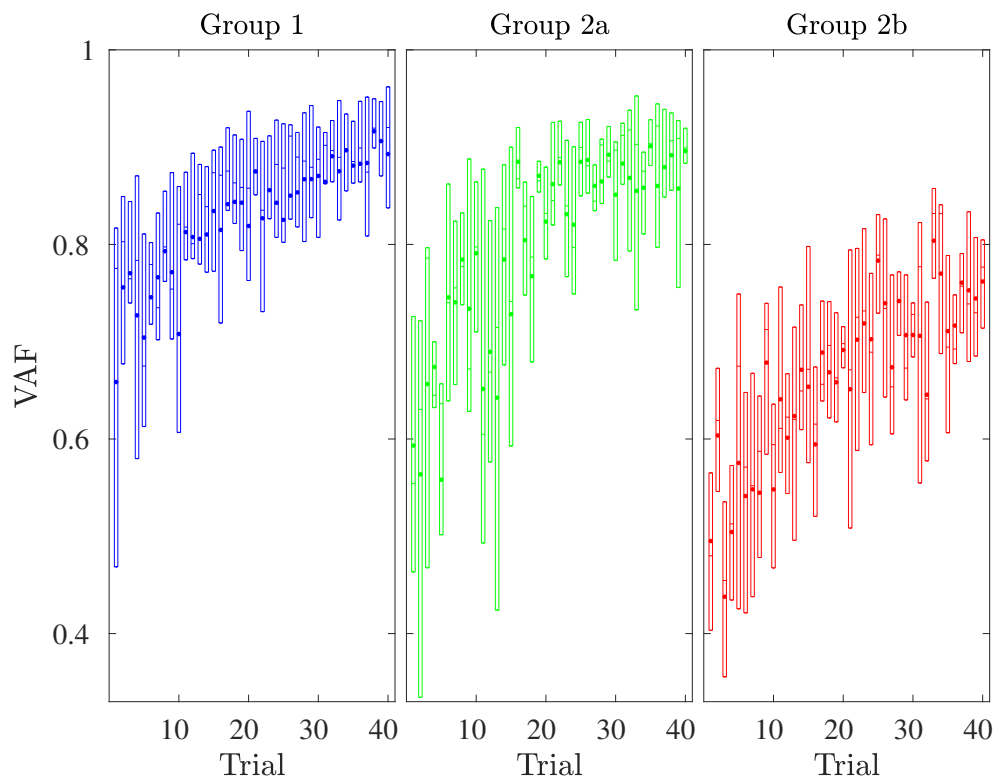
Figure B.2: Mean, median, first quartile, and third quartile of VAF on each trial. For all three groups, the mean and median VAF increase over the 40 trials. ● is the mean, and the boxplot shows the median, first quartile, and third quartile.

Bibliography

[1] D. M. Wolpert, R. C. Miall, and M. Kawato. Internal models in the cerebellum. *Trends in Cognitive Sciences*, 2:338–347, 1998.

[2] M. Ito. Neurophysiological aspects of the cerebellar motor control system. *International Journal of Neurology*, 7:162–176, 1970.

[3] R. A. Schmidt. A schema theory of discrete motor skill learning. *Psychological Review*, 82:225–260, 1975.

[4] M. Kawato. Internal models for motor control and trajectory planning. *Current Opinion in Neurobiology*, 9:718–727, 1999.

[5] C. Tin and C.P. Poon. Internal models in sensorimotor integration: perspectives from adaptive control theory. *Journal of Neural Engineering*, 2:S147–S163, 2005.

[6] H. Gomi and M. Kawato. The cerebellum and VOR/OKR learning models. *Trends in Neuroscience*, 15:445–453, 1992.

[7] R. Happee. Goal directed arm movements. iii. feedback and adaptation in response to inertia perturbations. *Journal of Electromyography and Kinesiology*, 3:112–122, 1993.

[8] R. Shadmehr and F. A. Mussa-Ivaldi. Adaptive representation of dynamics during learning of a motor task. *The Journal of Neuroscience*, 14:3208–3224, 1994.

[9] F. Gandolfo, F. A. Mussa-Ivaldi, and E. Bizzi. Motor learning by field approximation. *Proceedings of the National Academy of Sciences*, 93:3843–3846, 1996.

[10] R. L. Sainburg, C. Ghez, and D. Kalakanis. Intersegmental dynamics are controlled by sequential anticipatory, error correction, and postural mechanisms. *Journal of Neurophysiology*, 81:1045–1056, 1999.

[11] J. V. Cohn, P. Dizio, and J. R. Lackner. Reaching during virtual rotation: context specific compensations for expected coriolis forces. *Journal of Neurophysiology*, 83:3230–3240, 2000.

[12] J. R. Flanagan and J. R. Tresilian. Grip-load force coupling: a general control strategy for transporting objects. *Journal of Experimental Psychology: Human Perception and Performance*, 20:944–957, 1994.

[13] J. R. Flanagan and A. M. Wing. The role of internal models in motion planning and control: evidence from grip force adjustments during movements of hand-held loads. *Journal of Neuroscience*, 17:1519–1528, 1997.

[14] B. Mehta and S. Schaal. Forward models in visuomotor control. *Journal of Neurophysiology*, 88:942–953, 2002.

[15] A. J. Nagengast, D. A. Braun, and D. M. Wolpert. Optimal control predicts human performance on objects with internal degrees of freedom. *PLOS Computational Biology*, 5:e1000419, 2009.

[16] D. Liu and E. Todorov. Evidence for the flexible sensorimotor strategies predicted by optimal feedback control. *Journal of Neuroscience*, 27:9354–9368, 2007.

[17] E. Guigon, P. Baraduc, and M. Desmurget. Computational motor control: redundancy and invariance. *Journal of Neurophysiology*, 97:331–347, 2007.

[18] J. B. Dingwell, C. D. Mah, and F. A. Mussa-Ivaldi. Experimentally confirmed mathematical model for human control of a non-rigid object. *Journal of Neurophysiology*, 91:1158–1170, 2004.

[19] J-L. Vercher, F. Sares, J. Blouin, C. Bourdin, and G. M. Gauthier. Role of sensory information in updating internal models of the effector during arm tracking. *Progress in Brain Research*, 142:203–222, 2003.

[20] J. B. Dingwell, C. D. Mah, and F. A. Mussa-Ivaldi. Manipulating objects with internal degrees of freedom: evidence for model-based control. *Journal of Neurophysiology*, 88:222–235, 2002.

[21] N. Bhushan and R. Shadmehr. Computational nature of human adaptive control during learning of reaching movements in force fields. *Biological Cybernetics*, 81:39–60, 1999.

[22] D. M. Wolpert, Z. Ghahramani, and M. I. Jordan. An internal model for sensorimotor integration. *Science*, 269:1880–1882, 1995.

[23] R. C. Miall, D. J. Weir, D. M. Wolpert, and J. F. Stein. Is the cerebellum a smith predictor? *Journal of Motor Behavior*, 25:203–216, 1993.

[24] Y. Wada and M. Kawato. A neural network model for arm trajectory formation using forward and inverse dynamics models. *Neural Networks*, 6:919–932, 1993.

[25] M. Katayama and M. Kawato. Virtual trajectory and stiffness ellipse during multijoint arm movement predicted by neural inverse models. *Biological Cybernetics*, 69:353–362, 1993.

[26] T. Flash and N. Hogan. The coordination of arm movements: an experimentally confirmed mathematical model. *Journal of Neuroscience*, 5:1688–1703, 1985.

[27] Hiroaki Gomi and Mitsuo Kawato. Learning control for a closed loop system using feedback-error-learning. In *29th IEEE Conference on Decision and Control*, pages 3289–3294. IEEE, 1990.

[28] R. C. Miall and D. M. Wolpert. Forward models for physiological motor control. *Neural Networks*, 9:1265–1297, 1996.

[29] Maurice A Smith, Jason Brandt, and Reza Shadmehr. Motor disorder in huntington's disease begins as a dysfunction in error feedback control. *Nature*, 403(6769):544, 2000.

[30] M. I. Jordan and D. E. Rumelhart. Forward models: supervised learning with a distal teacher. *Cognitive Science*, 16:307–354, 1992.

[31] A. Tustin. The nature of the operator's response in manual control and its implications for controller design. *Journal of the Institution of Electrical Engineers - Part IIA: Automatic Regulators and Servo Mechanisms*, 94:190–206, 1947.

[32] Duane T. McRuer and Ezra S. Krendel. The human operator as a servo system element. *Journal of the Franklin Institute*, 267(5):381 – 403, 1959.

[33] D. Mcruer, D. Graham, E. Krendel, and W. Reisener. Human pilot dynamics in compensatory systems: Theory, models, and experiments with controlled element and forcing function variations. *Air Force Flight Dynamics Laboratory, Research and Technology Division, Air Force Systems Command, Wright-Patterson Air Force Base, Tech. Rep. AFFDL-TR-65-15*, 1965.

[34] D. T. McRuer, D. Graham, and E. S. Krendel. Manual control of a single-loop system: Part i. *Journal of the Franklin Institute*, 1(283):1–29, 1967.

[35] D. T. McRuer, D. Graham, and E. S. Krendel. Manual control of a single-loop system: Part ii. *Journal of the Franklin Institute*, 2(283):145–168, 1967.

[36] R. L. Stapleford, D. T. McRuer, and R. E. Magdaleno. Pilot describing function measurements in a multiloop task. *IEEE Trans. Human Factors in Electronics*, 8(2):113–125, 1967.

[37] D. McRuer and D. H. Weir. Theory of manual vehicular control. *IEEE Transactions on Man-Machine Systems*, 10(4):257–291, Dec 1969.

[38] R. J. Wasicko, D. T. McRuer, and R. E. Magdaleno. Human pilot dynamics in single-loop systems with compensatory and pursuit displays. Technical Report AFFDL-TR-66-137, Air Force Flight Dynamics Laboratory, Research and Technology Division, Air Force Systems Command, Wright-Patterson Air Force Base, 1965.

[39] R. A. Hess. Pursuit tracking and higher levels of skill development in the human pilot. *IEEE Trans. Systems, Man, and Cybernetics*, 11(4):262–273, 1981.

[40] Duane T. McRuer and Ezra S. Krendel. Mathematical models of human pilot behavior. *AGARDograph*, no. 188, 1974.

[41] A. Abdel-Malek and V. Z. Marmarelis. Modeling of task-dependent characteristics of human operator dynamics pursuit manual tracking. *IEEE Transactions on Systems, Man, and Cybernetics*, 18(1):163–172, Jan 1988.

[42] PD Neilson, MD Neilson, and NJ O'dwyer. Internal models and intermittency: A theoretical account of human tracking behavior. *Biological Cybernetics*, 58(2):101–112, 1988.

[43] PD Neilson, NJ O'dwyer, and MD Neilson. Stochastic prediction in pursuit tracking: An experimental test of adaptive model theory. *Biological cybernetics*, 58(2):113–122, 1988.

[44] Vincent A. Laurense, Daan M. Pool, Herman J. Damveld, Marinus René M. van Paassen, and Max Mulder. Effects of controlled element dynamics on human feedforward behavior in ramp-tracking tasks. *IEEE Transactions on Cybernetics*, 45(2):253–265, 2015.

[45] Max Mulder, D.M. Pool, K. van der El, F.M. Drop, and M.M. van Paassen. Manual control with pursuit displays: New insights, new models, new issues. *IFAC-PapersOnLine*, 52(19):139–144, 2019. 14th IFAC Symposium on Analysis, Design, and Evaluation of Human Machine Systems HMS 2019.

[46] Kasper van der El, Daan M. Pool, Marinus René M. van Paassen, and Max Mulder. Effects of target trajectory bandwidth on manual control behavior in pursuit and preview tracking. *IEEE Transactions on Human-Machine Systems*, 50(1):68–78, 2020.

[47] Xingye Zhang and Jesse B. Hoagg. Frequency-domain subsystem identification with application to modeling human control behavior. *Systems & Control Letters*, 87:36–46, 2016.

[48] X. Zhang, T. M. Seigler, and J. B. Hoagg. The impact of nonminimum-phase zeros on human-in-the-loop control systems. *IEEE Transactions on Cybernetics*, doi: 10.1109/TCYB.2020.3027502, 2020.

[49] X. Zhang, S. Wang, J. B. Hoagg, and T. M. Seigler. The roles of feedback and feedforward as humans learn to control unknown dynamic systems. *IEEE Transactions on Cybernetics*, 48(2):543–555, Feb 2018.

[50] S. Alireza Seyyed Mousavi, Xingye Zhang, T.M. Seigler, and Jesse B. Hoagg. Subsystem identification of feedback and feedforward systems with time delay. *Results in Control and Optimization*, 1:100002, 2020.

[51] J. Randall Flanagan and Ashwini K. Rao. Trajectory adaptation to a nonlinear visuomotor transformation: evidence of motion planning in visually perceived space. *Journal of Neurophysiol*, 74(5):2174 – 2178, 1995.

[52] Paul R Davidson, Richard D Jones, Harsha R Sirisena, and John H Andreae. Detection of adaptive inverse models in the human motor system. *Human Movement Science*, 19(5):761 – 795, 2000.

[53] Herbert Heuer and Mathias Hegele. Learning new visuo-motor gains at early and late working age. *Ergonomics*, 50(7):979–1003, 2007.

[54] Herbert Heuer and Mathias Hegele. Adaptation to a nonlinear visuomotor amplitude transformation with continuous and terminal visual feedback. *Journal of Motor Behavior*, 40(5):368 – 379, 2008.

[55] Willem B Verwey and Herbert Heuer. Nonlinear visuomotor transformations: locus and modularity. *The Quarterly Journal of Experimental Psychology*, 60(12):1629–1659, 2007.

[56] Martina Rieger, Willem B Verwey, and Cristina Massen. The effect of continuous, nonlinearly transformed visual feedback on rapid aiming movements. *Experimental brain research*, 191(1):1, 2008.

[57] Asim Ghous and Peter D Neilson. Evidence for internal representation of a static nonlinearity in a visual tracking task. *Human Movement Science*, 21(5):847 – 879, 2002.

[58] Seyyed Alireza Seyyed Mousavi, Xingye Zhang, T. Michael Seigler, and Jesse B. Hoagg. Characteristics that make linear time-invariant dynamic systems difficult for humans to control. *IEEE Transactions on Human-Machine Systems*, 51(2):141–151, 2021.

[59] S. Alireza Seyyed Mousavi, Faina Matveeva, Xingye Zhang, T. Michael Seigler, and Jesse B. Hoagg. The impact of command-following task on human-in-the-loop control behavior. *IEEE Transactions on Cybernetics*, pages 1–15, 2020.

[60] S. Prakriya and D. Hatzinakos. Blind identification of linear subsystems of LTI-ZMNL-LTI models with cyclostationary inputs. *IEEE Trans. Sig. Proc.*, 45:2023–2036, 1997.

[61] W. Zhao and H. Chen. Recursive identification for Hammerstein system with ARX subsystem. In *Proc. Chin. Contr. Conf.*, pages 473–476, Harbin, China, August 2006.

[62] D. Schmid and G. Enzner. Robust subsystems for iterative multichannel blind system identification and equalization. In *Proc. Pacific Rim Conf. on Communications, Computers and Signal Processing*, pages 889–893, Victoria, Canada, August 2009.

[63] M. Roth, J. Leasage, and L. Litz. Block-box identification of discrete event systems with optimal partitioning of concurrent subsystems. In *Proc. Amer. Contr. Conf.*, pages 2601–2606, Baltimore, MD, June–July 2010.

[64] M. Suzuki, N. Takatsuki, J. Imura, and K. Aihara. Node knock-out based structure identification in networks of identical multi-dimensional subsystems. In *Proc. Euro. Contr. Conf.*, pages 2280–2285, Zurich, Switzerland, July 2013.

[65] J. C. Spall. Identification for systems with binary subsystems. *IEEE Trans. Auto. Contr.*, 59:3–17, 2014.

[66] S. Hatakeyama, M. Iwase, and S. Yamaura. Analysis of human operation utilizing closed-loop identification method. In *Proc. IEEE Workshop on Intelligent Data Acquisition and Advanced Computing System: Technology and Applications*, pages 232–236, Sofia, Bulgaria, September 2005.

[67] S. Gillijns and B. D. Moor. Data-based subsystem identification for dynamic model updating. In *Proc. Conf. Dec. Contr.*, pages 3303–3308, San Diego, CA, December 2006.

[68] H. J. Palanthandalam-Madapusi, S. Gillijns, B. D. Moor, and D. S. Bernstein. Subsystem identification for nonlinear model updating. In *Proc. Amer. Contr. Conf.*, pages 3056–3061, Minneapolis, Minnesota, June 2006.

[69] A. V. Morozov, A. A. Ali, A. M. D'Amato, A. J. Ridley, S. L. Kukreja, and D. S. Bernstein. Retrospective-cost-based model refinement for system emulation and subsystem identification. In *Proc. Conf. Dec. Contr.*, pages 2142–2147, Orlando, FL, December 2011.

[70] A. M. D'Amato, A. J. Ridley, and D. S. Bernstein. Retrospective-cost-based adaptive model refinement for the ionosphere and thermosphere. *Statistical Analysis and Data Mining*, 4:446–458, 2011.

[71] X. Zhang and J. B. Hoagg. Subsystem identification of multivariable feedback and feedforward systems. *Automatica*, 72:131–137, October 2016.

[72] F. Chang and R. Luus. A noniterative method for identification using hammerstein model. *IEEE Transactions on Automatic Control*, 16(5):464–468, October 1971.

[73] G. Burnham, Jinbom Seo, and G. Bekey. Identification of human driver models in car following. *IEEE Transactions on Automatic Control*, 19(6):911–915, December 1974.

[74] R. Hess, J. K. Moore, and M. Hubbard. Modeling the manually controlled bicycle. *IEEE Transactions on Systems, Man, and Cybernetics - Part A: Systems and Humans*, 42(3):545–557, May 2012.

[75] M. Mulder, A. Abbink, E. R. Boer, F. M. Drop, K. van der El, and M. M. Paasen. Manual control cybernetics: State-of-the-art and current trends. *IEEE Transactions on Human-Machine Systems*, 48(5):468–485, 2018.

[76] A. Tustin. The nature of the operator's response in manual control, and its implications for controller design. *Journal of the Institution of Electrical Engineers - Part IIA: Automatic Regulators and Servo Mechanisms*, 94(2):190–206, May 1947.

[77] D. T. McRuer and H. R. Jex. A review of quasi-linear pilot models. *IEEE Trans. Human Factors in Electronics*, 8(3):231–249, 1967.

[78] Duane T. McRuer, Lee Gregor Hofmann, Henry R. Jex, G P Moore, Anil V. Phatak, D. H. Weir, and J. Wolkovitch. New approaches to human-pilot/vehicle dynamic analysis. *Air Force Flight Dynamics Laboratory*, Tech. Rep. AFFDL TR 67-150, 1968.

[79] Reza Shadmehr, Maurice A. Smith, and John W. Krakauer. Error correction, sensory prediction, and adaptation in motor control. *Annual Review of Neuroscience*, 33(1):89–108, 2010.

[80] M. Kawato. A hierachical neural-network model for control and learning of voluntary movement. *Biological Cybernetics*, 57:169–185, 1987.

[81] M. Kawato and H. Gomi. A computational model of four regions of the cerebellum based on feedback-error learning. *Biological Cybernetics*, 68:95–103, 1992.

[82] Peter D Neilson, Megan D Neilson, and Nicolas J O'Dwyer. What limits high speed tracking performance? *Human movement science*, 12(1-2):85–109, 1993.

[83] M. Haruno, D. M. Wolpert, and M. Kawato. *Advances in Neural Information Processing Systems*, chapter Multiple paired forward-inverse models for human motor learning and control, pages 31–37. MIT Press, 1999.

[84] D. A. Nowak, J. Hermsdorfer, S. Glasauer, L. Meyer, and N. Mai. The effects of digital anaesthesia on predictive grip force adjustments during vertical movements of a grasped object. *European Journal of Neuroscience*, 14:756–762, 2001.

[85] D. A. Nowak, S. Glasauer, L. Meyer, N. Mai, and J. Hermsdorfer. The role of cutaneous feedback for anticipatory grip force adjustments during object movements and externally imposed variation of the direction of gravity. *Somatosensory and Motor Research*, 19:49–60, 2002.

[86] O. Bock. Early stages of load compensation in human aimed arm movements. *Behavioural Brain Research*, 55:61–68, 1993.

[87] J. R. Flanagan and A. M. Wing. Modulation of grip force with load force during point-to-point movements. *Experimental Brain Research*, 95:131–143, 1993.

[88] J. R. Flanagan, J. R. Tresilian, and A. M. Wing. Coupling of grip force and load force during arm movements with grasped objects. *Neuroscience Letters*, 152:53–56, 1993.

[89] D. L. Weeks, M.-P. Aubert, A. G. Feldman, and M. F. Levin. One-trial adaptation of movement to changes in load. *Journal of Neurophysiology*, 75:60–74, 1996.

[90] S. J. Goodbody and D. M. Wolpert. Temporal and amplitude generalization in motor learning. *Journal of Neurophysiology*, 79:1825–1838, 1998.

[91] C. G. Atkeson. Learning arm kinematics and dynamics. *Annual Review of Neuroscience*, 12:157–183, 1989.

[92] J. Diedrichsen, T. Verstynen, A. Hon, Y. Zhang, and R. B. Ivry. Illusions of force perception: The role of sensori-motor predictions, visual information, and motor errors. *Journal of Neurophysiology*, 97:3305–3313, 2007.

[93] A. J. S. Sheffler, S. A. S. Mousavi, E. Hellström, M. Jankovic, M. A. Santillo, T. M. Seigler, and J. B. Hoagg. Effects of reference-command preview as humans learn to control dynamic systems. In *2019 IEEE International Conference on Systems, Man and Cybernetics (SMC)*, pages 4199–4204, Oct 2019.

[94] K. van der El, D. M. Pool, H. J. Damveld, M. R. M. van Paassen, and M. Mulder. An empirical human controller model for preview tracking tasks. *IEEE Transactions on Cybernetics*, 46(11):2609–2621, Nov 2016.

[95] W. M. Haddad and D. S. Bernstein. Explicit construction of quadratic lyapunov functions for the small gain, positivity, circle, and popov theorems and their applications to robust stability. part II: Discrete-time theory. *International Journal of Robust and Nonlinear Control*, 4:249–265, 1994.

[96] Kaoru Amano, Naokazu Goda, Shin'ya Nishida, Yoshimichi Ejima, Tsunehiro Takeda, and Yoshio Ohtani. Estimation of the timing of human visual perception from magnetoencephalography. *Journal of Neuroscience*, 26(15):3981–3991, 2006.

[97] Jean-Jacques Orban de Xivry and Philippe Lefèvre. Saccades and pursuit: two outcomes of a single sensorimotor process. *The Journal of physiology*, 584 Pt 1:11–23, 2007.

[98] Seyyed Alireza Seyyed Mousavi. *The Effects of System Characteristics, Reference Command, and Command-following Objectives on Human-in-the-loop Control Behavior*. PhD thesis, University of Kentucky, 2019.

[99] C von Hofsten and L Rönnqvist. Preparation for grasping an object: a developmental study. *Journal of experimental psychology*, 14:610–621, 1988.

[100] RS Johansson. How is grasping modified by somatosensory input. *Motor control: Concepts and issues*, pages 331–355, 1991.

[101] R. S. Johansson and G. Westling. Roles of glabrous skin receptors and sensorimotor memory in automatic control of precision grip when lifting rougher or more slippery objects. *Experimental Brain Research*, 56:550–564, 1984.

[102] R.S. Johansson, C. Häger, and L. Bäckström. Somatosensory control of precision grip during unpredictable pulling loads. *Experimental Brain Research*, 89:204—213, 1992.

[103] Alan M. Wing. 15 - anticipatory control of grip force in rapid arm movement. In Alan M. Wing, Patrick Haggard, and J. Randall Flanagan, editors, *Hand and Brain*, pages 301–324. Academic Press, San Diego, 1996.

[104] G Cadoret and AM. Smith. Friction, not texture, dictates grip forces used during object manipulation. *Journal of neurophysiology*, 75:1963–1969, 1996.

[105] D. A. Nowak, S. Glasauer, and J. Hermsdorfer. How predictive is grip force control in the complete absence of somatosensory feedback. *Brain*, 127:1–11, 2004.

[106] Shinya Takamuku and Hiroaki Gomi. Better grip force control by attending to the controlled object: Evidence for direct force estimation from visual motion. *PubMed*, 9:2045–2322, 2019.

[107] Bo Yu, R. Brent Gillespie, James S. Freudenberg, and Jeffrey A. Cook. Identification of human feedforward control in grasp and twist tasks. In *2014 American Control Conference*, pages 2833–2838, 2014.

[108] J. I. Elkind and C. D. Forgie. Characteristics of the human operator in simple manual control systems. *IRE Transactions on Automatic Control*, AC-4(1):44–55, 1959.

[109] E. Krendel and D. McRuer. A servomechanisms approach to skill development. *Journal of The Franklin Institute-engineering and Applied Mathematics*, 269:24–42, 1960.

[110] O. H. Gerlach. Developments in mathematical models of human pilot behavior. *Aeronautical Journal*, 7:293–305, 1977.

[111] Poulton Ec. Learning the statistical properties of the input in pursuit tracking. *Journal of Experimental Psychology*, 54:28–32, 1957.

[112] E. Poulton. Perceptual anticipation in tracking with two-pointer and one-pointer displays. *The British journal of psychology. General section*, 43:222–229, 1952.

[113] R. Chernikoff, H. P. Birmingham, and F. Taylor. A comparison of pursuit and compensatory tracking under conditions of aiding and no aiding. *Journal of experimental psychology*, 49 1:55–9, 1955.

[114] R. W. Allen and D. T. McRuer. The man/machine interface–Pursuit control. *Automatica*, 15(6):683–686, 1979.

[115] P Neilson, Nicholas O'Dwyer, and M Neilson. Stochastic prediction in pursuit tracking: An experimental test of adaptive model theory. *Biological cybernetics*, 58:113–22, 02 1988.

[116] Bo Yu, Brent Gillespie, J.s Freudenberg, and Jeffrey Cook. Human control strategies in pursuit tracking with a disturbance input. *Proceedings of the IEEE Conference on Decision and Control*, 2015:3795–3800, 02 2015.

[117] T.B. Sheridan. Three models of preview control. *IEEE Transactions on Human Factors in Electronics*, HFE-7(2):91–102, 1966.

[118] K. Ito and M. Ito. Tracking behavior of human operators in preview control systems. *Electrical Engineering in Japan*, 95(1):120–127, 1975.

[119] Kasper van der El, Daan M. Pool, Herman J. Damveld, Marinus René M. van Paassen, and Max Mulder. An empirical human controller model for preview tracking tasks. *IEEE Transactions on Cybernetics*, 46(11):2609–2621, 2016.

[120] Kasper van der El, Daan M. Pool, Marinus René M. van Paassen, and Max Mulder. Effects of preview on human control behavior in tracking tasks with various controlled elements. *IEEE Transactions on Cybernetics*, 48(4):1242–1252, 2018.

[121] Kasper van der El, Daan M. Pool, Marinus M. van Paassen, and Max Mulder. Effects of linear perspective on human use of preview in manual control. *IEEE Transactions on Human-Machine Systems*, 48(5):496–508, 2018.

Vita

Sajad Koushkbaghi received the B.Sc. degree in Aerospace Engineering in 2011 and the M.Sc. degree in Aerospace Engineering with a focus on Dynamics and Control in 2013 from Amirkabir University of Technology. He started his Ph.D. studies in Mechanical Engineering at the University of Kentucky in 2016.